Systematic Studies of the interaction between Amyloid ß-Protein and Lipids

Dissertation zur Erlangung des Grades
"Doktor der Naturwissenschafen"

am Fachbereich Biologie
der Johannes Gutenberg-Universität
in Mainz

vorgelegt von
Haipeng Song
aus Changchun, Jilin, V. R. China

Mainz, June, 2005

Tag der mündlichen Prüfung: 28th, June 2005

Die vorliegende Arbeit wurde unter Betreuung von Herrn Prof. Dr. H. Paulsen und Herrn Prof. Dr. W. Knoll im Zeitraum zwischen August 2001 bis Februar 2005 am Max-Planck-Institute für Polymerforschung, Mainz, Deutschland angefertigt.

CONTENTS

1 INTRODUCTION

1.1 The Amyloid hypothesis of Alzheimer's disease

Alzheimer's disease (AD) is the most frequent form of intellectual deterioration in elderly individuals and the fourth leading cause of death in developed nations. Although the cause of AD remains unknown, this disorder is a progressive degenerative disorder of insidious onset and is characterized by memory loss, confusion and a variety of cognitive disabilities. Clearly, this disease is a major social and health-care problem for which there is no cure or effective treatment. AD can be divided into a familial form, which usually has an early onset (before 60 years), and a sporadic late-onset form.[2]

The molecular mechanisms and hypothesis of Alzheimer's disease can be incredibly complex. So far, the prevalent hypothesis is that amyloid ß-peptides (Aß), aggregating outside nerve cells in the brain, are the primary influence driving AD pathogenesis.[3] Two variants of Aß have been found in these plaques: Aß1-40 and Aß1-42. The evidence that Aß aggregates play an important role in the early pathogenesis of AD comes mainly from studies of individuals affected by the familial form of the disease or by the so-called Down syndrome.[4] Almost all patients with Down syndrome develop AD neuropathology at an early age.[5] In a survey of brains from Down syndrome patients, diffuse amyloid deposits were observed in younger subjects in the absence of any other cerebral abnormality,[6] indicating that the formation of amyloid aggregates is perhaps the first neuropathological alteration. Furthermore, the fact that mutations in the gene encoding the ß-amyloid precursor protein (*APP*) are associated with the familial AD is a strong indication of the importance of amyloid in the pathogenesis of the disease.[7] These mutations promote the generation of Aß by favoring proteolytic processing of APP by ß- or γ- secretase. In addition to *APP*, three other genes have so far been linked with AD:

apolipoproein E (*apoE*, chromosome 19), presenilin 1 (*PS1*, chromosome 14) and presinilin 2 (*PS2*, chromosome 1). Mutations or polymorphisms in these genes induce an increase in the production or amyloidogeneicity of Aß, [8-11] and thus appear to be implicated in the disease through the formation of amyloid. These exciting observations provide a framework for the emerging amyloid hypothesis. A sequence of the pathogenetic steps of familial forms of AD was proposed according to the amyloid hypothesis (Fig. 1).

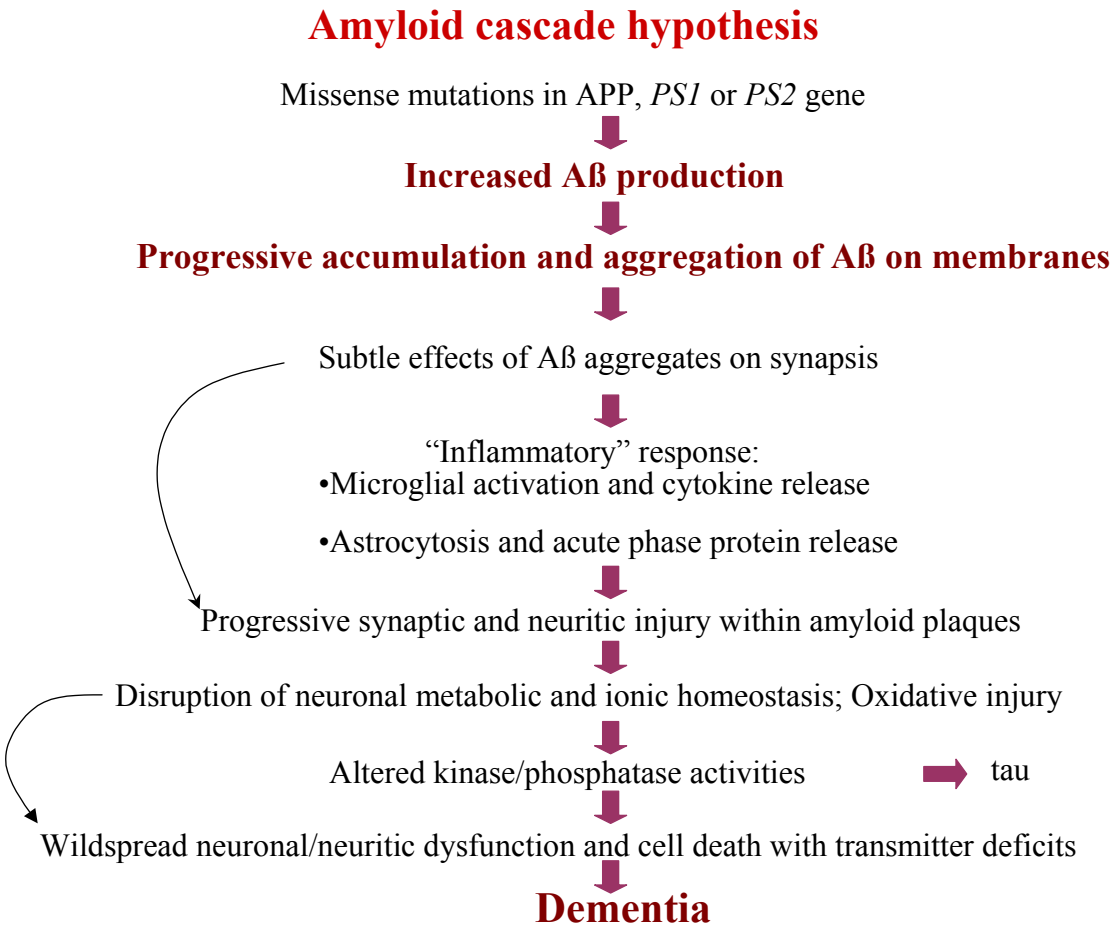

Figure 1.1: The sequence of pathogenic events leading to AD proposed by the amyloid cascade hypothesis.

Neuropathological studies have shown that neurodegenerative changes occur around compact amyloid plaques. Several different mechanisms have been proposed to mediate

amyloid toxicity,[12] including: (1) an increase in intracellular Ca^{2+}; (2) the formation of ion channels; (3) the increase of free radicals; and (4) the activation of signal transduction by interaction with specific cellular receptors. Two variants of Aß (Aß1-40 and Aß1-42) were recognized as primary component in these plaques of AD patient brain tissues.

1.2 Factors affecting Aß aggregation

The process of plaque formation in the development of Alzheimer's disease is complex and includes many steps. As mentioned above, APP is a transmembrane glycoprotein, and the Aß domain starts close to the membrane on the extracellular side and ends within the membrane. Because APP has to be cleaved within the membrane to release Aß, it was speculated that abnormal APP processing or membrane damage was the first pathological alternation in AD. However, it is now clear that low levels of a peptide identical to the one deposited in the AD amyloid are constitutively produced by most cell types,[13] and Aß is a normal constituent of human biological fluids.[14;15] These findings suggest that abnormal APP processing is not required for the amyloid formation and that Aß fibrilliogenesis might be the earliest pathological event in the disease. Regardless of whether soluble Aß is the precursor of the fibrillar Aß, it is certain that the same sequence can adopt two different states with distinct structure and biological properties. The key question in AD amyloidogenesis is why Aß is soluble under certain conditions but aggregates under others.

The relationship between the structure and fibrillogenicity of Aß has also been extensively studied. Several reports indicate that the conformation adopted by Aß peptides is crucial in amyloid formation.[16-18] Under the conditions in which the peptide adopts the random coil/α-helical structure, it aggregate slowly, but if Aß adopts the ß-sheet conformation, it aggregates rapidly.[19-21] By using synthetic analogs of Aß (1-40) that contain single amino-acid substitutes, it was found that a transition between a random coil/α-helix structure and a ß-strand conformation in the Aß N-terminal domain modulates amyloid formation, rendering two different species of Aß in solution: one 'able' and another one 'unable' to form amyloid. Therefore, it seems likely that a key

event in amyloidogenesis is the conversion of the normal soluble Aß conformer into the ß-sheet-rich amyloidogenic intermediate. Furthermore, Aß peptides with high contents of ß-sheets become partially resistant to proteolytic degradation, and this may be a crucial mechanism in amyloid deposition.[22] Most of the experimental evidence indicates that the central hydrophobic region of Aß plays an important role in modulating amyloid formation. On the other hand, it has been shown that the length of the C-terminal domain of Aß can influence the rate of Aß assembly by accelerating nucleus formation, suggesting that the C-terminal domain might play an important role in the modulation of fibrillogenesis. In summary, both the central and C-terminal domains of Aß appear to be crucial for amyloid formation,[23] and the basic unit for fibrillogenesis might be the Aß conformer adopting an antiparallel ß sheet that consists of strands involving the regions 12-24 and 28-40/42.

Increasing evidence suggests that the possibility for conversion of soluble Aß peptides into aggregated ones may be mediated by direct interaction of Aß and the membrane lipids. It was demonstrated that interactions between Aß and phosphatidylinositol accelerate amyloid fibril formation presumably through the structure conversion from a random coil to ß-sheet structure.[24] Sialic acid was also found to be an essential requirement for the binding to the ganglioside.[25;26] Furthermore, the increases not only in ganglioside but also the cholesterol contents in the lipid bilayers facilitate the binding of Aß to the membranes by altering the binding capacity.[27;28] Ganglioside-bound Aß undergoes a conformational transition from an α-helix-rich structure to a ß-sheet-rich structure with the increase in the peptide density on the membrane. It was hypothesized that, once underwent conformational change, Aß was able to acts as a "seed" for the formation of amyloid fibrils in intracellular cholesterol-rich microdomains, suggesting lipid composition including gangliosides and cholesterol strictly controls amyloid formation. If Aß recognizes gangliosides more readily in membranes that are rich in cholesterol, then the increased levels of cholesterol present in the human body as a function of aging would increase one's risks for AD. However, it was suggested that the increase of cholesterol, also changing with age, might be a compensatory factor reducing extracellular Aß by membrane insertion.[29] It was reported that Aß adopts mainly an α-helix after reacting with rich cholesterol-containing PC vesicles. This effect could be

beneficial in reducing the formation of aggregation by depressing the ß-sheet conformation, suggesting that a possible pathway of Aß aggregation which ultimately induces the formation of plaques may be prevented by its membrane insertion. This notion was further supported by the other report that the addition of >30mol% cholesterol to the membranes leads to the formation of channels.[30] By increased incorporation of Aß into membranes, cholesterol helps not only to inhibit the tendency of Aß to fibrillate but also to reduce the imbalance of the cellular ions induced by membrane depolarization, which could be one of the factors responsible for cytotoxicity in AD. In addition, oxidatively damaged phospholipid membranes were also found to promote ß-sheet formation of Aß,[31] suggesting a possible role for lipid peroxidation in the pathogenesis of AD. These observations implicate that subtle lipid changes within the membranes of neuronal cells could induce the aggregation process of Aß.

1.3 Aim of the Study

The interactions between Aß and membranes play a potential role in the formation of Aß aggregation, and thus the focus of this study is on how lipid membranes affect the behavior of Aß. Although many concepts about Aß-lipid interactions have been proposed, the interpretation of experimental results from different types of model systems is sometimes controversial. In preparing any model membrane, it is generally important that the lipids remain well mixed throughout the sample preparation procedure. However, the model system of lipid-vesicle containing cholesterol prepared by conventional solvent-drying/hydration protocols entails the risk that lipid and sterol components may dry at different rates as the solvent evaporates, yielding an inhomogeneous final sample. This problem can be mitigated somewhat by the proper choice of solvents and sample drying conditions, but remains a challenge for samples with elevates cholesterol contents (>ca. 40mol%). Obviously, the mechanisms of Aß-lipid interactions derived from these model membranes using the aforementioned preparation methods require further exploring. In addition, relatively simple membrane system, such as monolayers at the air-water interface, may not be suitable for properly evaluating the incorporation of Aß into the

membranes, because membrane's inner layer surely has an influence on the interaction of Aß with membranes. In order to address these problems, hence, our prime interest presented in Chapter 4 is to develop a model system which is more complex and close to a cell membrane.

Several lines of evidence have explored the roles of molecules such as cholesterol and gangliosides in the formation of Aß aggregates, but the interactions between Aß and phospholipid/cholesterol membranes especially composed of zwitterionic lipids (POPC and sphingomyelin) remain to be systematically investigated by further research due to the reasons mentioned above. In addition, cholesterol is rather susceptible to oxidation leading to the formation of cholesterol oxidation products (COPs). However, many questions concerning the importance of oxysterols in AD development remain to be answered. For these reasons model membranes containing different lipid compositions were used to investigate Aß-lipid interactions. Immunosensitive analysis based on monoclonal antibodies play today an important role as a tool for analytical applications. In chapter 5, we combined the immunoassay methodology with surface plasmon field-enhanced fluorescence spectroscopy (SPFS) to probe the binding ability of Aß to the model membranes.

In recent years, "lipid rafts" made of cholesterol and sphingolipid in AD have been to be considered potential candidates for Aß binding sites. Cell studies show that APP, ß-secretase and presenilin 1 all reside in "lipid rafts". Thus, the production and accumulation of Aß might occur primarily in these micro-domains. In order to clarify whether the binding of Aß is related to the specific micro-domains, we apply fluorescence microscopy to the study of monolayers of membrane lipids at the air-water interface. The phase behaviors of Langmuir films composed of different lipid componets will be presented in chapter 6.

It is well-known that peptides with a ß-structure conformation cannot penetrate the membrane as readily as α-helices because of the problem of satisfying the hydrogen bonding capability of the amide bonds. The formation of Aß aggregates definitely correlates with the orientation of Aß at the membrane plane. Therefore, knowledge of the orientation of Aß at the membrane surface is significant to evaluate the tendency of Aß to

aggregate. In chapter 7, pair-wise binding tests of monoclonal antibodies (mAbs) against distinct epitopes to different sites of Aß were performed in order to determine the possible orientation of Aß adsorbed at the membrane containing both sphingomyelin and 25-hydroxycholesterol, which are potential binding sites for Aß. In addition, we will detect the conformational change of Aß caused by melatonin at the membranes using the pair-wise binding tests, which provides a novel tool for the investigation on the effects of membranes on the Aß conformation and for screening new inhibitors of Aß aggregates.

2 Methods and theories

2.1 Langmuir films

Langmuir monolayers are produced and characterized in an apparatus that has been traditionally referred to as a Langmuir trough. It consists of a trough, usually made from a hydrophobic material like Teflon to contain the subphase water and movable barrier(s) that span across the water surface. A typical Langmuir trough is shown in Fig. 2.1. Langmuir film studies have mostly been carried out with amphiphilic molecules that contain a polar head group and a non-polar tail, as in the typical example of stearic acid, with COOH at the polar head and with a C_{17} alkyl chain attached.

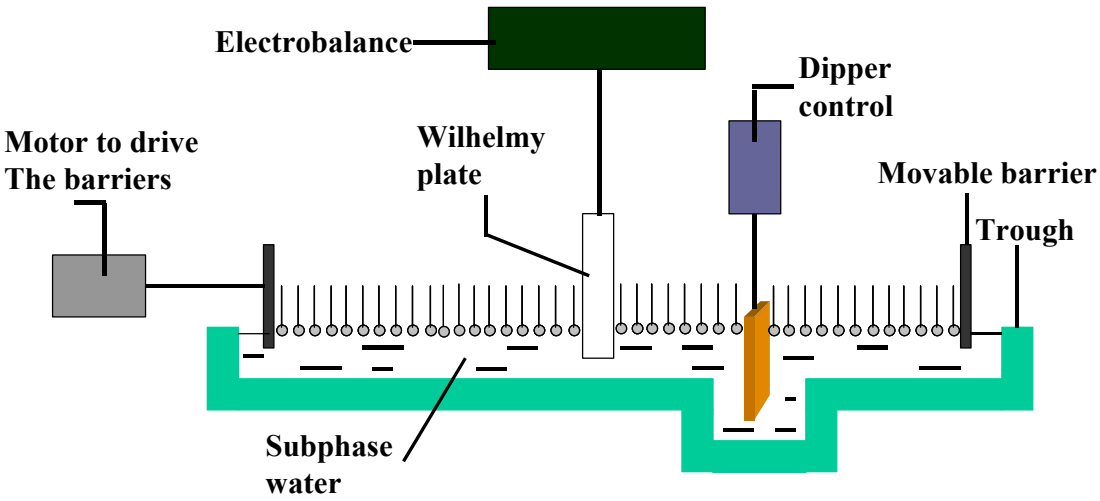

Figure 2.1: Schematic representation of a Langmuir trough that conatains the Wilhemy plate for measuring surface pressure using an electrobalance. Also shown is the dipper employed for transferring Langmuir-Blodgett onto a solid substrate.

In a common Langmuir film experiment, a known amount of amphiphilic material dissolved in a water-immiscible, volatile organic solvent such as chloroform is placed on the water surface. After evaporation of the solvent, the monolayer material is compressed with the movable barriers. Monolayer formation is usually monitored by recording surface-area isotherms. Stringent conditions must be adopted for obtaining reproducible results with a Langmuir film. These include: (i) the use of pure materials and spreading solvents, where HPLC grade organic solvents and AR grade salts are normally recommended; (ii) accurate weighing of the monolayer material; (iii) selection of suitable spreading solvents; (iv) careful filtration of non-dissolved materials, also taking into account the filtered material during area calculation; (v) regular and thorough cleaning of the trough and barriers; (vi) the use of ultrapure water for the subphase; and (vii) a clean and vibration-free environment for carrying out the experiments with controllable subphase temperature, which may be achieved by water circulation underneath the trough bottom.

2.1.1 Surface pressure-area isotherms

Molecules in a liquid are subject to attractive forces; in the bulk of the liquid these forces are equal. However, at a surface or interface the forces are unbalanced and the net effect is to pull the peripheral molecules into the bulk of the solution. This effect gives rise to surface tension. The surface tension can be defined as “the work required to expand the surface isothermally by a unit area”. The tendency of surface-active molecules to accumulate at interfaces favors expansion of the interface and hence reduces the surface tension. Such behaviour makes it possible to monitor the surface pressure as a function of the area occupied per molecule provided that the number of molecules deposited on the surface is known.

The basic and widely used tool to characterize a Langmuir monolayer is the surface pressure (π)-area (A) isotherm, which is a plot of the change in surface pressure (a measure of the decrease in surface tension, i.e, the two-dimensional analogue of pressure) as a function of the area available to each molecule on the aqueous subphase surface. The reduction of surface tension is known as the surface pressure. Pressure readings are made by means of a “Whilhemy” plate attached to a microbalance.

2.1.2 Forces at the subphase surface

The isotherm can usually shows three distinct regions (Fig. 2.2):

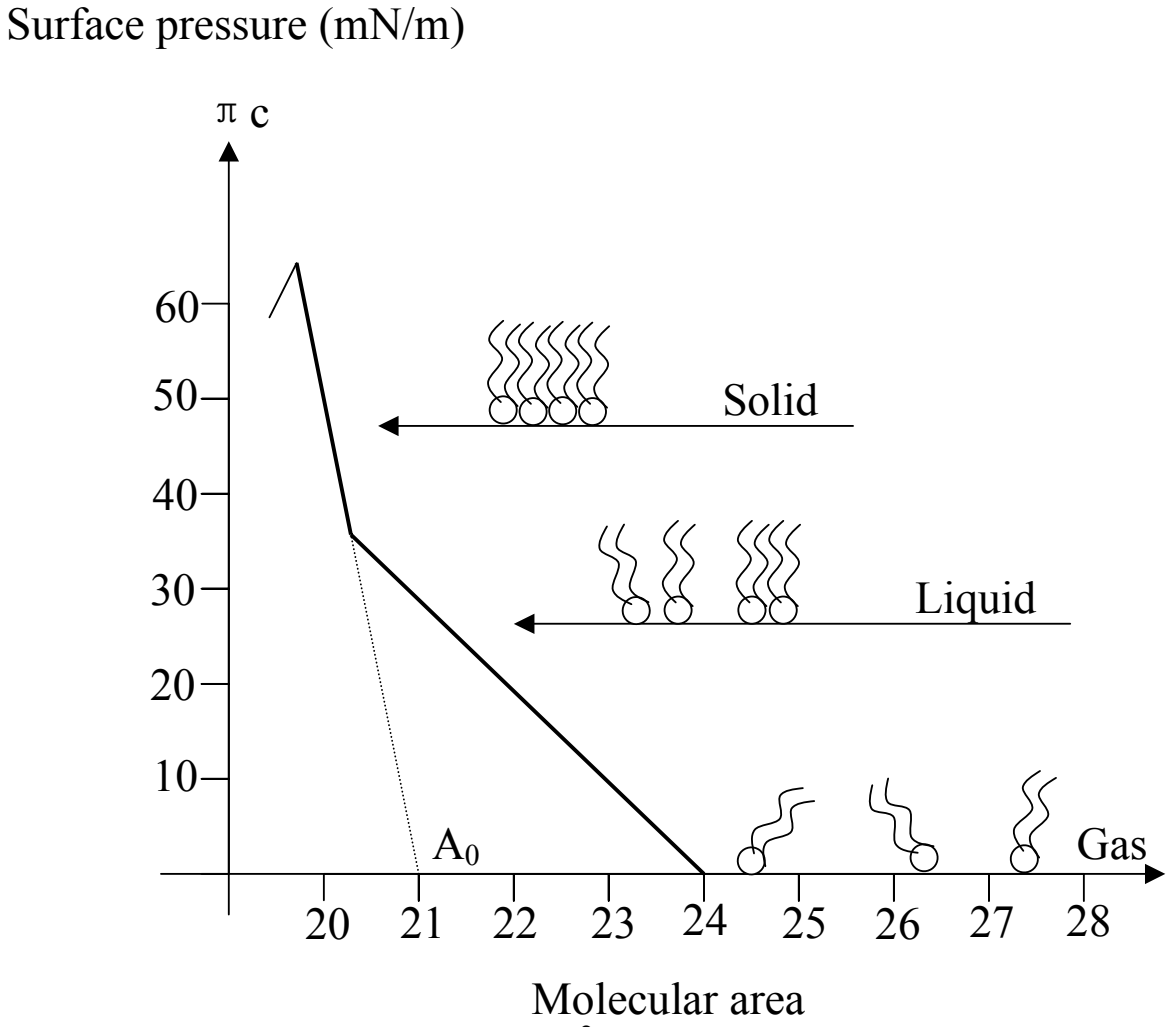

Figure 2.2: A stearic acid isotherm on pure water

After initial spreading onto the subphase, no external pressure is applied to the monolayer and the molecules behaves as a two-dimensional gas, which can be described by :

$$\pi A = kT$$

where π is the surface pressure, A the molecular area, k the Boltzmann constant and T is the thermodynamic temperature. In this "gaseous" state (G), the molecules are far apart and believed not to interact with each other. The free energy of the aqueous subphase and therefore the surface tension remain unchanged. If the area of the monolayer is reduced by film compression, the molecules become closer and start to interact [so-called "liquid" state (L)]. Under further compression [so-called "solid" or crystalline" (C), film molecules are closely packed and assumed to be vertically oriented. This solid state is characterized by a steep and usually linear relationship between surface pressure and molecular area. On further compression monolayer collapse occurs. The shape of π/A isotherms is strongly influenced by many factors including the experimental conditions and chemical modification of the molecule's structure. It is well known that for an insoluble monolayer to be obtained, the molecule should possess at least 12 carbon atoms. Otherwise, solubility in the aqueous subphase causes monolayer loss with a decrease in monolayer area. Lauric acid, which lies on the border, forms slightly soluble, gaseous monolayers (Fig. 2.3). The addition of two more carbon atoms causes myristic acid to exhibit a condensed gaseous phase region as well as an expanded phase[32] and further increase in hydrocarbon chain length results in the additional formation of a solid phase,[33] as illustrated in Fig. 2.3. The presence of an unsaturated double or triple bond changes the isotherm characteristics. The two parts of the molecule linked with a double bond cannot rotate and thus the bond may disrupt chain ordering. This is more pronounced for the cis- than for the trans-isomers.[34]

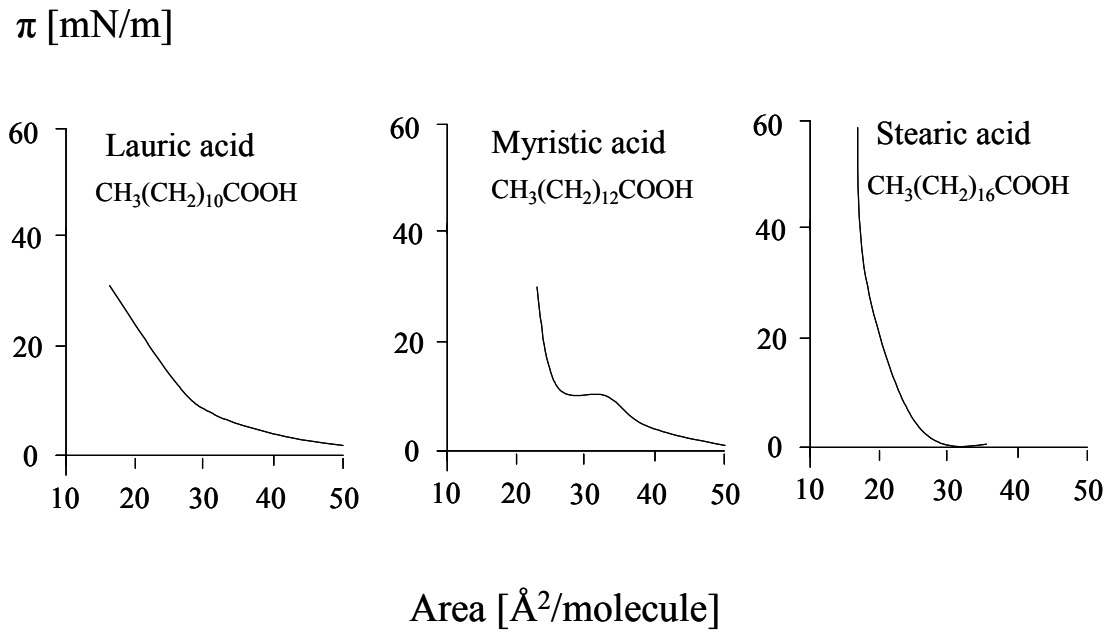

Figure 2.3: Surface pressure-area (π/A) isotherms of lauric acid, myristic acid spread on 10-3 M HCl aqueous subphase (20°C, compression speed 7.5×1017 $Å^2$ min^{-1}). The mere change in the size of the hydrophobic tail causes the nature of the isotherm to vary considerably.

Eventually the collapse pressure, π_c, is reached at which the film irretrievably loses its monomolecular form. The forces acting upon it become too strong for confinement in two dimensions and molecules are ejected out of the monolayer plane into either the subphase (more hydrophilic molecules) or the superphase (more hydrophobic molecules). However, collapse is not uniform across the monolayer but is usually initiated near the leading edge of the barrier or at discontinuities in the trough such as corners or the Wilhelmy plate. Usually a "collapsed" film will consist of large areas of uncollapsed monolayer interspersed with "mountain ridges" where monolayers have been crushed together to form bulky aggregates. This is rather like mountain formation at the collision of the earth's tectonic plates, but on a vastly different scale. The collapse pressure can be defined as the maximum to which a monolayer can be compressed without any detectable expulsion of molecules from the Langmuir film. It depends upon the details of the experimental procedures, i.e. the chemical substances used, the temperature, the rate at which the film is compressed, etc.

Quantitative information can be obtained on the molecular dimensions and the shape of the molecule under study. If the monolayer is in the two-dimensional “solid” or “liquid condensed” phase the molecules are relatively well oriented and closely packed and the zero-pressure molecular area (Å) can be obtained by extrapolating the slope of the “solid” phase to zero pressure- the point at which this line crosses the x-axis is the hydrothetical area occupied by one molecule in the condensed phase at zero pressure.

It is important to study the isotherm of the monolayer of the film forming material as a pre-requisite to the determination of dipping characteristics. Information can be obtained as to the way in which the molecules pack at the interface and the stability of the compressed layer at high pressures. Improved quality can be obtained by “annealing” the film, which is by compressing (never going above π_c) then expanding a number of times. Such a procedure encourages more efficient packing and usually a shift to lower molecular areas is observed. Recent work suggests that the Langmuir film exists in a number of different liquid crystal phases on the water surface, depending on the film temperature and pressure.

2.1.3 Surface pressure measurement

The measurement of the surface pressure is usually carried out at pseudo-equilibrium conditions, by continuously compressing the monolayer while monitoring the surface pressure, though one can obtain equilibrium values by compressing the monolayer on a point-to-point basis. There are two main methods to measure the surface pressure during monolayer compression: the Langmuir balance and the Wilhemy plate. In this study, the latter one is used to measure the surface pressure. The Wilhemy method is an absolute method in which the forces acting on the plate, usually made of platinum or filter paper, partially immersed in the subphase are measured (Fig. 2.3). Such forces, the downward forces, such as gravity and surface tension, and upward forces, such as buoyancy due to the displacement of water, are normally measured with a sensitive electrobalance.

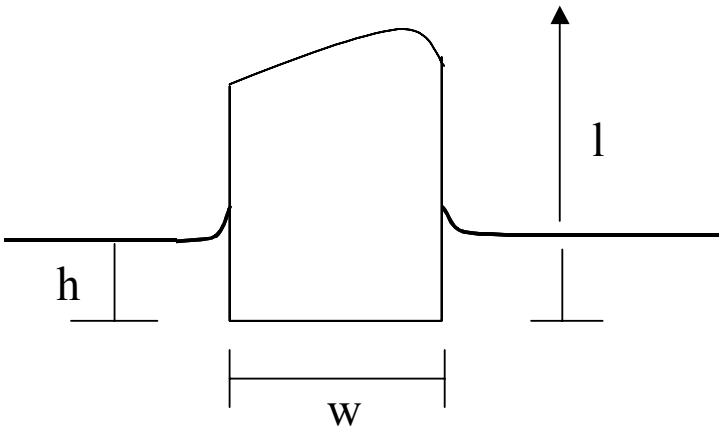

Figure 2.4: The Wilhemy plate

If the plate has the dimensions l×w×t (length, width, thickness) and a density, ρ, and is immersed in water to a depth, h, then the net force downward, F, is describe by the equation:

$$\text{Force} = (\rho_p lwt)\cdot g - (\rho_L hwt)\cdot g + 2.(w + t)\cdot\gamma\cdot\cos\theta \qquad (1)$$

(Force = weight – upthrust + surface tension)

With ρ_p being the density of the plate, ρ_L the density of the liquid, γ the surface tension of the liquid, θ the contact angle of liquid to plate and g the acceleration due to gravity.
Before making any measurements, the pressure reading is zeroed, thereby eliminating the weight term from Eq. 1:

$$\text{Force} = -(\rho_L hwt)\cdot g + 2\cdot(w + t)\cdot\gamma\cdot\cos\theta \qquad (2)$$

(Force = - upthrust + surface tension)

The upthrust term is eliminated from Equation 2 as the plate is always kept at a constant level by the balance, no matter what the surface tension:

$$\text{Force} = 2\cdot(w + t)\cdot\gamma\cdot\cos\theta \quad (3)$$

Finally, use of paper plates ensures a contact angle of the liquid to the plate of $\theta = 0°$ and the expression reduces to:

$$\text{Force} = 2\cdot(w + t)\cdot\gamma \quad (4)$$

Hence for a plate, the surface tension is:

$$\gamma_{plate} = \text{Force} / 2\cdot(\text{width} + \text{thickness}) \quad (5)$$

with the surface tension (γ) in mN/m, the force in mN and the perimeter in metres.
Generally therefore, the surface tension is given by:

$$\gamma = \text{Force} / \text{perimeter} \quad (6)$$

Thus for a ring, the surface tension is given by:

$$\gamma_{ring} = \text{Force} / (\pi d + \pi (d-2t)) \quad (7)$$

Where “d” is the outer diameter of the ring and “t” is the thickness of the wire in metres. The surface tension is in mN/m and the force is in mN.
Hence for a 10.25mm wide, 0.25mm thick paper plate, a 100 mg weight will give a reading of 46.7mN/m. This is useful figure when checking the pressure sensor.

2.1.4 Langmuir-Blodgett (LB) films

The Langmuir-Blodgett (LB) technique has been frequently used to produce thin film of amphiphilic molecules on solid supports. The two-dimensional assembly of biomolecules has been shown to be of great value in many applications, such as 2D crystallization of

proteins, investigations of ordering and phase behavior of model membranes and development of biological sensor.[35;36]

Irving Langmuir and Katharine Blodgett developed this method in the early twentieth centrury. They found that amphiphilic molecules spread on a water surface are arranged with a specific orientation in monolayers. This allows the transfer of a compressed fatty acid monolayer from the air-water interface onto a solid substrate by consecutively moving a plate vertically through the LB-film. A schematic illustration of the procedure is shown in fig. 2.5. Langmuir-Blodgett films consist of mono-molecular layers stacked sequentially onto a solid substrate. A solid substrate is lowed into the water, breaking through the Langmuir film, and provided that certain criteria have been met, the Langmuir film attaches itself to the substrate, coating it by a mono-molecular layer. The LB technique, by definition, requires amphiphilic molecules to be trapped at the interface of two phases (either liquid-liquid or liquid-gas). Two types of surfaces can be coated by the lB technique-hydrophobic (water repelling) and hydrophilic (water attracting). Here we only discuss the deposition on the hydrophilic substrates.

Deposition onto hydrophilic substrates proceeds in a similar manner, with the exception that first layer is deposited on the film up-stroke.

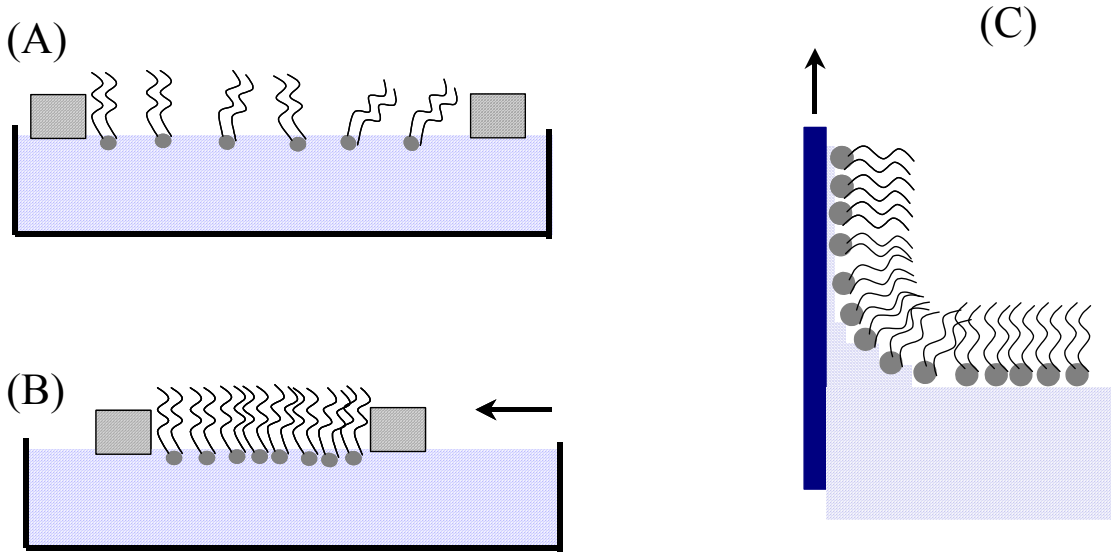

Figure 2.5: Schematic representation of the LB-monolayer formation. The procedure is as follows: (A) amphiphilic molecules dissolved in an organic solvent are spread at the air-liquid interface of a LB-trough and the solvent is then allowed to evaporate. (B) the molecules are compressed into an ordered film by a lateral phaysical force produced by a moving a barier. (C) If the solid support is hydrophilic a monolayer of amphiphilic molecules can be transferred to the surface on the upsroke of the vertical dipping procedure. The surface pressure is controlled with a Wilhelmy plate and kept constant during the dipping procedure.

This is a result of the water meniscus onto a hydrophilic surface being curved upwards. If the substrate is moved down into the subphase, the curvature of the meniscus and the direction of motion do not coincide. Hence, molecules cannot be deposited. Thus the first monolayer on a hydrophilic substrate is deposited on the first “up” stroke through the monolayer, as the direction of the meniscus now favors the headgroup of the molecule to attach to the surface.

A good measure of how well a film has been transferred to a substrate is the transfer ratio, given by:

$$TR = \frac{areea\ of\ \ monolayer\ removed\ \ from\ the\ \ subphase\ at\ \ cons\tan t\ \ pressure}{area\ of\ \ substrate\ immersed\ in\ the\ water}$$

Such a ratio is usually measured for each substrate pass through the air-water interface. However, it must be remembered that the measured transfer ratio is an average value over the entire immersed surface and often require interpretation. It is possible, for instance, to measure a TR of 0% if 100% deposition takes place on one face of the substrate and 100% of film is peeled off from the other face.

2.2 Contact angle measurement

Contact angle, θ, is a quantitative measure of the wetting of a solid by a liquid. The possibility of estimating solid surface tensions from contact angles relies on a relation which has been reported by Young in 1805.[37]

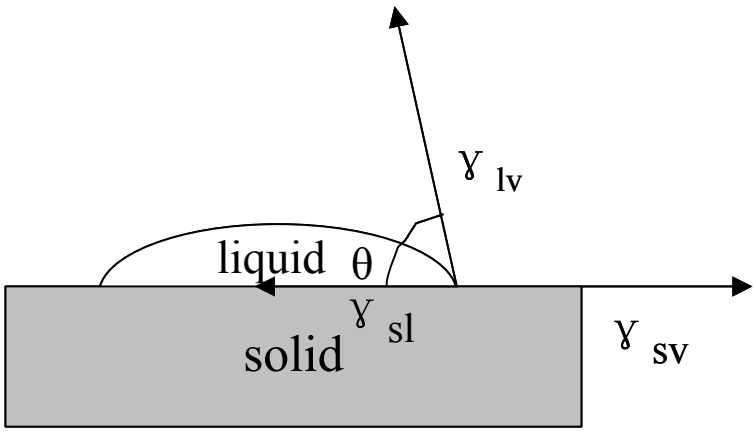

Figure 2.6: Schematic of a sessile-drop contact angle system

The contact angle of a liquid drop on a solid surface is defined by the mechanical equilibrium of the drop under the action of three interfacial tensions (Fig. 2.6): solid-vapor, $\gamma_{sv,}$ solid-liquid, γ_{sl}, and liquid-vapor, γ_{lv}. This equilibrium relation is known as Young's equation:

$\gamma_{lv} \cos \theta_Y = \gamma_{sv} - \gamma_{sl}$

where θ_Y is the Young contact angle, i.e. a contact angle which can be inserted into Young's equation. This analysis involves the interfacial free energies between the three phases. Contact angle measurements are easily performed by establishing the tangent (angle) of a liquid drop with a solid surface at the base. The attractiveness of using contact angles θ to estimate the solid-vapor and solid-liquid interfacial tensions is due to the relative ease with which contact angles can be measured on suitably prepared solid surfaces. It can be seen from Fig.2.6 that low values of θ indicate that liquid spreads, or wets well, while high values indicate poor wetting. If the angle θ is less than 90 the liquid is said to wet the solid. If it is greater than 90 it is said to be non-wetting. A zero contact angle represents complete wetting.

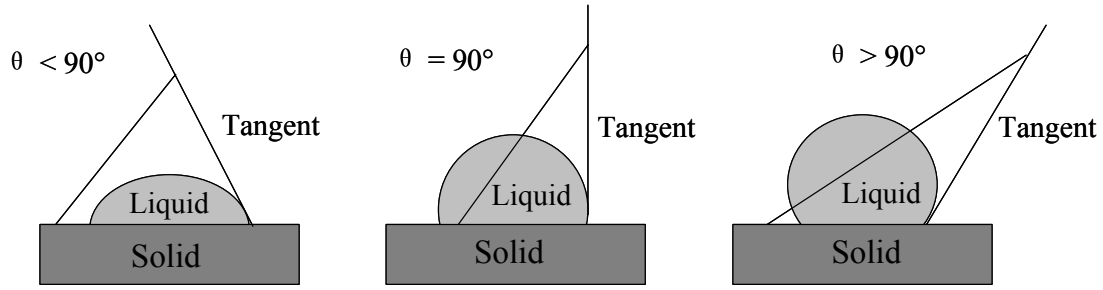

Figure 2.7: Schematic of the angle formed by a liquid at the three-phase boundary (liquid/gas/solid).

For any given solid/liquid interaction there exists a range of contact angles which may be found. The values of static contact angles are found to depend on the recent history of the interaction. If the drop has recently been expanded the angle is said to represent the "advancing" contact angle. If the drop has recently been contracted the angle is said to represent the "receding" contact angle. These angles fall within a range with the advancing angles approaching a maximum value and the receding angles approaching a minimum value. Dynamic contact angles may be assayed at various rates of speed. Dynamic contact angles measured at low velocities should be equal to properly measure

static angles. Since $\gamma_{lv,}$ $\gamma_{sv,}$ and γ_{sl} are thermodynamic properties of the liqid and solid, Young's equation implies a single, unique contact angle; in practice, however, contact angle phenomena are complicated. In particular, the contact angle made by an advancing liquid (θ_a) and that made by a receding liquid (θ_r) are not identical; nearly all solid surfaces exhibit contact angle hysteresis, *H* (the difference between θ_a and θ_r)

$H = \theta_a - \theta_r$

Because of these various complexities, models have been employed to gain a deeper understanding of the thermodynamic status of contact angles. In general, it has been found that experimentally observed apparent contact angle, θ, may or may not be equal to the Young contact angle, θ_Y:

1. On ideal solid surfaces, there is no contact angle hysteresis and the experimentally observed contact angle is equal to θ_Y.
2. On smooth, but chemically heterogeneous solid surfaces, θ is not necessarily equal to the thermodynamic equilibrium angle. Nevertheless, the experimental advancing contact angle, $\theta_{a,}$ can be expected to be a good approximation of $\theta_{Y.}$ Therefore, care must be exercised to ensure that the experimental apparent contact angle, θ, is the advancing contact angle on a heterogeneous and smooth surface can also be a Young angle, it is usually found to be non-reproducible often because of sorption of the liquid into the solid and swelling of the solid by the liquid.
3. On rough solid surfaces, no such equqlity between θ_a and θ_Y exists: all contact angles on rough surfaces are meaningless in terms of Young's equation.

Several contact angle approaches,[38-44] of current interest, were largely inspired by the idea of using Young's equation for the determination of surface energetics (Fig. 2.7). While these approaches are, logically and conceptually, mutually exclusive, they share, nevertheless, some basic assumptions:

1. All approaches rely on the validity and applicability of Young's equation for surface energetics from experimental contact angles.
2. Pure liquids are always used; surfactant solutions or mixtures of liquids should not be

used, since they would introduce complications due to preferential adsorption.

3. The values of γ_{lv}, γ_{sv} (and γ_{sl}) are assumed to be constant during the experiment, i.e. there should be no physical or chemical reaction between the solid and the liquid.
4. The liquid surface tensions of the testing liquids should be higher than the anticipated solid surface tension.
5. The values of γ_{sv} going from liquid to liquid are also assumed to be constant, i.e. independent of the liquid used.

In order to assure that the experimentally measured contact angles do not violate any of the above assumptions, one requires careful experimentation and suitable metholodogy.

Two different approaches are commonly used to measure contact angles of non-porous solids, goniometry and tensiometry. Goniometry involves the observation of a sessile drop of a test liquid on a solid substrate. Tensiometry involves measuring the forces of interaction as a solid is contacted with a test liquid. In this study, goniometry is applied to the measurement of contact angles, and hence we only describe this technique below.

Analysis of the shape of a drop of a test liquid placed on a solid is the basis for goniometry. The basic elements of a goniometer include a light source, sample stage, lens and image capture. Contact angle can be assessed directly by measuring the angle formed between the solid and the tangent to the drop surface.

The production of drops with advanced and receded edges involves one of two strategies. Drops can be made to have advanced edges by addition of liquid. Receded edges may be produced by allowing sufficient evaporation or by withdrawing liquid from the drop. Alternately, both advanced and receded edges are produced if the stages on which the solid is held is tilted to the point of incipient motion. Goniometry can be used in many situations where tensiometry cannot. A great variety of solid substrates can be used provided they have a relatively flat portion for testing and can fit on the stage of the instrument. Testing can be performed using very small quantities of liquid. It is also easy to test high temperature liquids such as polymer melts.

2.3 Preparation of liposomes (vesicles)

2.3.1 Mechanism of vesicle formation

Liposomes (lipid vesicles) are formed if a thin lipid film or lipid cakes are hydrated and stacks of liquid crystalline bilayers become fluid and swell. The hydrated lipid sheets detach during agitation and self-close to form large, multilamellar vesicles (LMV) which prevents interaction of water with the hydrocarbon core of the bilayer at the edges (Fig. 2.7). Once these particles have formed, reducing the size of the particle requires energy input in the form of sonic energy or mechanical energy (extrusion).

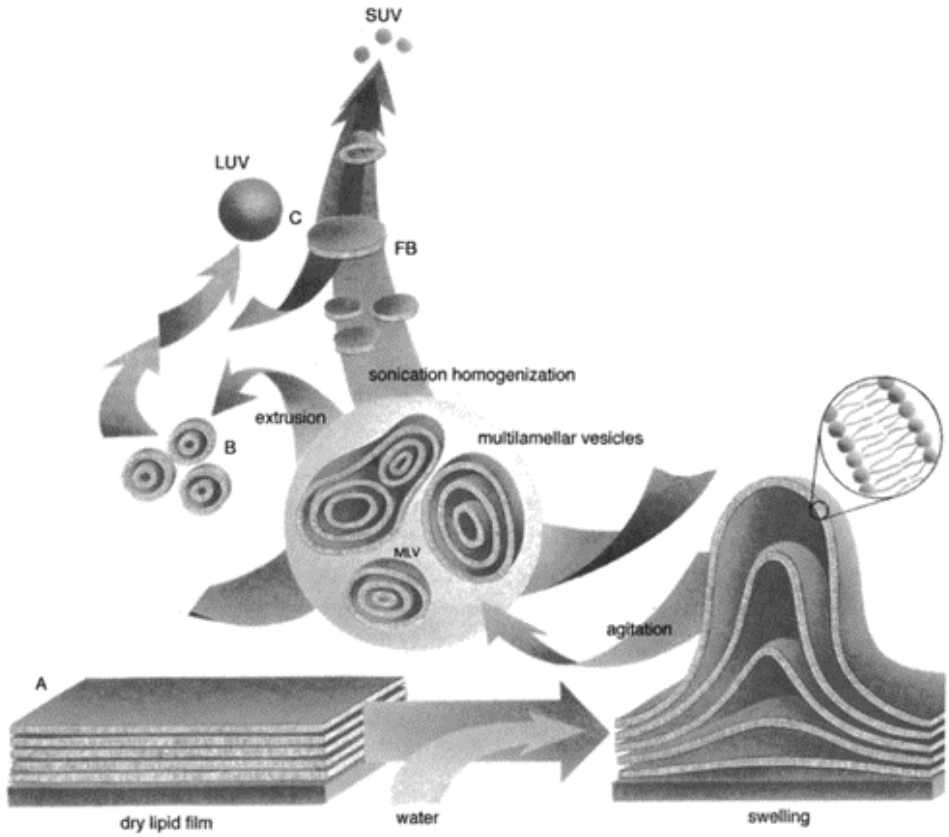

Figure 2.8: Schematic of vesicle formation

2.3.2 Procedures of liposome preparation

Properties of lipid formulations can vary depending on the composition (cationic, anionic, neutral lipid species), however, the same preparation method can be used for all lipid vesicles regardless of composition. The general elements of the procedure involve preparation of the lipid for hydration, hydration with agitation, and sizing to a homogeneous distribution of vesicles.

2.3.2.1 Preparation of lipid for hydration

When preparing liposomes with mixed lipid composition, the lipids must first be dissolved and mixed in an organic solvent to assure a homogeneous mixture of the lipids. Usually this process is carried out using chloroform or the mixture of chloroform and methanol. The intent is to obtain a clear lipid solution for complete mixing of lipids. Once the lipids are thoroughly mixed in the organic solvent, the solvent is removed to yield a lipid film. For small volumes of organic solvent (<1ml), the solvent may be evaporated using a dry stream of nitrogen or argon in a fume hood. For larger volumes, the organic solvent should be removed by rotary evaporation yielding a lipid film on the sides of a round bottom flask. The lipid film is thoroughly dried to remove residual organic solvent by placing the vial or flask on a vacuum pump overnight. Dry lipid films or cakes can be removed from the vacuum pump, the container closed tightly and taped, and stored frozen until ready to hydrate.

2.3.2.2 Hydration of lipid film/cake

Hydration of the dry lipid film/cake is accomplished simply by adding an aqueous medium to the container of dry lipid and agitating. The temperature of the hydrating medium should be above the gel-liquid crystal transition temperature (T_c or T_m) of the lipid with the highest T_c before adding to the dry lipid. After addition of the hydrating medium, the lipid suspension should be maintained above T_c during the hydration period. For high transition lipids, this is easily accomplished by transferring the lipid suspension to a round bottom flask and placing the flask on a rotory evaporation system without a

vacuum. Spinning the round bottom flask in the warm water bath maintained at a temperature above T_c of the lipid suspension allows the lipid to hydrate in its fluid phase with adequate agitation. Hydration times may differ slightly among different lipid species and structures, however, a hydration time of 1 hour with vigorous shaking, mixing, or stirring is highly recommended. It is also believed that allowing the vesicle suspension to stand overnight (aging) prior to downsizing makes the sizing process easier and improves the homogeneity of the size distribution. Aging is not recommended for high transition lipids as lipid hydrolysis increases with elevated temperatures.

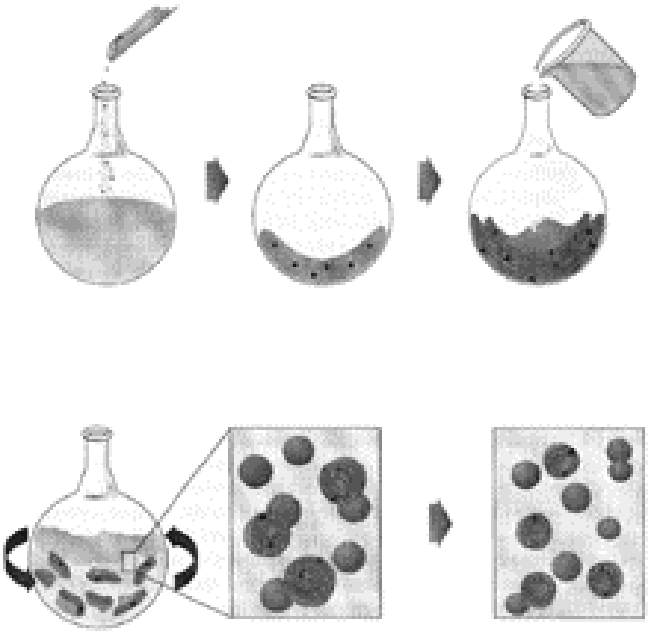

Figure 2.9: Schematic of the procedure of the formation and the hydration of lipid film.

Suitable hydration media include distilled water, buffer solutions, saline, and nonelectrolytes such as sugar solutions. During hydration some lipids form complexes unique to their structure. Highly charged lipids have been observed to form a viscous gel when hydrated with low ionic strength solutions. The prolem can be alleviated by addition of salts or by downsizing the lipid suspension. Poorly hydrating lipids such as phosphatidylethanolamine have a tendency to self aggregate upon hydration. Lipid

vesicles containing more than 60mol% phosphatidylethanolamine form particles having a small hydration layer surrounding the vesicle. As particles approach one another there is no hydration repulsion to repel the approaching particles and the two membranes fall into an energy well where they adhere and form aggregates. The production of hydration is a large, multilamellar vesicle (LMV) analogous in structure to an onion, with each lipid bilayer separated by water layer. The spacing between lipid layers is dictated by composition with polyhydrating layers being closer together than highly charged layers which separated based on electrostatic repulsion. Once a stable, hydrated LMV suspension has been produced, the particles can be downsized by various techniques, including sonication or extrusion.

2.3.2.3 Sizing of lipid suspension

i Sonication

Disruption of LMV suspensions using sonic energy (sonication) typically produces small, unilamellar vesicles (SUV) with diameters in the range of 15-50nm. The most common instrumentation for preparation of sonicated particles are bath and probe tip sonicators. Probe tip sonicators deliver high energy input to the lipid suspension but suffer from overheating of the lipid suspension causing degradation. Sonication tips also tend to release titanium particles into the lipid suspension which must be removed by centrifugation prior to use. For theses reasons, bath sonicators are the most widely used instrumentation for preparation of SUV. Sonication of an LMV dispersion is accomplished by placing a test tube containing the suspension in a bath sonicator (or placing a tip of the sonicator in the test tube) and sonicating 5-10 minutes above the T_c of the lipids. The lipid suspension should begin to clarify to yield a slightly opalescent transparent solution. The haze is due to light scattering induced by residual large particles remaining in the suspension. These particles can be removed by centrifugation to yield a clear suspension of SUV. Due to the high degree of curvature of these membranes, SUV are inherently unstable and will spontaneously fuse to form larger vesicles if stored blow their transition temperature.

ii Extrusion

Lipid extrusion is a technique in which a lipid suspension is forced through a polycarbonate filter with a defined pore size to yield particles having a diameter near the pore size of the filter used. Prior to extrusion through the final pore, LMV suspensions are disrupted either by several freeze-thaw cycles or by prefiltering the suspension through a larger pore size (typically 0.2μm-1.0μm). This method helps prevent the membranes from fouling and improves the homogeneity of the size distribution of the final suspension. As with all procedures for downsizing LMV dispersions, the extrusion should be done at a temperature above the T_c of the lipid. Attempts to extrude below Tc will be unsuccessful as the membrane has a tendency to foul with rigid membranes which cannot pass through the pores. Extrusion through filters with 100nm pores typically yields large, unilamellar vesicles (LUV) with mean diameter of 120-140nm. Mean particle size also depends on lipid composition and is quite reproducible from batch to batch.

2.4 Fluorescence microscopy

The application of fluorescence microscopy to the study of monolayers of membrane lipids has been fruitful and relevant to the understanding of membrane processes.[45-48] The analysis of steady-state fluorescence emitted upon excitation of components in a Langmuir film can provide structural information as well as dynamics of possible chemical/structural changes. Fluorescence of a monolayer material or dye incorporated in a mixed monolayer can be excited by incident light either from the air or from the water, in total reflection or in the transmission mode. Since solubility of the fluorescent probe depends on the monolayer state, contrast is generated upon changing these states.

2.4.1 Experimental apparatus for florescence microscopy

A schematic diagram of the general features of an apparatus fluorescence microscopic study of monolayers is shown in Fig. 2.10.

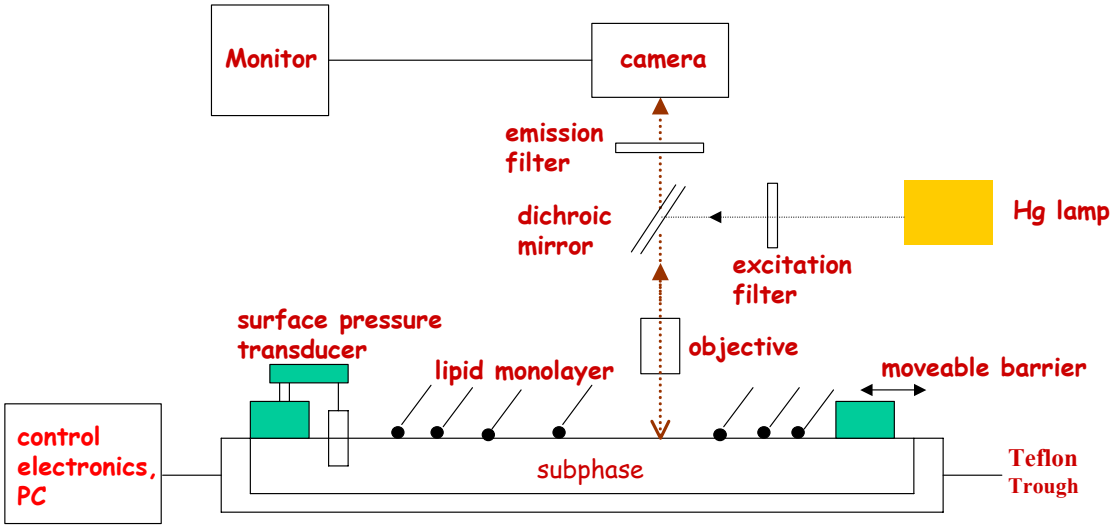

Figure 2.10: Schematic of an apparatus for fluorescence microscopic investigations of lipid monolayers, shown for an upright microscope configuration.

An upright microscope is used to simplify the trough design and the necessary machining. The surface textures of Langmuir films are often heterogeneous and it can be informative to be able to translate the trough in the x and y directions and observe different areas, at least within several square centimeters of area. If a trough is placed on an upright microscope, the microscope stage can be translated to examine different regions of the surface film.

The microscope should be acquired with a mercury lamp and lamp power supply and a selection of filter cube assemblies to allow for the use of the expected fluorescence labels Fig 2.11). One or more long-working-distance objectives of different magnifications (10×, 20×, and 50× would be typically available) allow for the variation in the field of view for instances in which the monolayer shows large structure as well as for cases in which the domains are smaller in size. It is important that the system be placed on a vibration-free and levelled surface. Vibrations will affect both the image quality and the resolution of the surface pressure readings, and a tilt of the surface will lead to problems with water

spillage out of the trough. The area around the trough should be covered to protect the monolayer from air currents and accumulation of airborne impurities.

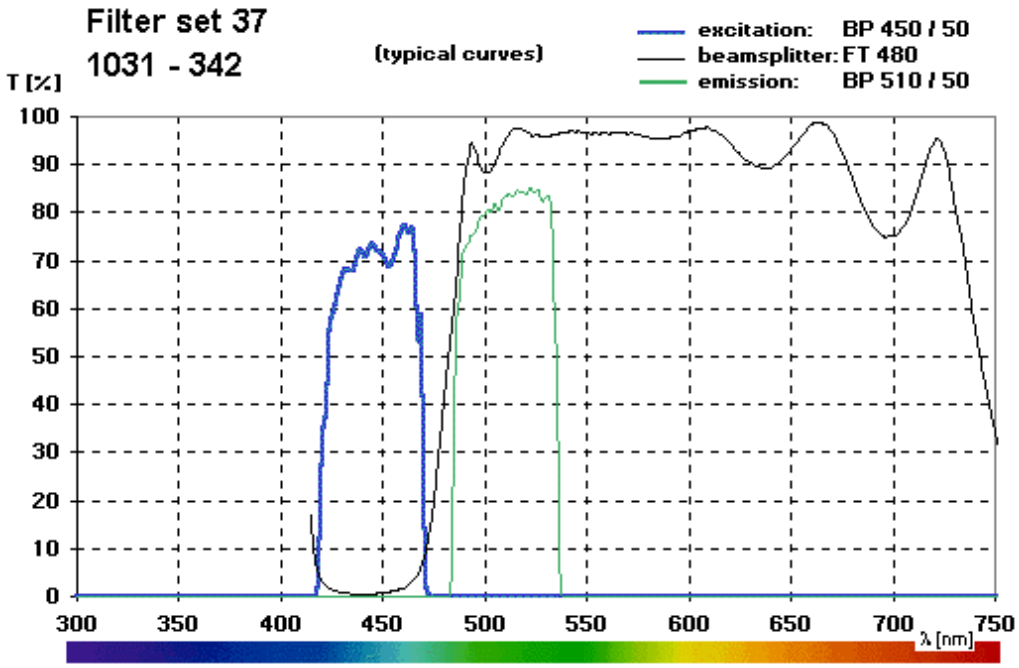

Figure 2.11: Typical curves of the filter set for the fluorophore (NBD)

Another important decision is the choice of camera for detection of the monolayer image. Our system employs a CCD (charge-coupled device) camera. The use of CCD cameras has become more popular and is preferable because the CCD is more rugged. The intensities of the pixels in the CCD depend on the number of bits in the gray scale. For imaging Langmuir films by fluorescence microscopy, a standard 8 bits is adequate. The light level for fluorescence from a monolayer doped with < 1% of a fluorescent tag is in the low to very low region and a CCD camera coupled to an image intensifier is needed.

2.4.2 Image acquisition and data analysis

It is generally the practice to record fluorescence images of the Langmuir film throughout the course of the experiment or at selected times. Later retrieval of selected images for

detailed analysis or labeling and preparation for presentation can be aided by an image analysis system. The most economical choice is a personal computer (PC)-based frame grabber board so that images can be captured and stored in files in a common picture format (jpg, gif, tif, etc.). Images can be enhanced and their contrast improved using various solftware filters applied to the image gray scale. Units accomplishing this in real time as the monolayer is viewed are also available. These units allow real-time contrast enhancement, brightness enhancement, and integration, a process in which the displayed image is a composite of a certain number of frames. Integration does not work well with Langmuir films in most cases, as the domains tend to drift slowly on the water surface, especially if the barrier is moving. If it is necessary to observe the same domains over a long period of time, a Teflon collar with a slit can be placed over the objective and through the interface to trap the same domains and prevent them from slowlydrifting away.

2.5 Surface plasmon resonance spectroscopy (SPR) & surface plasmon field-enhanced fluorescence spectroscopy (SPFS)

2.5.1 SPR

For more than a decade, biosensors based on surface plasmon resonance (SPR) have been commercially available, making real-time, tagless biomolecular interaction analysis accessible to those in biochemistry and related fields. In parallel with (and largely driven by) these commercial successes, there have been large increases in the number of academic persuits involving biosensing and bioassays with SPR.

For a more mathematically rigorous discussion of surface plasmon resonance, people are referred to work concerning the optical properties of thin metal films. Originally described by Ritchie in the 1950s[49] surface plasmons are coherent fluctuations in the electron density occurring at a “free-electron” metal dielectric interface. Examples of free-electron metals (those with a lone electron in the valence shell) are Ag, Au, Al, and Cu, with Au being the most commonly used in biosensing. As is typical for surface-

confined modes, the transverse component (perpendicular to the metal surface) of the dielectric field vector decays exponentially into the dielectric medium from a maximal value at the metal surface. With typical decay lengths being ~200nm (at mid-visible excitation wavelength), surface plasmons are exquisitely sensitive to changes in the properties of the interface. Specially, changes in the thickness and/or refractive index of a thin layer in contact with the metal film result in a change in the propagation of the surface plasmon mode. This sensitivity can be described by the magnitude of the electric field propagation in the plane of the metal film:

$$E_x(x,z,t) = E_x^0(x)\exp(i\omega t - ik_z z) \qquad (1)$$

where ω is the optical frequency, and the complex propagation constant along the z-axis is given by

$$Kz = K_z' + ik_z'' \qquad (2)$$

It is this value (often refered to as K_{sp}, the wavevector of the surface plasmon) that is dependent on the refractive index at the interface.

$$K_{sp} = \frac{\omega}{c}\sqrt{\frac{\varepsilon_m \varepsilon_s}{\varepsilon_m + \varepsilon_s}} \qquad (3)$$

In equation (3), ε_m and ε_s contain the real and imaginary parts of the metal and sample dielectric functions, respectively, and c is the speed of light in vacuum. Given this, it is apparent that radiation impinging upon the metal film with the same propagation wavevector can be used to excite this mode. The wavevector for the photon in the sample is

$$K_{light} = \frac{\omega}{c}\sqrt{\varepsilon_s} \qquad (4)$$

However, a simple calculation shows that for a plasmon-supporting metal (large, negative negative real part of ε_m), K_{sp} is always greater than K_{light}. Surface plasmons therefore cannot be excited by photos propagating in free space.

To overcome this problem, one must use illumination conditions that allow for modulation of the incident (momentum) wavevector magnitude. The most common method for accomplishing this was proposed originally by Kretschmann in 1971.[50] In this technique, the thin metal film is optically coupled to a prism made of a high-refractive-index material (e.g. glass). Illumination of the film through this prism under total internal reflection conditions allows for the excitation of the surface plasmon via an evanescent wave. Mathematically, the wavevector of the evanescent field is

$$K_{ev} = \frac{\omega}{c}\sqrt{\varepsilon_g}\sin\theta \qquad (5)$$

where ε_g is the real part of the glass dielectric function and θ is the incident angle of excitation. From this we can see that light of a specific frequency can excite a plasmon of that frequency if θ satisfies the equality $K_{ev}=K_{sp}$. Experimentally, this is observed to result in a sharp minimum in the plot of reflectance versus incident angle. Because is K_{sp} dependent on the refractive index above the metal film, θ is likewise sensitive to this value. Furthermore, since the resonance condition can now be experimentally observed, it can be correlated with the optical properties of the sample as indicated by Eq. (3); the position of the reflectance minimum is used to quantitatively determine the sample refractive index.

A number of practical experimental conditions, such as metal film thickness and incident wavelength, must be considered when designing an SPR experiment for optimal sensitivity. A 47-nm-thick gold film is the optimal substrate for sensing applications. In the optimal (47 nm) film, a fraction of the incident radiation is reflected from the glass/Au interface, while another fraction propagates through the film to the Au/sample interface and excites surface plasmons, which in turn radiates back into the metal film. The back-scattered radiation is then out of phase with the incident radiation, thereby

resulting in a destructive interference process and, hence, a decrease in reflectance. For a thicker Au film, much of the wave propagating into the metal has decayed before reaching the Au/sample surface, resulting in a decrease in the magnitude of the back-reflected plasmon radiation. Conversely, the thin film displays a back-reflected field that is much greater in magnitude and therefore increases the reflectance of the ATR device near the plamon angle.

Because the optical constants for thin metal films are varying functions of the incident wavelength, the photon energy can be used to change the shape and position of the SPR curve. SPR curves become sharper at longer wavelength, reflecting a decrease in the amount of damping experienced by the surface mode. Quantitatively, this damping is related to the decay length of plasmons at the Au/sample interface:

$$I(x) = \exp(-2k_x'' x) \qquad (6)$$

in which the imaginary part of the plasmon wavevector is

$$K_x'' = \frac{\omega}{c}\left(\frac{\varepsilon_m' \varepsilon_s}{\varepsilon_m' + \varepsilon_s}\right)^{3/2} \frac{\varepsilon_m''}{2(\varepsilon_m')^2} \qquad (7)$$

Equation (7) assumes that the real (‘) and imaginary (“) parts of the metal dielectric function are frequency dependent. From these equations, it follows that a decrease in the optical frequency will result in a reduction of the plasmon damping and, hence, a longer propagation of the plasmon mode [i.e. Eq. (6) decays more slowly]. This effect has been exploited by Corn’s group, which used IR-excited plasmons to obtain higher SPR sensitivity.[51;52]

Taken alone, the above discussion of the surface plasmon effect suggests numerous advantages of the technique with respect to biomolecular interaction analysis. This technique is label-free; no enzyme, fluorophore, or radioisotope labeling for detection or amplification of a binding event. SPR can also be performed in real time, thereby allowing for kinetic as well as thermodynamic parameters to be determined. Finally, the

technique is noninvasive due to a “back-side” illumination geometry that is employed; the source beam does not have to travel through the sample solution during operation. This decreases any interference that could arise from turbid or strongly absorbing solutions. Despite these advantages, it is still desirable in some applications to utilize “tagging” to either amplify or differentiate observation in the SPR experiment.

2.5.2 SPFS

One of the major advantages of surface plasmon spectroscopy is the fact that it allows for label-free detection of binding events. It is the mere presence of the bound analyte at the interface, or more precisely, it is the optical contrast that a molecular unit bound to the interface generates with respect to the surrounding medium within the evanescent field of the surface plasmon mode propagating along the metal/dielectric interface, that is detected. For not too small proteins binding from an aqueous solution to the interface this typically gives a sufficient signal. For example, a monomolecular layer of streptavidin, a tetrameric protein of a molecular mass of 60 000 g mol^{-1}, at a maximum lateral packing density of ca. 60% generates an angular shift of the surface plasmon resonance curve corresponding to a dielectric layer of d = 4.0 nm (assuming a refractive index of n=1.45 @=633 nm).[53;54]With a lower limit for a reliable signal detection corresponding to an effective layer of about 0.1–0.2 nm this generates a sufficient signal-to-noise level allowing for a detailed kinetic analysis and determination of binding affinities.[55] However, problems arise if only a very dilute lateral packing of the proteins can be achieved or if very small analytes of low molecular mass are to be detected. In these cases, only very thin effective layers are generated, eventually resulting in angular shifts, too low to be detected.[56] This then generates severe sensitivity limitations and, as a consequence, the concept of using (fluorescence) label techniques in connection with surface plasmon spectroscopy as a means to enhance the signal of the interfacial binding events are to be considered.

As shown in Figure 2.11, the critical angle, θ_c, whose value is determined only by the refractive indices of the prism and the dielectric medium, indicates the onset of the attenuated total reflection (ATR) phenomenon. The resonance minimum angle, θ_0, on the other hand, suggests the condition at which the incident photons wavevector matches the

surface plasmon wavevector at the metal/dielectric interface. At this resonance angle, almost all the energy of the incident radiation is converted into surface plasmon excitation and the intensity of the electromagnetic field is greatly enhanced, expressed as the lowest reflectivity.

2.5.2.1 Field Enhancement

The enhancement factor is given by the ratio of the magnetic field intensity on the metal surface at the dielectric side divided by the incoming magnetic field intensity for p-polarized light[57]. The calculated intensities are normalized to the incident intensity and are plotted together with the corresponding reflectivity in Figure 2.12 depending on the angle of incidence for three-layer systems prism/Ag/water and prism/Au/water. Peak intensities scaled against the incoming intensity can reach an enhancement factor of 58 for the former and 16 for the latter. Generally, the smaller the imaginary dielectric constant ε'', i.e. the lower the absorption and hence dissipation of the optical field intensity, the higher the enhancement factor.

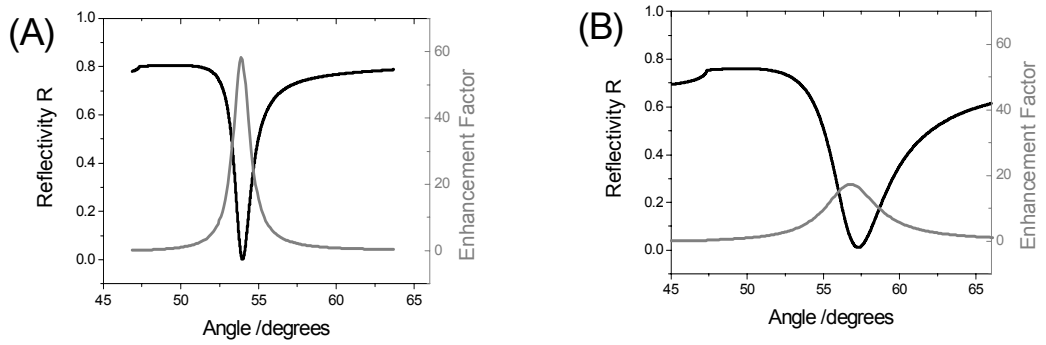

Figure 2.12: Simulation curves of the reflectivity and the relative field intensity as a function of the He-Ne laser light incident angle on three-phase systems prism/Ag/water (A) and prism/Au/water (B).

This field enhancement phenomenon is well known and widely applied in other spectroscopy technologies, *e.g.* in surface-enhanced Raman scattering (SERS).[58]

The peak intensity is found at a slightly lower angle of incidence than the minimum in the reflectivity. The reason again is related to the resonance character of the PSP excitation:

as one sweeps through the resonance the phase difference of the surface mode relative to the driving photon field changes as for any other resonator: for a fictive loss-free metal the phase would change from 0° below the resonance to 180° above it, with a sharp step at the resonance. Any damping (loss) in the system broadens and smears this phase change. Since we are observing in reflection a coherent superposition of a partial wave directly reflected from the metal/prism interface with (a fraction of) the surface mode re-radiated via the prism, the minimum in the total reflection then is the destructive interference of the two partial waves differing in phase by 180° which is reached just above the angle of maximum surface plasmon intensity. Again, the higher the loss of metal ($\varepsilon''_{Au} > \varepsilon''_{Ag}$) the more smeared-out is the phase change of the PSP resonance and hence the larger the difference in the angular position of the surface mode peak intensity and the reflectivity minimum (cf. Fig. 2.12 (a) for Ag and Fig. 2.12 (b) for Au).

2.5.2.2 Fluorescence at the Metal/Dielectric Interface

In the case of total internal reflection, only a moderate field enhancement by a factor of 4 is obtained at the critical angle due to constructive interference between the incoming and reflected electromagnetic field. This enhancement together with the evanescent character of this surface light triggered its successful use in total internal reflection fluorescence (TIRF).[59] As mentioned above, the electromagnetic field enhancement of SPR is more substantial than that of TIR, as a consequence, much stronger fluorescence emission should be obtained if the fluorophores are excited by surface plasmon evanescent wave.

The evanescent field decays exponentially into the dielectric layer adjacent to the metal film with the characteristic parameter, the penetration depth, at which the surface field intensity drops down to *1/e* of the interface value, typically several hundred nanometers into the dielectric medium. Therefore, surface plasmon sensitive fluorescence measurements will only be possible if the dyes are in close proximity to the metal film.

However, the electronic coupling of the molecular orbits localized in the chromophore with the extended band structure of the metallic electrons in the solid substrate generates new decay channels for the excitation energy of the dye, leading to a strong modification of radiative lifetimes and fluorescence intensities as the fluorophores are coming closer

and closer to the metal surface.[60] Figure 2.13 summarizes some of the observed distance-dependent energy transfer mechanisms.

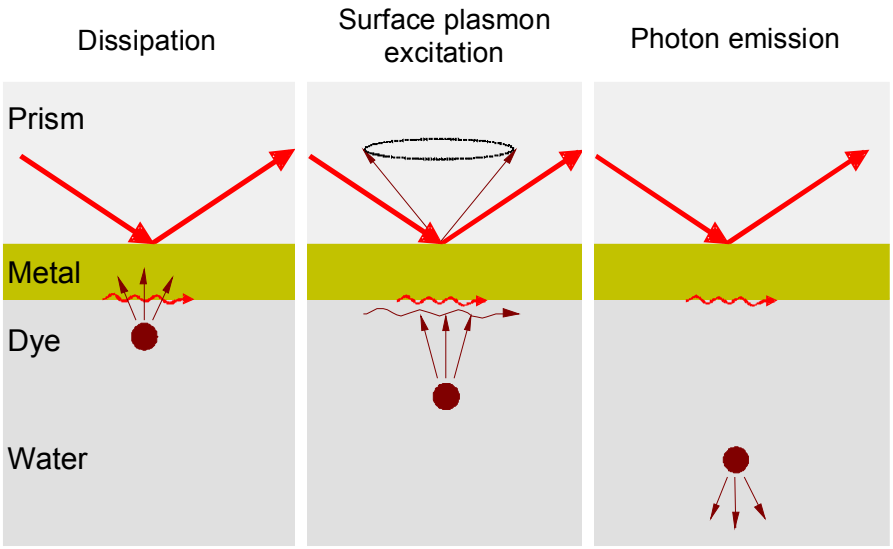

Figure 2.13: Schematic of the different electronic coupling regimes for a fluorophore in water at different distances to a metal film surface.

If a dye is positioned at a distance within 10 nm to the metal surface, a substantial 'radiation-less' de-excitation with a corresponding reduction of the radiative lifetime and the fluorescence intensity is found. The fluorescence is 'quenched', dissipating the excitation energy in the metal as heat. This quenching phenomenon can be modeled by the Förster resonance energy transfer, showing a R^{-6} dependence of the transfer efficiency to the separation distance. However, integrating over all possible sites of an entire surface of acceptors will yield a R^{-4} dependence (cf. dashed curve in Fig. 2.14).

At an intermediate-distance regime (a few nm up to ~20 nm), the optically excited chromophores can effectively couple back to the plasmonic states of the metal substrate. Since some of the excitation energy is dissipated in the dye molecule via vibronic excitation, the corresponding back-coupled surface plasmon mode is red-shifted relative to the excitation and hence re-radiates in a cone via the prism at a slightly smaller angle.

At sufficient separation distances (>20 nm), free emission of the fluorophores can be achieved. The fluorescence intensity only depends on the intensity of the evanescent field except for some (negligible) interference effects between the radiation field directly emitted and the one reflected from the metallic surface.

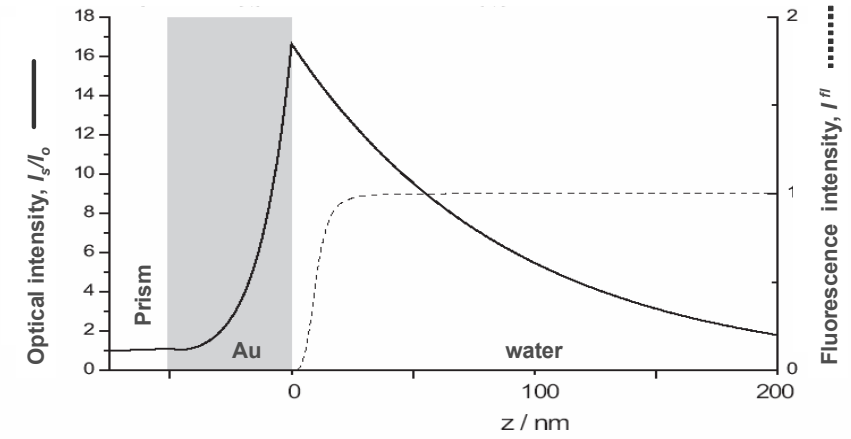

Figure 2.14: Comparative presentation of the distance dependence of the optical field enhancement of a surface plasmon evanescent wave mode excited at a prism/Au/water interface (solid curve), and the Förster energy transfer mechanism, expressed as the relative fluorescence intensity (dashed curve) placed at a certain distance above the metal/water interface.

Figure 2.14 summaries these findings in their consequence for the design of an interfacial architecture optimized for maximum sensitivity enhancement by combining the spatial characteristics of surface plasmon fields and the quantum efficiency for radiative dipoles near a metal surface. In contrast to the quenching processes that only occur for chromophores within 10-15 nm of the surface, the exponential decay of the surface plasmon field ranges on a much longer distance of several hundred nanometers. This means that fluorescent species placed at least 1 Förster distance (typically 5-7 nm) away from the surface experience a loss in the fluorescence intensity of a factor of 2 at most. They are still in the largely enhanced optical field of a resonantly excited surface plasmon mode used for chromophore excitation. Therefore, by carefully designing the supramolecular interfacial layers proving the binding sites for the recognition process of fluorescently labeled analyte, one can gain enormously in detection sensitivity by

exploiting the enhanced surface plasmon optical field without being compromised by the quenching mechanism.

2.5.2.3 Home-Made SPFS Setup

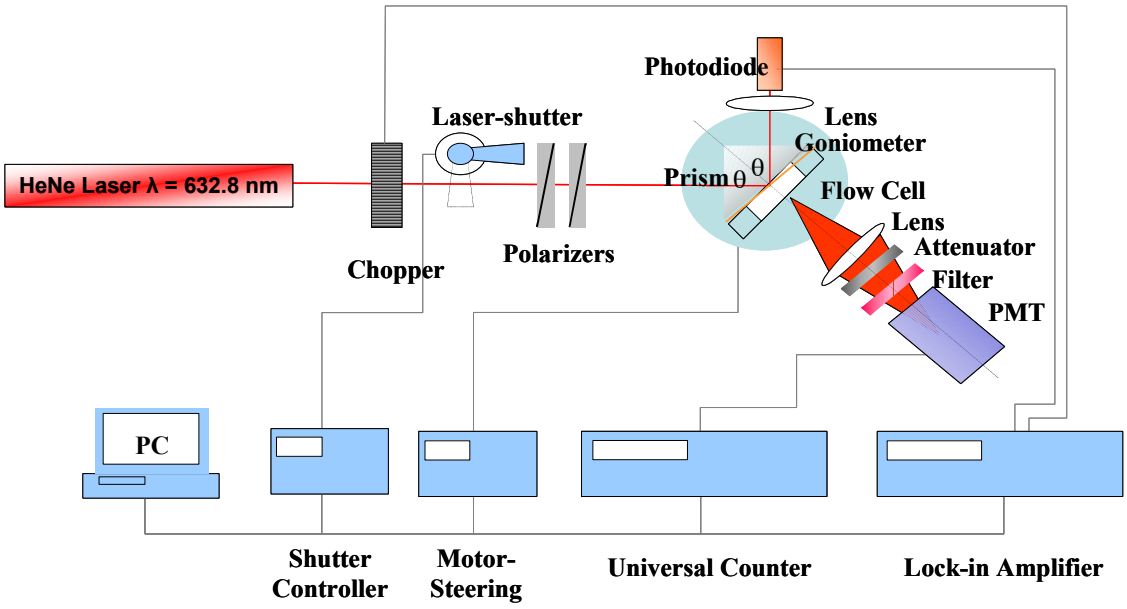

Figure 2.15: Schematic of a surface plasmon field-enhanced fluorescence spectroscopy setup with two separate excitation laser sources.

The experimental set-up is based on a 'conventional' surface plasmon spectrometer and is schematically depicted in Fig. 2.15. It allows for the simultaneous recording of reflectivity, as well as, fluorescence intensity data, either as a function of the angle of incidence, θ, or as a function of time in the kinetic mode. The wavelength of the laser light source has to be selected so as to allow for an efficient excitation of the fluorescence dye. The continuous laser beam passes through a chopper (Perkin Elmer, frequency = 1331 Hz) connected to a lock-in amplifier (Perkin Elmer). A PC-controlled shutter is also mounted in the optical path in order to minimize the photobleaching of the fluorophores. Two polarizers (Glan-Thompson) are used next, adjusting the plane of polarization and the intensity of the laser. Finally, the laser beam enters a right angle coupling prism (Schott, LASFN9, n = 1.85 @ λ = 632.8 nm) and is reflected off the metal/dielectric interface, focused by a convex lens (Owis, f = 50 mm) onto a photodiode detector which

is connected to the same lock-in amplifier as the chopper. The prism/sample unit and the photodiode detecting unit are mounted on two-axial goniometers (Huber) with the precision of 0.001° rotational movements, enabling an independent tuning of respective angular positions. Normally, the former unit rotates at θ, while the latter unit rotates at 2θ, relative to the fixed excitation laser beam, in the surface plasmon resonance scan measurements.

The fluorescence detection module is mounted along the normal direction of the metal-dielectric interface, rotating together with the prism/sample unit. In a general surface plasmon field-enhanced fluorescence mode, the fluorescence emission emitted normal to the meta/dielectric base plane is collected by a focusing lens (Owis, f = 50 mm) and passes through an interference filter (LOT, λ = 671 nm, transmittance = 60%, for Alexa Fluor 647 (from Molecular Probes Inc.) excitation, λ = 620 nm or 560 nm, to block the scattered and out-coupled excitation light, before it's finally gathered by a photomutiplier tube (PMT, Hamamatsu), which is connected to a universal counter (Agilent) via a home-made electronic interface to convert analog to digital data, expressed in counts per second (cps). In the case where the fluorescence light intensity is beyond the PMT's linear input-versus-output range (< 2.5×10^6 cps), an appropriate attenuator (neutral filter, LOT) is added to weaken the intensity according to its attenuation factor.

Two modes of operation are possible: an angular scan mode in a θ–2θ reflection geometry, or a kinetics mode in order to resolve time-dependent processes at a fixed angle of observation. For both modes, the reflectivity channel as well as the fluorescence intensity channel can be recorded simultaneously. Data acquisition and electronics control are accomplished by custom programs.

2.6 Interfacial kinetics based on Langmuir adsorption model

Biomolecules carry out their roles *in vivo* by interaction with one or more binding partners. Hence, a quantitative analysis of these recognition events *in vitro* provides an illuminating insight into biological function and mechanism[61]. The classical Langmuirian model of interaction in free solution is used as a foundation for the development of

analytical methodologies for the interaction analysis. The simplest physically plausible isotherm is based on three assumptions[62]:

1) Adsorption cannot proceed beyond monolayer coverage;
2) All sites are equivalent and the surface is uniform;
3) The ability of a molecule to adsorb at a given site is independent of the occupation of neighboring sites.

For the reversible interaction observed between an immobilized ligand *B* and a soluble ligate *A*, we have:

$$A + B \underset{k_{off}}{\overset{k_{on}}{\Leftrightarrow}} AB\,.$$

The rate of complex *AB* formation is described by the association rate constant k_{on}, which has units of $M^{-1}s^{-1}$. The rate of complex dissociation is described by k_{off}, which has units of s^{-1}. The rate of association of *A* with *B* is equal to $k_{on}[A][B]$. The rate of dissociation of *AB* is equal to $k_{off}[AB]$. On mixing *A* and *B*, association and dissociation of *AB* will occur. Equilibrium will eventually be reached if the rates of association and dissociation of *AB* are equal. At equilibrium, [*AB*], [*A*] and [*B*] are constant. Hence, at equilibrium:

$$k_{on}[A][B] = k_{off}[AB]\,.$$

This may be rearranged as follows:

$$\frac{[A][B]}{[AB]} = \frac{k_{off}}{k_{on}} = K_D$$

where K_D is termed the dissociation equilibrium constant, and has units of M. The lower the value of K_D, the greater the affinity. The reciprocal term K_A, the association equilibrium constant, having units of M^{-1}, is sometimes used in the literature as the measure of affinity, where:

$$K_A = \frac{1}{K_D}\,.$$

3 Construction of peptide-tethered lipid membranes

3.1 Introduction/background

The membrane surrounding the living cell serves functions such as control of solute permeability and reognition events. All biological membranes have the same general structure. In the currently accepted concept, a membrane is a bimolecular lipid layer. The remarkable ability of lipids to self-organize into supramolecular structures such as monolayers, micelles, planar bilayers, and vesicles is not only essential for cell-based life, but also is the absolute prerequisite for the built-up of the model membranes. Self-organization arises from inherent properties of lipid molecules and intermolecular interactions between lipids and water. These interactions are nominally referred to as hydrophobic, hydrophilic, dipolar, hydrogen bonding, and electrostatic. It is the self-organization of lipids that brought the development of artificial cells and biomembrane mimics. These model membranes play a key role in the investigations on the structures and functions of biomembranes.

Much of the knowledge concerning the interactions between amyloid ß-protein (Aß) and lipids has been gained from the studies of the model membranes mainly including monolayer,[63] vesicles,[64] black lipid membranes (BLMs),[65] and supported monolayers. The simplest model systems frequently used in the studies on Aß-lipid interactions are monolayers formed at the air-water interface. The protein-membrane interactions can be measured by the change in the surface pressures of the monolayer. Recently, it has been reported that Aß insertion into membranes can be detected using the monolayer technique.[66] However, this conclusion can be challenged by the fact that the interaction of

peptides and membranes is critically dependent on the inner layer of the membranes. Binding affinities of the peptides to lipid monolayers and bilayers measured by SPR indicated that the binding between melittin with lipid monolayer is markedly lower as compared with their binding to bilayers.[67]

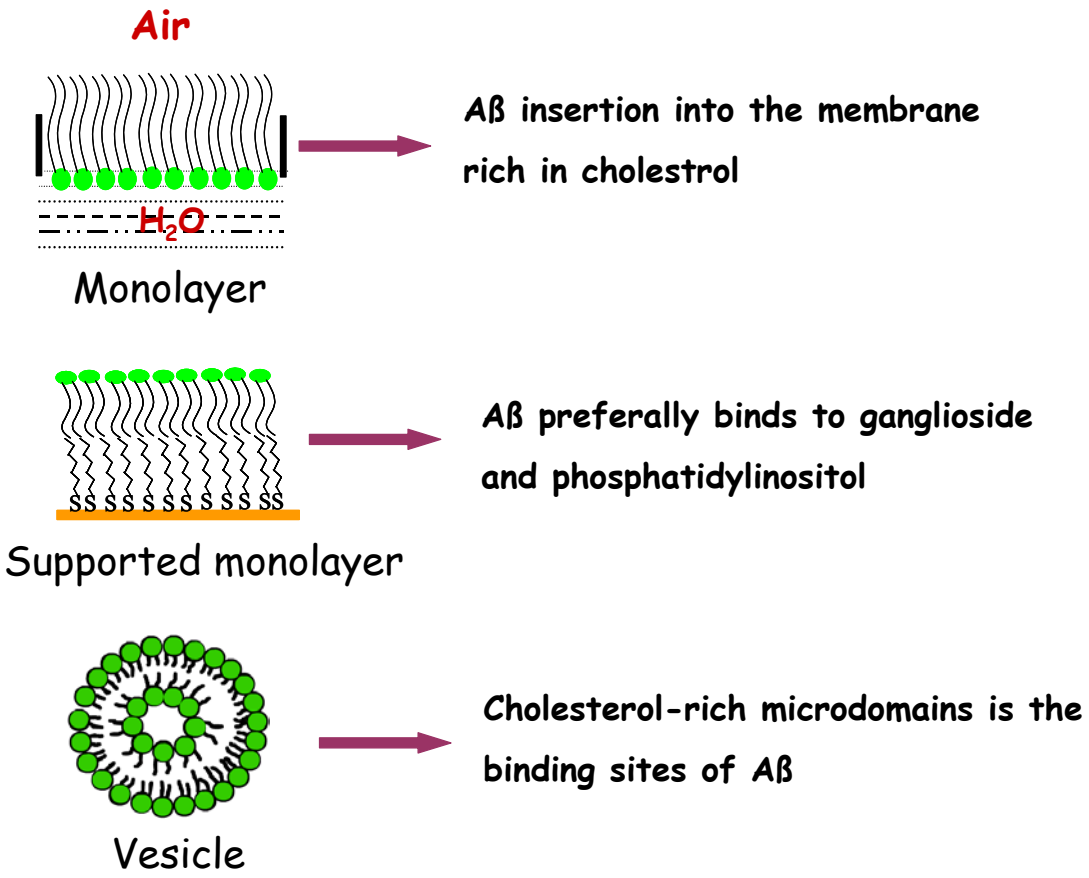

Figure 3.1: The model systems for the investigation of Aß-lipid interactions. (A) Langmuir monolayers; (B) support monolayer; (C) vesicle (liposome)

A more complex model system than monolayers is lipid vesicles (liposomes). Lipid vesicles can provide a bilayer model for the investigations of Aß-lipid interactions. An assumption that Aß preferentially binds to gangliosides in raft-like membranes composed of cholesterol and sphingomyelin has been obtained using this model system of lipid vesicles.[68] However, the role of cholesterol and gangliosides in the formation of Aß

plaques also need to be further explored, because the method of lipid-vesicle preparation used in that research yielded an inhomogeneous final sample containing more than 40mol% cholesterol.[69;70] Therefore, the real effects of cholesterol on the binding of Aß to gangliosides in biomembranes cannot be deduced from the observations in the model membrane of the lipid vesicles. Certainly, the supported membranes formed by vesicles containing more than 40mole% cholesterol, which are prepared by the conventional method, are also not ideal membrane mimics for the investigtion of the interaction between Aß and membranes. Obviously, the establishment of the model membranes much more close to a cell membrane is very significant for getting insight into the mechanism on membrane mediated amyloid plaque formation.

Solid-supported lipid bilayers have been popular biomimetic membrane systems since they allow examining peptide interactions at the lipid/water interface while at the same time limiting lipid motion through surface immobilization. Constricting lipid mobility in supported lipid layers might make such systems a more realistic model compared to Langmuir films since this better resembles lipid dynamics within real membranes.[71] In addition, the stable arrangement of such an ultrathin fragile lipid lamella with the robustness of a solid support in a planar configuration allows for the application of a number of powerful surface- or interface-sensitive experimental techniques (such as surface plasmon resonance) that should give very detailed information of protein-membrane interactions in these systems.[72]

In order to address the above problems, we developed peptide-tethered lipid membranes based on the concept of solid-supported membranes by the Langmuir-Blodgett (LB) and/or Langmuir-Schaefer (LS) methods. Tethered lipid bilayer membranes conceptually resemble BLMs as a planar biomimetic model system. The artificial membrane in this arrangement is created by covalently binding a lipid monolayer onto gold substrates, followed by deposition of another lipid film resulting in the formation of a tethered bilayer. The advantages of the LB and LS techniques originate from the fact that the transfer of lipid layers is carried out under controlled surface pressure, and well-defined layers can be deposited. With the appropriate choice of composition and deposition conditions, lateral organization and membrane asymmetry can be specified. In contrast, vesicle fusion is restricted to the deposition of fluid-phase lipids and cannot be used to

create asymmetric bilayers. In our case, each layer was transferred to the substrate always at a surface pressure of π = 30mN/m, which is the pressure of a biological membrane. In addition, the LB and LS methods allow for the construction of the architecture containing random composition of lipids at will. For our model membranes, DMPE always constitutes the proximal layer resembling the lipid on the inner side of a cell membrane. However, the lipid components of the distal layers are changeable. A peptide sequence used as a spacer was covalently linked on one side to the gold surface, and on the other end to a DMPE molecule as a part of the proximal monolayer of the tethered membrane. This tethering leads to a stable and robust coupling of the bilayer to the sensor surface and at the same time decouples the membranes sufficiently from the substrate to allow for the lipid matrix to exist in a fluid state as it is required for a number of membrane proteins (receptors, channels, carriers, etc) for their proper functions.

3.2 Materials

A 19-mer peptide (P19) derived from the α-laminin subunit was obtained from American Peptide Company, Inc. N-ethyl-N'-(dimethylaminopropyl) carbodiimide (EDC) were purchased from Sigma-Aldrich. N-hydroxysuccinimide (NHS) was obtained from Perbio Science Deutschland GmbH. EDC and NHS were each dissolved in 10ml Milli-Q water at the concentration of 75mg/ml and 11.5mg/ml, respectively, and stored in 500µl aliquots at –20°C until use.

1-Palmitoyl-2oleoyl-sn-glycerol-3-phosphocholine (POPC) and 1,2-dimyristoyl-*sn*-glycero-3-phosphoethanolamine (DMPE) were purchased from Avanti Polar Lipids, Inc.

N-octyl-ß-D-glucopyranoside was purchased from Merck Biosciences GmbH.

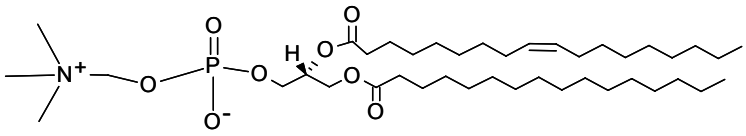

POPC

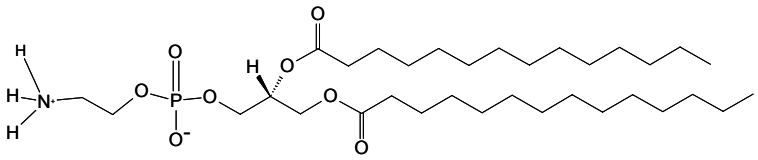

DMPE

HS- Cys-Ser-Arg-Ala-Arg-Lys-Gln-Ala-Ala-Ser-Ile-Lys-Val-Ala-Val-Ser-Ala-Asp-Arg-C(=O)-OH

P19

Figure 3.2: The structures of lipids and the peptide used in the construction of the model membranes.

3.3 The construction of peptide-tethered lipid bilayers (t-LBs)

LaSFN9 glass slides, which were used to prepare planar gold substrates, were carefully cleaned and coated with about 2nm chromium and 50nm gold on top by evaporation under vacuum in a commercial instrument (Edwards). For the peptide (P19) modification, a fresh planar gold surface was incubated with the peptide at a concentration of 40µg/ml in 0.02% ammonia solution for at least 24 hours. A stable monomolecular peptide layer was formed by the strong gold-sulfur interaction of the N-terminal cysteine moiety. The excess of unbound peptide was removed by extensive rinsing with Milli-Q water and the resulting optical thickness was monitored by SPS. The carboxyl groups of the peptide (P19) layer were activated with EDC/NHS for the subsequent reaction with amines from the polar head of DMPE. EDC and NHS were mixed in equal amounts in a volume of 1ml (50mM NHS, 200mM EDC) just before the immediate use and applied to the

peptide-modified gold surface for less then 10 minutes. A schematic of the reaction chemistry is present in Fig. 3.3.

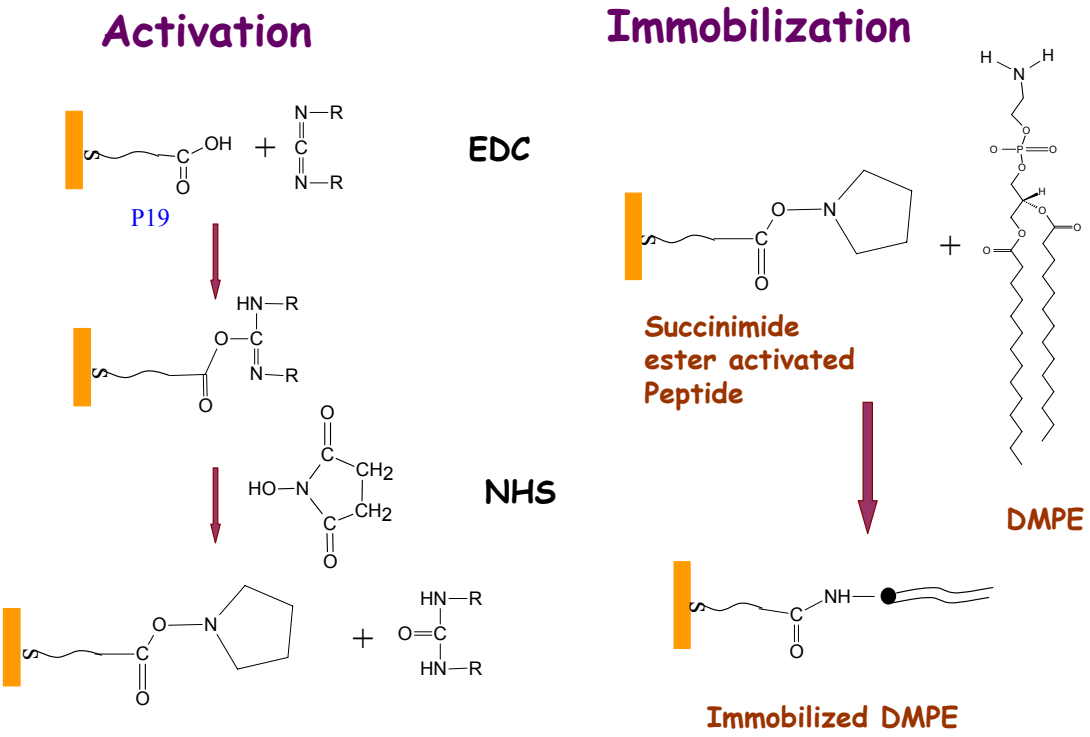

Figure 3.3: Schematic of the immobilization of DMPE on the gold substrate. (A) the carboxyl group at the peptide was activated by EDC/NHS; (B) Succinimide ester reacted with primary amide at the polar head of DMPE to form the covalent compound.

For the Langmuir-Blodgett (LB) transfer, pure DMPE monolayers were spread at room temperature from a chloroform solution (0.5mg/ml) at the air/water interface in a Teflon trough with a dipping well. Following Wilhelmy's method the barriers are made to approach and surface pressure can be easily measured, using a roughened platinum plate, with a precision of 1mN/m. A symmetric, non-linear compression was achieved by making the two barriers approach at a constant rate of 35mm/min. DMPE monolayers were transferred from the air/water interface of the Langmuir trough to the activated peptide-covered surface at a vertical withdrawal speed of 2mm/min at a constant surface

pressure of π = 30 mN/m which was maintained using a computer feedback loop. Transfer ratios were approximately 1.

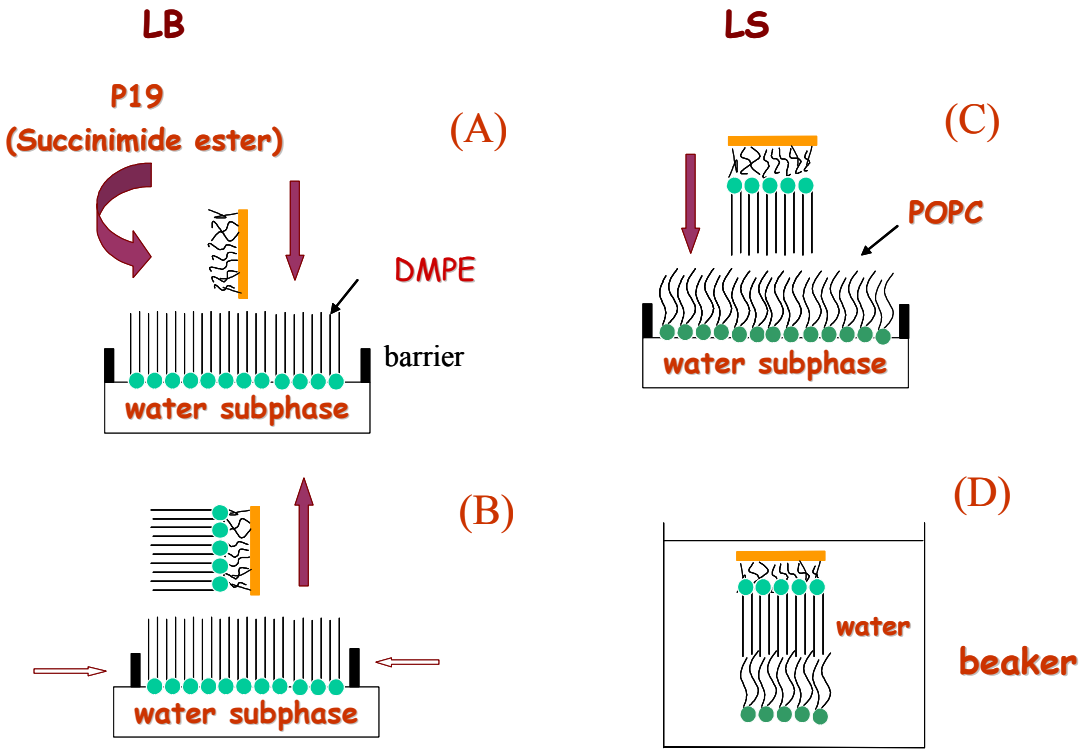

Figure 3.4: Schematic of the procedure for the establishment of the peptide-tethered lipid bilayers. (A)- (B) The formation of the proximal layer on the peptide by the Langmuir-Blodgett (LB) technique; (C)-(D) The formation of the distal layer on the proximal layer by the Langmuir-Schaefer (LS) technique. The model membranes after formation should be kept in water more than half hour.

The distal lipid monolayer was obtained by Langmuir-Schaefer transfer. The substrate with the bilayer is then collected in a dish, avoiding any subsequent exposure to air. With both methods, fully hydrated high quality bilayers were obtained. The proximal lipid monolayer in all cases was pure DMPE. Fig. 3.4 shows that The Langmuir-Schaefer transfer allows for any change in the lipid composition of the distal lipid monolayers. In this study, six artificial model systems with different distal lipid monolayers were built up.

3.4 Results and Discussions

The establishment of the model system was motivated by the fact that plasma membranes of cells are asymmetric,[73;74] that is, phosphatidylcholine and sphingomyelin have been found on the external leaflet of the plasma membrane whereas the aminophospholipids phosphatidylserine and phosphatidylethanolamine are predominantly on the inner side.[75] Hence, DMPE always resides on the proximal layers in our model systems. The lipids mainly comprising cellular membranes were chosen as the distal layers of the model systems that interact with Aß. In this study, a gold substrate was used as a solid support for lipid lamellas characterized by SPR and SPFS measurements. A hydrophilic peptide was employed as spacer molecules to tether the proximal lipid layer to the gold surface thus providing good stability and preserving the native state of the bilayer on the support.
SPR was used to demonstrate the formation of peptide-tethered lipid bilayers. Fig. 3.5 shows the quantitative evaluation of the surface modification via the stepwise attachment of peptide and lipid bilayers onto the gold substrate. A full angular scan was recorded for every single layer after its surface attachment. All respective angular shifts were Fresnel-analyzed. From Fresnel's equations, one can calculate the optical thickness of the coating (assuming for the peptide a refractive index of n=1.41, and for the lipids a refractive index of n=1.5).[76;77] The idea with respect to the selection of the 19mer peptide as a spacer between the gold surface and the lipid bilayers originated from the following consideration: 1) the peptide, which contains 12 polar amino acids, creates a soft, hydrated cushion that act as both a lubricating surface and a spacer. 2) the presence of a cysteine residue at the amino-terminus of the peptide allows for its covalent binding to the gold surface via a strong Au-thiolate bond, forming a rigid molecular layer with the orientation of the C-terminus of the peptide away from the gold surface. The carboxyl groups then allow for the covalent coupling to the primary amines at the polar head of DMPE. The optical thickness of the peptide layers derived from SPR measurements was about 2.2nm, close to 2.8nm of the theoretical length of a 19mer peptide molecule in the alpha helical conformation.

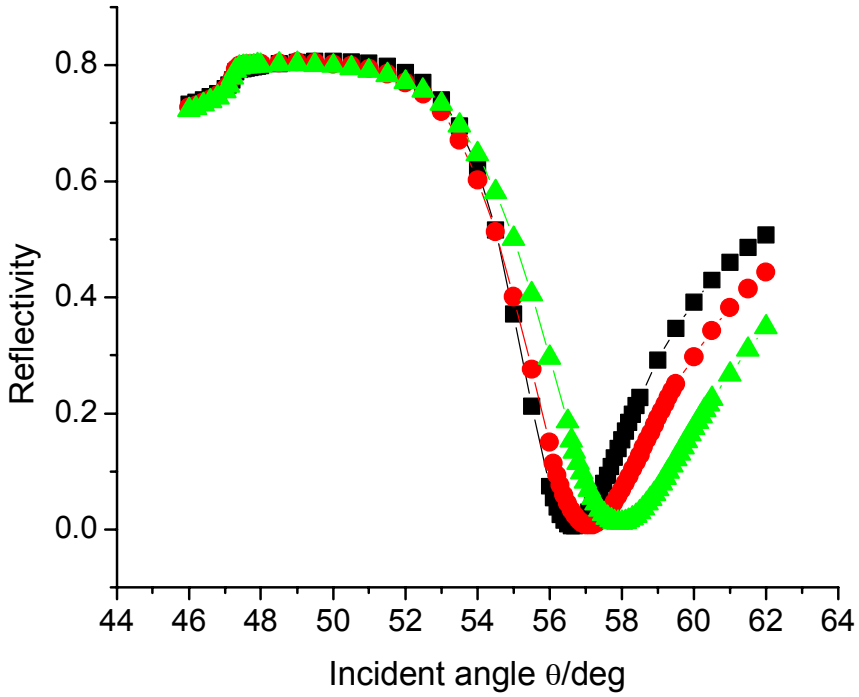

Figure 3.5: Assembly of a peptide-tethered lipid membrane on the gold surface. Angular scans of the reflected intensities for different interfacial architectures: the reference reflectivity curve (■) was measured for the Au surface in contact with water. The peptide monolayer resulted in an angular shift of the reflectivity curve (●); the lipid bilayer composed of DMPE and POPC were obtained by LB and LS transfer as described in the methods resulting in an additional angle shift (▲).

This indicated the formation of an ordered monomolecular layer of the peptide on the gold surface. The complete coverage of the gold surface and the resulting hydrophilic characters were further demonstrated by contact angle measurements (about $\theta = 35°$), which was sufficiently hydrophilic to allow for LB transfer.

The formation of bilayers deposited on the peptide was also checked by SPR. For the bilayers composed of POPC and DMPE, the thickness of 4.2nm thus obtained is quite reasonable compared to a DPPC bilayer thickness of 4.6nm obtained by X-ray diffraction. It is well-known that the membrane thickness decreases as the degree of unsaturated lipids increases. Thus, well-defined lipid bilayers can be obtained in the way described in the method section.

(A)

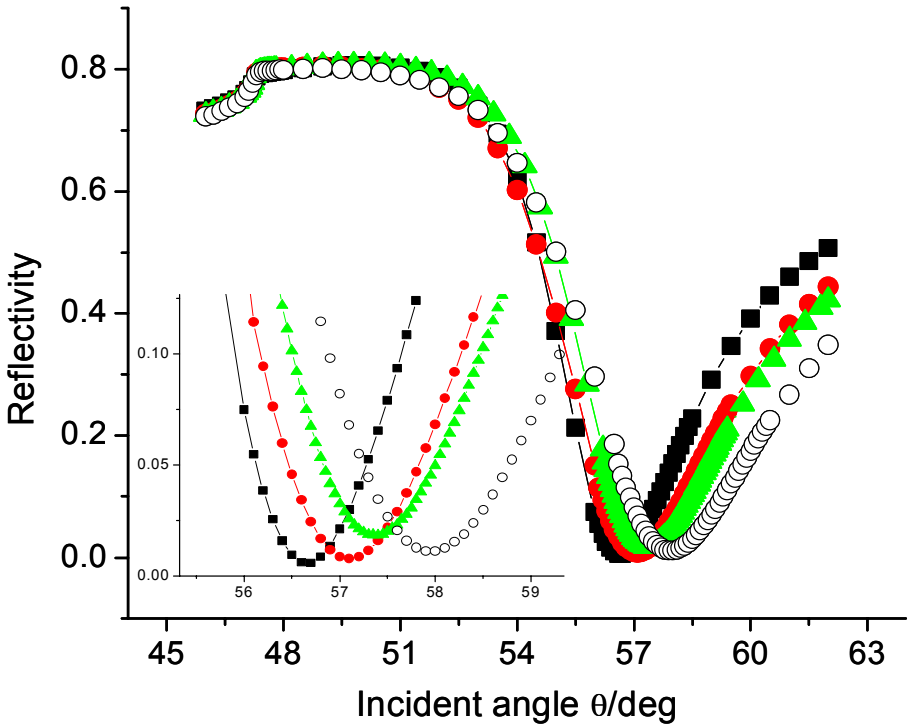
Reflectivity
0.0
0.2
0.4
0.6
0.8
45
48
51
54
57
60
63
Incident angle θ/deg
0.00
0.05
0.10
56
57
58
59

(B)

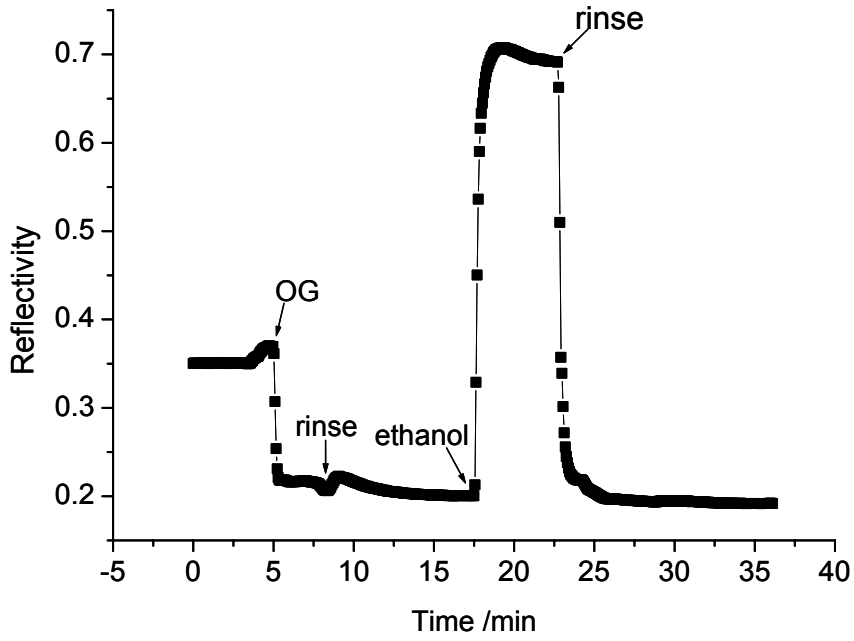
Reflectivity
0.2
0.3
0.4
0.5
0.6
0.7
-5
0
5
10
15
20
25
30
35
40
Time /min
OG
rinse
ethanol
rinse

Figure 3.6: Covalent binding of lipid molecules onto the surface-bound peptides. (A) Angular dependence of the reflected intensities for interfacial architectures after treatment with detergent and ethanol: the reference reflectivity curve (■) was measured for the Au surface in contact with water. The peptide monolayer resulted in an angular shift as the reflectivity curve (●); The layer of remaining lipid molecules (covalent binding to the surface) was obtained after treatment with detergent and ethanol resulting in a shift of the angular scan shifts to smaller angles (▲). The blow-up of the reflectivity curves is shown in the inset. The scan curve of the membrane before the treatment with the detergent and ethanol is also shown. (○). (B) The kinetic curve of the process for treatment of the peptide-tethered bilayers with the detergent and ethanol.

The model systems applied in the present work were in all cases constructed by the LB and the LS techniques at high surface pressures (30mN/m) that closely mimic the situation of a biomembrane.[78] The tethered bilayers were stable enough under continuous flow stream at a flow rate of 1ml/min for at least 24 hours.

The surface attached to the peptides was also checked (Fig. 3.6). Rinsing the tethered bilayer in the SPR flow cell with detergent (1-O-Octyl- β -D-glucopyranoside) and subsequently by ethanol removed all but the lipid molecules covalently bound to the surface.

The average thickness of the layer remaining after rinsing with the detergent and ethanol accounted for about 20%~30% of the theoretical surface coverage of a lipid monolayer. Contact angle measurements on the remaining layer showed a great increase in hydrophobicity of the surface from $\theta = 35°$ for the pure peptide to $\theta = 62°$ originating from contribution of the aliphatic chains of DMPE. Therefore, successful coupling of DMPE to the peptide surface was concluded. Taken together, it could be documented that a model system with some relevant features of a cell membrane was successfully constructed.

3.5 Conclusion

We successfully constructed a stable and a well-defined assay system with which the investigation of protein-lipid interactions can be carried out. Another important point is that the model membranes have the same packing density of lipids as a cell membrane. Therefore, adsorption behaviour of Aß studied in our model system should be more close

to that in biomembranes. The peptide-tethered artificial membranes should provide an ideal platform for the investigations on AD.

4 Investigation on the interaction between amyloid ß-protein (Aß) and lipids by surface plasmon field-enhanced fluorescence spectroscopy (SPFS)

4.1 Introduction/background

Amyloid ß-protein (Aß), a prominent constituent of brain plaques characteristic of Alzheimer's disease (AD), is a 40 or 42-residues polypeptide and is derived by the proteolytic cleavage of Aß precursor protein (APP). Although it remains unclear as to how exactly Aß plays a role in Alzheimer's disease (AD), the prevalent hypothesis is that neurotoxicity of Aß results from its direct interaction with membranes. It was reported that Aß has the ability to form ion channels in model membranes composed of phophatidyserine.[79] Silvia Micelli further demonstrated that the formation of ion channels in planar lipid membranes (PLM) was closely related to the membrane composition. Additionally, other membrane components promoted the formation of ß sheets of Aß, which is thought to be a striking feature of the Aß toxicity.[80;81] For example, the surface binding of Aß to negatively charged phospholipids has been shown to result in an induction of ß structure in Aß.[82] In recent years, evidence was reported that "lipid rafts" are the preferential sites for the formation of pathological forms of Aß,[83] as described in the case of the interactions of the Aß peptide with ganglioside-containing raft-like membranes made up of cholesterol and sphingomyelin, or with sphingolipid-containing domains.[84] However, it is not clear whether the complex of sphingomyelin and cholesterol are also potential binding sites for Aß. Systematic studies of the interaction between Aß and membranes especially composed of zwitterionic lipids can hardly be found, and thus, the interpretation of experimental results from different types of model systems is sometimes controversial. Moreover, much of the knowledge concerning the interaction between Aß and membranes is obtained from monolayer studies at the air-

water interface[85;86] or from vesicle/liposome model systems,[87;88] which are all relatively simple membranes. Hence, it is necessary to perform investigations in only one kind of model system, which is more complex and close to a cell membrane. In this study, we investigated Aß-membrane interactions using artificial peptide-tethered lipid membranes as described in Chapter 3.

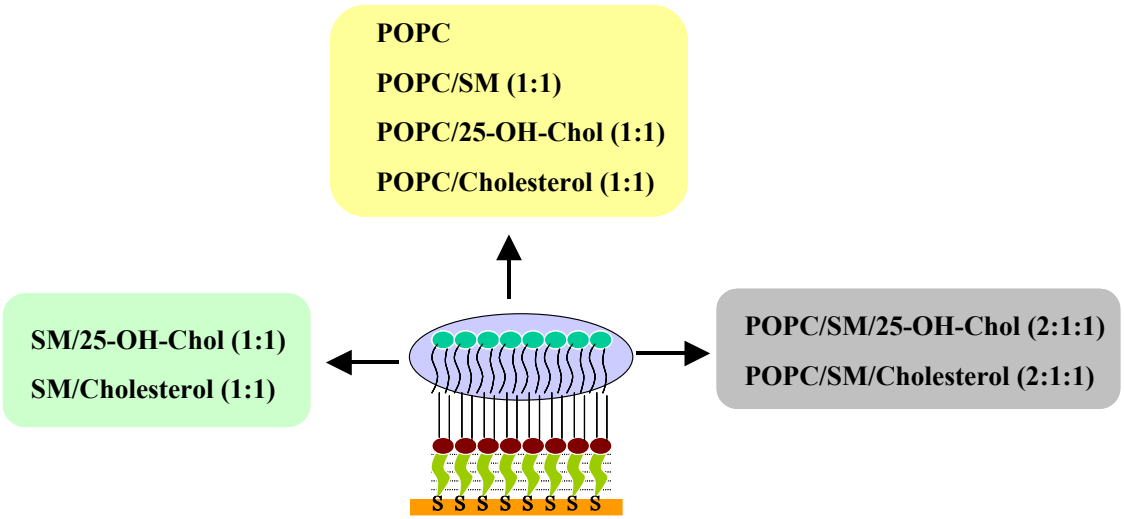

Figure 4.1: The model membranes applied to the investigation of protein-lipid interactions

Zwitterionic lipids (POPC and sphingomyelin), principal components in the outer monolayer of a plasma membrane, constitute the distal layers of the model systems. The importance of cholesterol in the Aß binding in model membranes has recently received considerable attention.[89;90] Hence, we incorporated cholesterol in the model membranes in order to study the role of these important membrane components. Cholesterol is rather susceptible to oxidation leading to the formation of cholesterol oxidation products (COPs). Oxysterols, oxidative derivates of cholesterol, are thought to potentially result from oxidative stress implicated in the central neuronal loss in AD.[91] It was shown by cell-culture studies that most neuronal cells were very sensitive to 25-hydroxycholesterol (25-OH-Chol) toxicity.[92] Judging from its molecular volume and its shape, 25-OH-Chol should be able to substitute for cholesterol in the cell membrane.[93] However, many

questions concerning the importance of oxysterols in AD development remain to be answered. Since cholesterol is a vital component of many membranes, we are very interested in the effects of substituting oxysterols for cholesterol on the Aß binding to the model membranes. For these reasons we used a peptide-tethered membranes comprising 25-OH-Chol as a model to assess whether the oxysterol influences the Aß adsorption, which may provide insight into some aspects of AD.

In order to enhance the signal of the interfacial binding events, we monitored the interaction of Aß with model membranes using surface plasmon field-enhanced fluorescence spectroscopy (SPFS), which is the combination of surface plasmon and fluorescence spectroscopy for sensor applications.[94] Anti-Aß40-mAb labeled with fluorophores was used to detect Aß adsorbed on membranes. Our results show that Aß binding is critically determined by the type and composition of the lipids in the model membranes. Meanwhile, non-specific binding of the antibody to the model membranes was also checked by SPFS.

4.2 Materials

Synthetic Aß40 peptide was purchased from Biopeptide Co., LLC., its purity (>95%) was analyzed by high performance liquid chromatography. Unless stated, Aß refers to Aß40 in the following text. The peptide (1mg) was initially dissolved in 1ml of 1,1,1,3,3,3-hexafluoro-2-propanol in order to avoid self-aggregation,[95] and then stored in 30µl aliquots at - 20°C until use. After removal of the solvent by nitrogen gas, the peptide was redissolved in PBS at the desired concentration.

Monoclonal anti-ß-Amyloid protein (epitope: 1-12) was purchased from Sigma-Aldrich.

All lipids, 1-palmitoyl-2oleoyl-*sn*-glycerol-3-phosphocholine (POPC), Cholesterol, 1,2-dimyristoyl-*sn*-glycero-3-phosphoethanolamine (DMPE), 25-hydroxycholesterol, 1-oleoyl-2-[12-[(7-nitro-2-1,3-benzo-xadiazol-4-yl)amino]dodecanoyl]-*sn*-glycero-3-phosphocholine(NBD-PC), sphingomye-lin (SM) from bovine brain were all purchased from Avanti Polar Lipids, Inc. N-octyl-ß-D-glucopyranoside was purchased from Merck Biosciences GmbH.

Alexa Fluor 647 monoclonal antibody kit was purchased from Molecular Probes Europe. B.V.

4.3 Fluorescence labelling of the monoclonal antibody

The procedures for the labelling were described in detail in the product information provided by Molecular Probes. Alexa Fluro 647 was used as a label for the monoclonal antibodies sensitive to an epitope within amino acid sequence 1-17 of the Aß40. The available dye-labeling kits enable a convenient mean to label small quantities (e.g. 100 µg) of proteins of interest with Mw > 30 kDa. Basically, three steps are required in the labeling procedure:

1) Reaction with dyes carrying reactive group, usually a succinimidyl ester (amine-reactive) or maleimide (thiol-reactive).
2) Purification of the labeled protein, usually by a gel-filtration column or dialysis.
3) Determination of the degree of labeling by UV adsorbances of proteins and dyes, respectively.

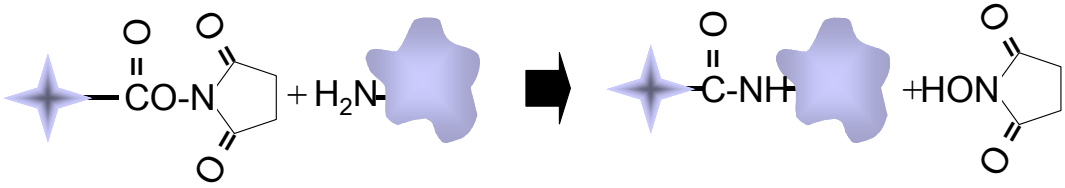

Figure 4.2: Schematic of the labeling of protein with Alexa Fluor 647 dye with a succinimidyl ester moiety.

For our experimental conditions (e.g. using the wavelength @ 633 nm as the excitation source), the commercial Alexa Fluor 647 dye (abbreviated as AF 647, from Molecular Probes, Inc.) was used taking advantage of its high fluorescence yield, less auto-quenching and in-sensitivity to pH conditions. The commercial labeling kit contains things needed to perform labeling reactions as well as to purify the resulting conjugates. In the kit, the AF 647 dye contains a succinimidyl ester moiety that reacts efficiently with

primary amines of the protein to form stable dye-protein conjugates at pH 7.5-8.5. The experimental protocol for labeling 100 μg monoclonal antibody is as the following:

1) Prepare 1 mg/mL antibody solution with sodium bicarbonate buffer (100 mM, pH 8.3)
2) Transfer 100 μL of the antibody solution to the vial of reactive dye. Incubate the solution for 1 hour at room temperature. Every 10-15 minutes, gently agitate the vial.
3) Prepare the spin column by adding the resin (30 kDa size exclusion) suspension into the column and allow it to settle, until the bed volume reaches 1.5 mL.
4) Centrifuge the column for 3 minutes at 1100 × g using a swinging bucket rotor. The Equation 3.1 converts the revolutions per minute (rpm) into the relative centrifugal force (g-force).
5) Load the 100 μL reaction volume dropwise onto the center of the column, allowing the solution to adsorb into the gel bed.
6) Place the column into a collection tube and centrifuge for 5 minutes at 1100 × g. The collection tube then contains labeled protein in ca. 100-150 μL of PBS, pH 7.2, with 2 mM sodium azide.
7) Dilute a small amount of the purified conjugate into suitable buffer and measure the absorbance in a cuvette with a 1 cm pathlength at both 280 nm (A280) and 650 nm (A650).

$$\text{The protein concentration (M)} = \frac{(A_{280} - (A_{650} \times 0.03)) \times dilution\_factor}{203{,}000} \qquad 4.1$$

with 203,000 being the molar extinction coefficient (() in cm-1M-1 of a typical IgG at 280 nm and 0.03 is a correction factor for the contribution of the fluorophore to the absorbance at 280 nm.

The degree of labeling, i.e., dye-to-protein ratio is:

$$\text{Mole dye per mole protein} = \frac{A_{650} \times dilution\_factor}{239{,}000 \times protein\_concentration(M)} \qquad 4.2$$

The degree of labelling was determined by UV-Vis absorbance spectroscopy. 4 moles of Alexa Fluro 647 were bound to one mole of antibody.

4.4 Interaction of anti-Aß-mAb and t-LBs

Anti-Aß40-mAb labelled with the fluorophore was used as a probe to detect Aß40 adsorbed on the lipid bilayers in this work. The antibody like other globular proteins inevitably interacts with lipid membranes, and thus it is the first task to know the mechanism on antibody-membrane interactions. The interactions of the antibody with the lipids were tested for the lipid matrices established as described above. Before the binding experiments, repeated rinsing with PBS ensured a proper environment for the protein binding. The antibody solutions diluted in PBS to a final concentration of 45nM were injected and allowed to interact with the lipid surface in the flow cell. After incubation for 30min, the surface was rinsed with PBS for 20min until equilibrium in order to remove free and loosely associated dye molecules on the membranes, where SPS/SPFS scan were performed to obtain the fluorescence signals of the antibody binding to the lipid surface.

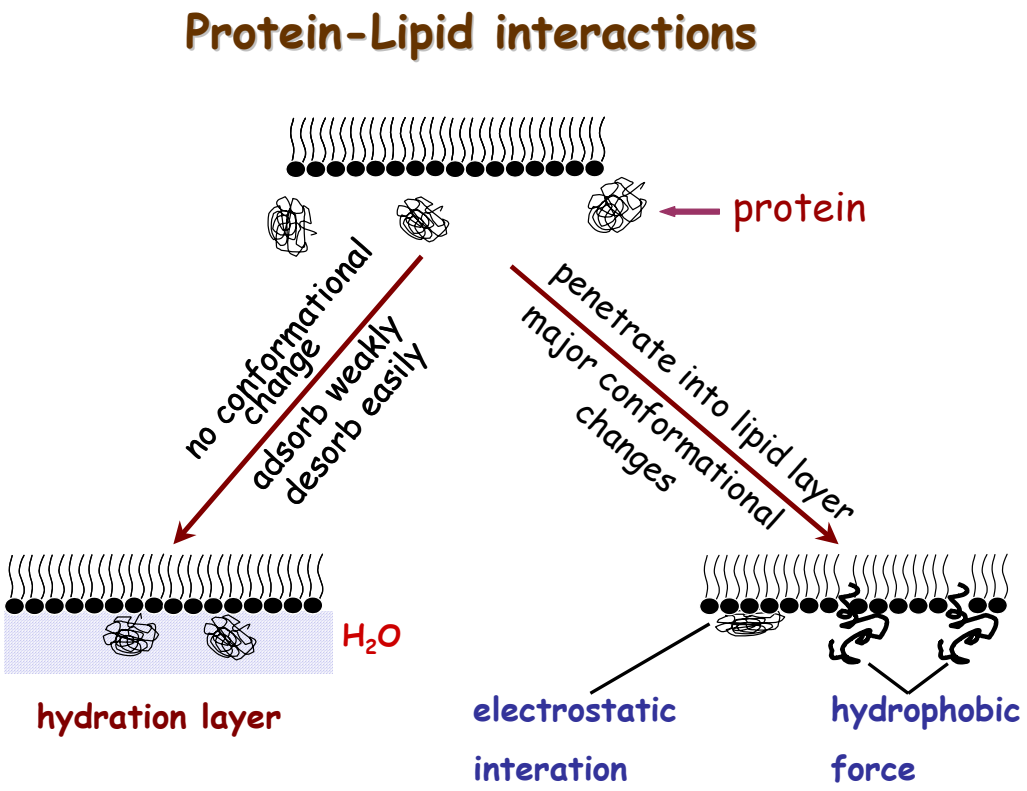

Figure 4.3: Schematic of protein-membrane interactions

It is well known that the adsorption of proteins at lipid membranes is the net result of the various interactions between and within the system components, which include the protein structures, lipid surfaces, and solvent (water). The driving force for lipid-protein interactions involves changes that include protein conformational changes,[96] variation of surface hydrations,[97;98]electrostatics and topological distortion.[99] Obviously, the outcome of the interaction depends on the structure and chemical composition of both protein and the lipid membrane. Zwitterionic lipids, which have zero net charge at neutral pH condition, were chosen in the present work as distal layers of t-BLs in order to investigate the adsorption of the antibody. Hence, electrostatic attraction between the antibody and lipids was excluded. In other words, hydrophobic forces will dominate the protein adsorption at the lipid membranes. In this case, the adsorption is strongly dependent on hydration layers of lipid surfaces, because it is necessary for hydrophobic interactions to

exchange the bound water between the protein and the surface.[100] Recently, a great attention has been paid to the influence of surface hydration layers on protein adsorption.[101-103] For example, the reduction of protein adsorption to PC surfaces has been extensively demonstrated.[104;105] These protein-resistant characteristics are believed to be due to the ability of the POPC groups to form large hydration layers. Our results also showed that membranes containing POPC had the weaker interaction with the antibody compared to that composed of sphingomyelin. (Fig. 4.4A).

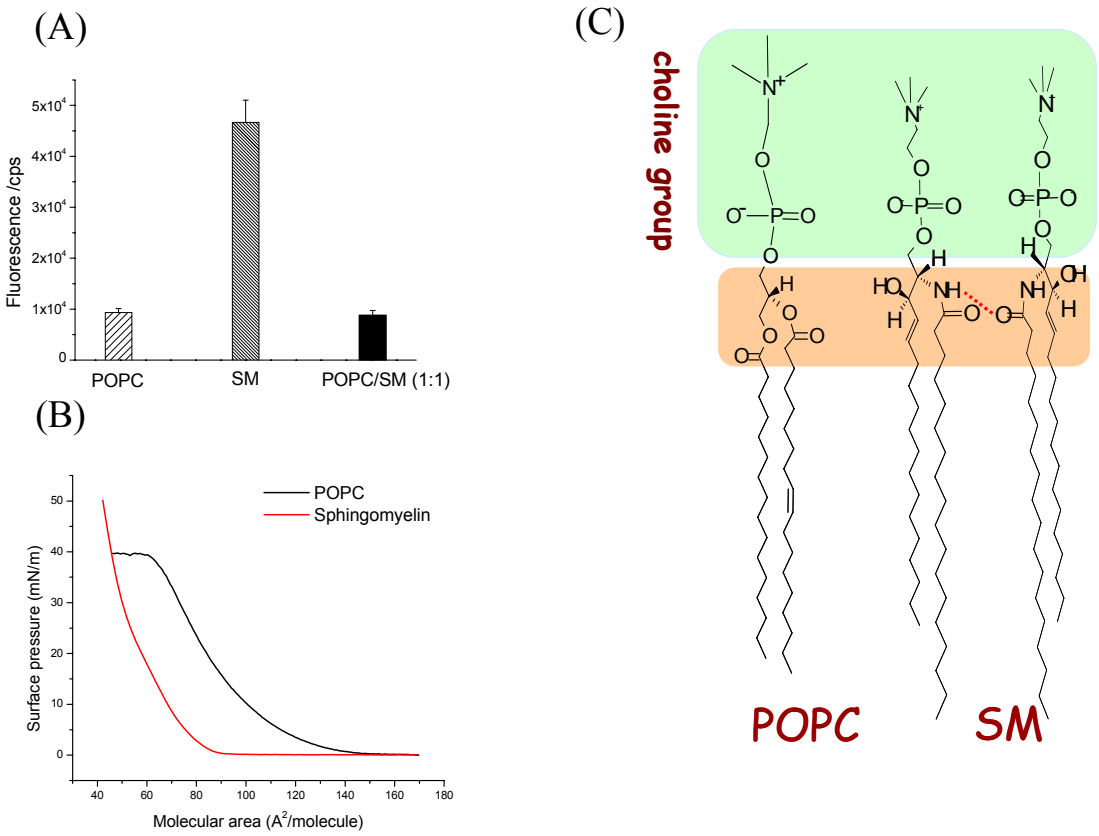

Figure 4.4: The relationship between lipid-antibody interaction and the structures of the lipids. (A) Interactions between the antibody labelled with the fluorophore and the model membranes containing POPC and sphingomyelin (SM). (B) Surface area-pressure isotherms, red curve: SM; black curve: POPC. (C) The structures of POPC and SM, the green area indicates the choline groups.

Indeed, there is strong evidence that a large free water fraction of POPC renders the

surface extremely hydrophilic, so that the hydration force provides a repulsive contribution to the protein-lipid interaction.[106] It is also suggested that the low protein adsorption of POPC is a result of the choline group having a high free-water fraction that disfavors protein conformational change at the membrane.[107]

However, the assumption that the choline in the head groups imparts the strong water binding character to phospholipids seems not to be true for sphingomyelins (SM). The SPFS results indicate that SM, which has the same phosphorylcholine head groups as PCs, is significantly more attractive to antibody adsorption (Fig. 4.4A). The remarkable increase in the protein adsorption is ascribed to the different interfacial features of SMs from PCs. The amide and hydroxyl groups in the interfacial regions of SM can act as hydrogen bond donors and acceptor, whereas the amide carbonyls in SM can only act as hydrogen acceptor. PC with two ester carbonyls in this region has only hydrogen bond-accepting features. These interfacial differences give SM the unique ability to form both intra- and intermolecular hydrogen bonding. It is assumed that the interactions of SM with itself giving rise to a network of hydrogen bonds formed by the amide residues at the interface can diminish the free water fraction at the lipid head groups. The surface pressure-area isotherms (Fig. 4.4B) showed that SM has higher packing density than POPC mainly due to the formation of intermolecular bonds. Both conditions, i.e., the average of orientation of the carbonyl group and the interfacial hydrogen bond network, seem to make the sphingomyelin lipid-water interface less hydrophilic as compared to the POPC interface. Another reason for SM being a strong protein adsorber is that a network structure of water molecules caused by the hydroxyl groups at the interface of SM presumably prolongs the contact of the antibody on the surface and enhances the chance for the interaction of the protein with the surface.

The adsorption of the antibody to a model membrane composed of an equimolar binary mixture POPC/SM rather closely resembled that for the pure POPC (cf Fig.4.4A). A plausible explanation is that POPC would disrupt the network of hydrogen within the SM if the two lipids mix and thus increase the free water content at the interface.[108] A small change in the fluorescence signals was observed in the equimolar mixtures of POPC/sterols compared to pure POPC systems, which further indicated that an important role is played by POPC in protein resistance. These results are in agreement with other

report in the literature.[109] However, significant difference of the effect of sterols (cholesterol and 25-OH-Chol) on protein adsorption was observed (cf Fig. 4.5). Slight decrease in the protein adsorption by the addition of cholesterol but significant increase by 25-OH-Chol compared to the pure SM alone was noted.

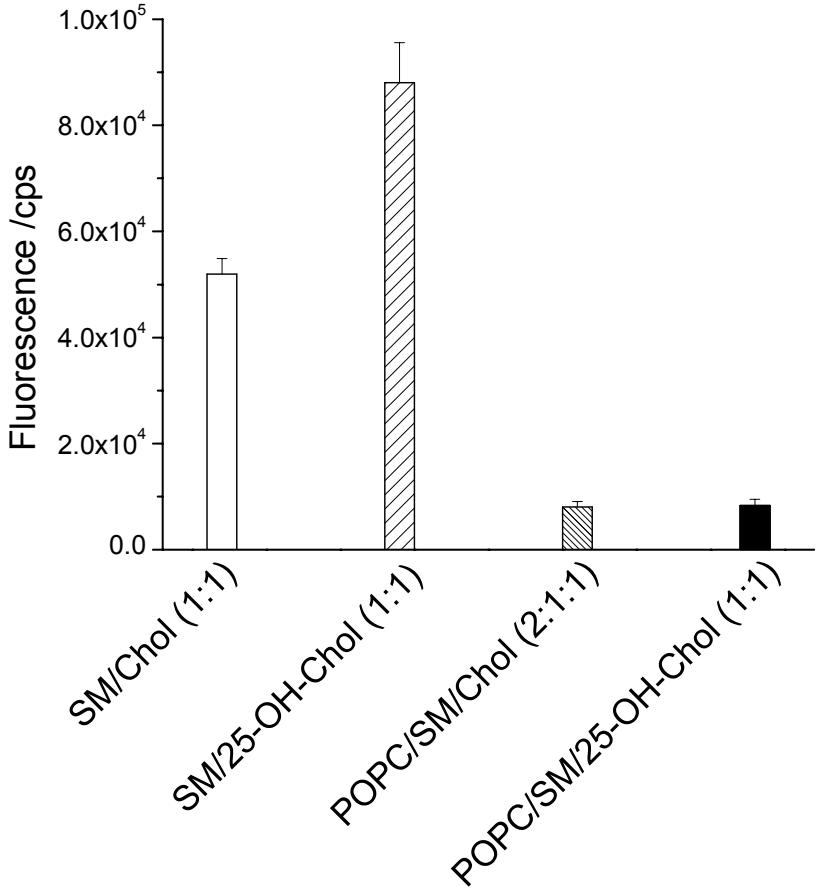

Figure 4.5: Effects of the sterols (cholesterol and 25-OH-Chol) on the antibody adsorption.

In view of the fact that cholesterol is thought to more strongly interact with SMs than with PCs,[110;111] such specificity could be expected to affect the hydration behavior of the SM-Chol system and further the protein adsorption. In the present work, however,

cholesterol has only a moderate effect on the protein-membrane interaction. Compared to cholesterol, 25-OH-Chol, which is different from cholesterol only in one additional hydroxyl group in position C_{25}, greatly promoted the protein adsorption.

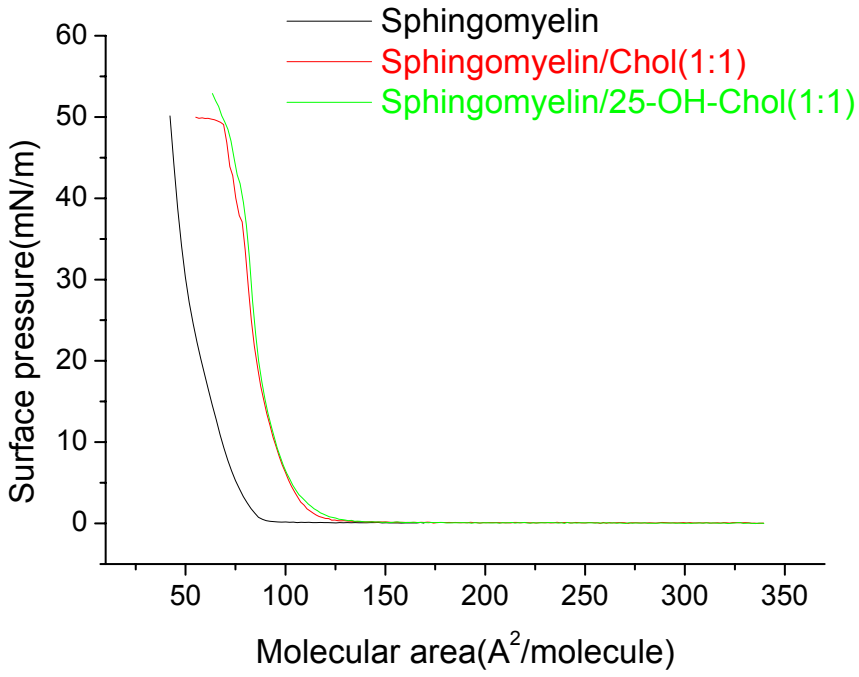

Figure 4.6: Pressure-area isotherms of the monolayers of pure sphingomyelin and the mixtures of sphingomyelin /the sterols

The surface pressure-area isotherms showed (Fig. 4.5) that cholesterol and 25-OH-Chol had an almost identical change of the phase behaviors at high surface pressures (>30mN/m). Hence, it was tentative that the interaction of the additional OH on C_{25} with SM affected the interfacial hydrogen network. However, addition of 50mol% POPC to the equalmolar mixtures of SM and sterols considerably decreased the protein adsorption. These results further indicate that POPC plays a key role in protein-resistent adsorption. Indeed, there is strong evidence that a large free water fraction of POPC renders the

surface extremely hydrophilic, so that the hydration force provides a repulsive contribution to the protein-lipid interaction.[112] In the tertiary mixtures, 50mol% POPC can form the hydration layers enough to preserve the natural conformation of the protein at the membrane surfaces. Therefore, any model membrane containing 50mol% POPC applied to the investigation of Aß-lipid interaction has low protein adsorption in this work.

4.5 Binding specificity of Aß to the model membranes

The interactions of Aß and the membranes were probed using SPFS by the detection of an antibody labeled with a fluorophore recognized Aß bound at the membranes (Fig. 4.6). Before the binding experiments, repeated rinsing with PBS ensured a proper environment for the protein binding. The Aß solutions were prepared as described above to a final concentration of 4.6µM. The matrices were rinsed with PBS before the solutions of the antibody labeled with Alexa Fluor 647 dye at a final concentration of 45nM were injected into the flow cell at a flow rate of 36µl/min. After incubation for 20min, the unbound peptide was rinsed out with PBS. The solutions of the antibody were injected and allowed to interact with Aß at the membranes in the flow cell. After incubation for 30min, the surface was rinsed with PBS for 20min until equilibrium was reached in order to remove free and loosely associated dye molecules on the membranes, where SPS/SPFS scan were performed to obtain the fluorescence signals of the antibody binding to the lipid surface. Binding specificity of Aß to the model membranes was determined by the fluorescent intensity of the antibody bound to Aß at the membranes.

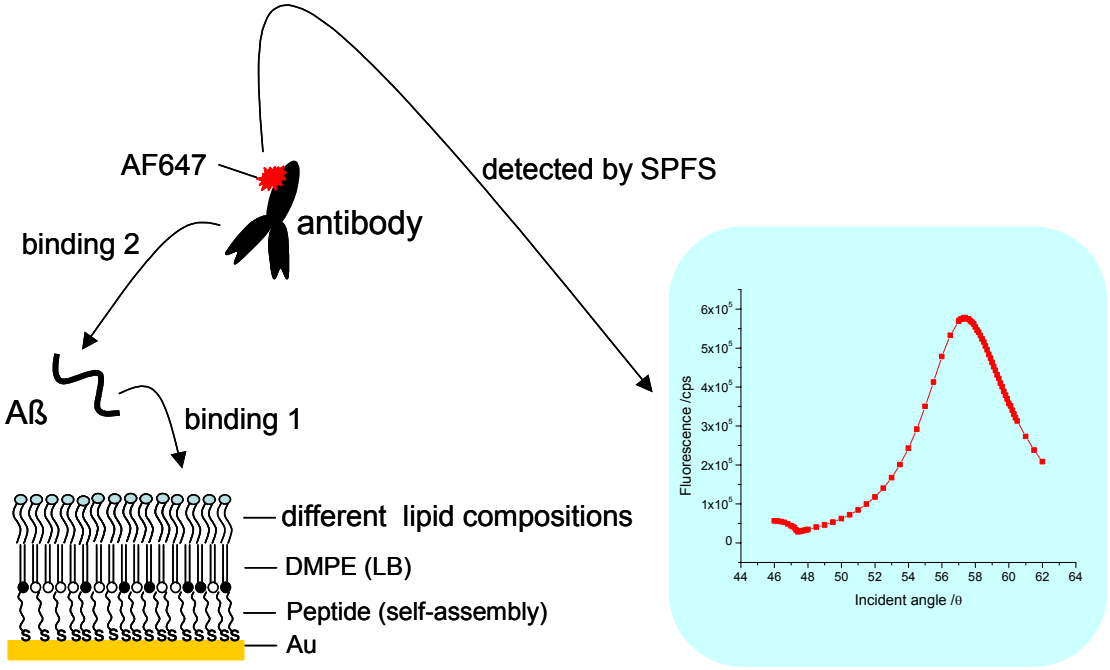

Figure 4.7: Schematic illustration of the detection of Aß-membrane interactions by the antibody labelled with a fluorephore using SPFS

In this work, anti-Aß40-mAb labelled with a fluorophore was used as a probe to detect Aß adsorbed to the model membranes. Different model membranes (POPC, POPC/sterols, POPC/SM and POPC/SM/sterols) were established to investigate the interactions between lipid bilayers of different composition and Aß. For monolayers with several components, the POPC accounts for 50mol% of the lipids in the distal layers of the model membranes in order to resist antibody adsorption. The aforementioned results indicate that 50mol% POPC is indeed resistant to the protein adroption. Therefore, there is almost no non-specific adsorption of the antibody to our model membranes. The fluorescence signals are thought to contain contributions only from the antibody binding to Aß at the membrane surfaces. We monitored the binding of Aß to the membranes by the detection of fluorescently labelled anti-Aß-mAb bound to Aß at the surfaces using SPFS. Hence, the interaction of Aß and the membranes was deduced from the fluorescent intensities of the bound antibodies.

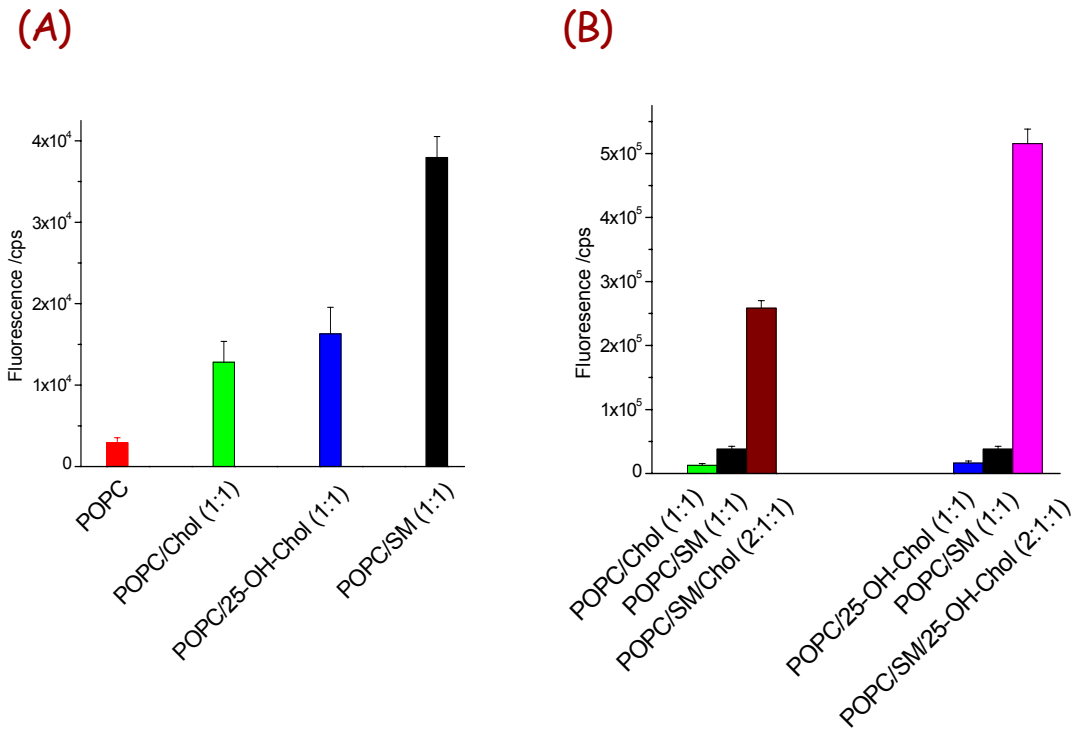

Figure 4.8: Effects of lipid composition on Aß adsorption. Fluorescence intensities (cps) were obtained at the maximum points of angular scan curves of fluorescence. (A) Fluorescence signal from pure POPC was the lowest and one from the mixture of SM/POPC was the strongest, indicating the strongest association of Aß with SM. (B) The fluorescence signal was significantly increased in the presence of SM and the sterols. And the most adsorption of Aß was found in the tertiary systems containing 25-hydroxycholesterol (25-OH-Chol).

Fig. 4.8A shows that the amount of antibody bound to Aß at a pure POPC membrane was the lowest among the four model systems, indicating Aß had the weakest interaction with POPC. The addition of 50mol% cholesterol (Chol) and 25-hydroxycholesterol (25-OH-Chol) to POPC increased the fluorescence signal, that is, Aß adsorption. These results are indicative of the role played by the sterols in Aß-membrane interaction, similar to what has been obtained by other methods.[113;114] It was reported that the sterols could facilitate Aß incorporation into the PC membranes if the content of the sterols is more than 30mol%. For binary equimolar mixtures of POPC and sphingomyelin, the strongest adsorption of Aß was observed. This preferential binding is possibly due to the specific

recognition of Aß to sphingomyelin. This assumption is confirmed by the fact that sphingolipid-binding domains have been identified in Alzheimer, Prion and HIV proteins.[115] These observations suggest that the Aß-membrane interaction is sensitive to the change in lipid composition. Compared to sphingomyelin, however, the above results do not show that sterols contribute considerably to the Aß adsorption even in the presence of 50mol% sterols in the systems.

In recent years, "lipid rafts" mainly composed of sphingolipid and cholesterol have received attention in the pathogenesis of Alzheimer's disease (AD). Studies from many laboratories showed that the production and adsorption of Aß occurred at raft-like domains.[116;117] It was reported[118;119] that Aß showed a significantly higher affinity for ganglioside within rafts of cholesterol and sphingomyelin. In the present work, the focus is on membranes containing sphingomyelin and cholesterol. The distal monolayer is composed of POPC/SM/Chol at a ratio of 2:1:1. In another tertiary system, cholesterol was replaced by 25-hydroxycholesterol (25-OH-Chol) in order to evaluate the effects of oxidative stress on Aß adsorption.

Fig. 4.8B shows that effects of the sterols or SM on Aß adsorption to the model membranes are remarkably amplified only if both components coexist in the membranes. Obviously, the greatly enhanced driving forces for Aß-membrane interaction to take place arise from the sterol-SM association. The most significant increase in the fluorescence signal was observed in the system POPC/SM/25-OH-Chol, suggesting that 25-OH-Chol may also be more tightly associated with SM than with POPC like cholesterol. These data implicate that the role of 25-OH-Chol could be of a certain importance for AD development.

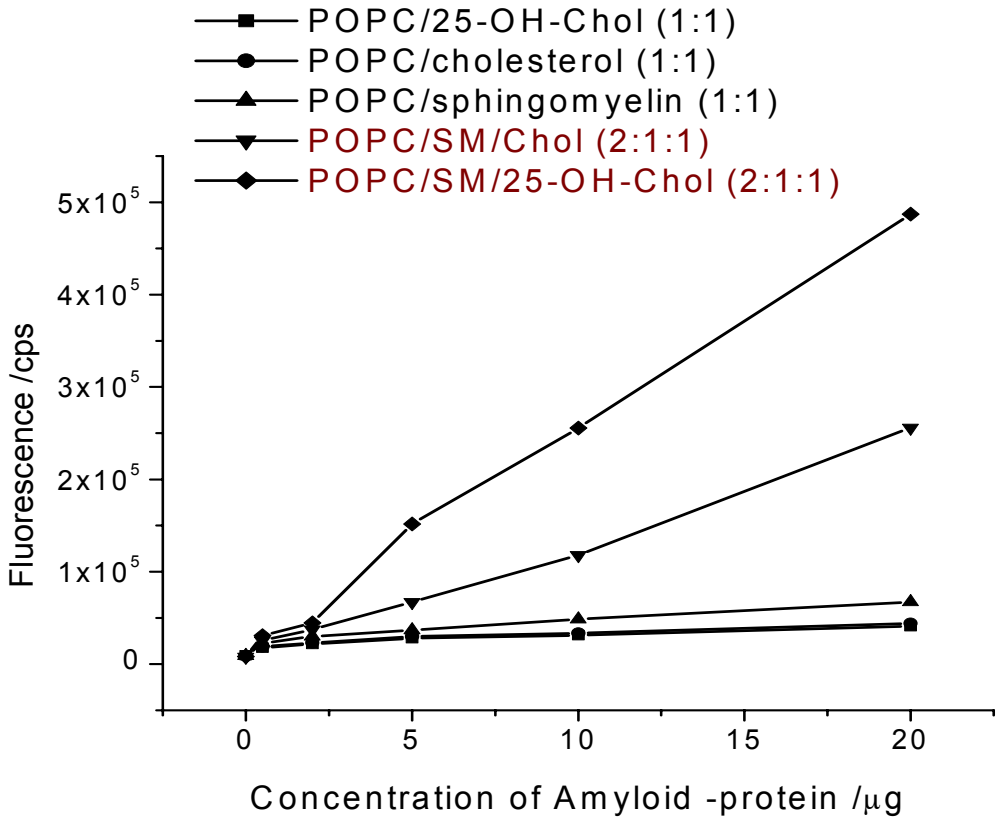

Figure 4.9: Effects of lipid composition on Aß adsorption. By step-wise increasing the solution concentration of Aß, the fluorescence intensity of each concentration was obtained at the peak of the scan curves of fluorescence. The specific binding of Aß to the membranes containing the sterols and SM gives a clear linear increase in fluorescence signals as a function of the concentration of Aß, which are shown as (●), (■), (▲), (▼) and (♦), respectively. The steepest linear curve was obtained in the tertiary mixtures of POPC/SM/Oxy (●); the curves form the membranes composed of binary mixtures are almost identical to the background.

Recent studies have pointed to the presence of oxidation products of cholesterol that easily occur during the aging process.[120] Further support for the hypothesis comes from the fluorescence measurements as a function of Aß concentrations, which is presented in Fig. 4.9. By a step-wise increase of the solution concentration of Aß, a strong linear increase of the fluorescence was obtained for the tertiary mixtures POPC/SM/sterols in contrast to that for the rest of the matrices. This indicates that the amount of Aß bound to

the model membranes POPC/SM/sterols is proportional to the increase in the concentration of the peptide. These experiments support the notion that Aß specifically recognises the SM/sterols and the absence of either one of them results in a substantial decrease in Aß adsorption, implying the selective binding of Aß to the special domains composed of SM and sterols.

4.6 Conclusions

By comparing experiments with membranes of different lipid composition, selective adsorption of Aß was observed. The simultaneous existence of SM and sterols in the model systems significantly enhanced Aß adsorption. In this work, an interesting observation is that the sterols (Chol and 25-OH-Chol) cannot increase Aß adsorption significantly unless SM is present in the model membranes. It can be assumed that the presence of SM modulates the interaction of Aß with the membranes. Among the model membranes used, the highest tendence of Aß to adsorb to the micro-domains containing 25-OH-Chol suggests that oxidation of cholesterol may relate to some aspects of AD. Sphingomyelin should receive much more attention in AD research than before, although cholesterol is prevalently thought to be an important factor in AD.

Our findings may also correlate with a recent report in which it was shown that the level of SM is increased in the brain of Alzheimer's patients.[121] High levels of SM in the central nervous system also give a hint as to its potential role in AD development. Of particular interest is the observation that the SM content increases with age in the cerebral cortex.[122] The present work also clearly demonstrates an important role of SM in Aß-membrane interaction.

5 The interactions of the sterols (cholesterol and 25-hydroxycholesterol) with sphingomyelin

5.1 Introduction/background

In 1972 Singer and Nicholson presented a fluid mosaic model of the cell membrane which showed the membrane as a fluid-like bilayer in which proteins are able to move freely. This model of the plasma membrane has evolved considerably since then.[123] Lipids that attract and/or pack with each other more effectively should naturally separate into domains within membranes. A growing body of evidence has shown that specialized lipid domains exist in membranes.[124;125] Among these domains, those containing sphingolipids and cholesterol, referred to as membrane or lipid rafts, have received much attention in the past years. A schematic model of lipid organization in the plasma membranes is proposed in Fig. 5.1. This model, based on the work of Israelachvili et al.[], takes into account the shape of each membrane lipid and the coexixtence of different lipid phases (L_c and L_0) within the membrane. It should be emphasized that this modern interpretation of membrane structure challenges the tranditional view that lipids and proteins are uniformaly istibuted in a homogenous bilayer.

It is widely accepted that lipid rafts are involved in signaling events and intracellular trafficking of proteins (including bacterial toxins).[126] In addition, there is also increasing evidence that lipid rafts are preferential sites of formation for pathological forms of the ß-amyloid peptide (Aß) associated with Alzheimer's disease (AD).[127-129] In the above Chapter, we also demonstrated that Aß selectively binds to membranes containing sterols and sphingomyelin, suggesting that the specific binding possibly implicates in the micro-domains. Heterogeneous distributions of sphingomyelin and cholesterol have been extensively studied by microscopy for lipid monolayers. However, it is not clear whether 25-hydroxycholesterol (25-OH-Chol) can also play a role in the formation of the micro-

domains. Furthermore, we are very interested in the phase behaviors of these lipids if the Langmuir monolayers are compressed to the pressure (π = 30mN/m) under which the model bilayers are constructed. In this study, we investigated the phase behaviors of sphingomyelin and 25-OH-Chol in mixed with 50mol% POPC by fluorescence microscopy. The occurrence and properties of domains can be monitored with lipid probes. The use of fluorescent lipid probes is particularly convenient because they allow direct visualization of domains large enough to be resolved microscopically. The application of fluorescence microscopy to the study of monolayers of membrane lipids has been fruitful and relevant to improving the understanding of membrane processes. Fluorescence microscopy revealed that 25-OH-Chol also could form micro-domains with sphingomyelin as cholesterol even at the pressure of the model bilayers.

5.2 Materials

All lipids, 1-palmitoyl-2oleoyl-*sn*-glycerol-3-phosphocholine (POPC), Cholesterol, 1,2-dipalmitoyl-*sn*-glycero-3-phosphocholine (DPPC), 25-hydroxycholesterol, 1-oleoyl-2-[12-[(7-nitro-2-1,3-benzo-xadiazol-4-yl)amino]dodecanoyl]-*sn*-glycero-3-phosphocholine(NBD-PC), sphingomye-lin (SM) from bovine brain were all purchased from Avanti Polar Lipids, Inc. Triton X-100 was obtained from Sigma. Solution containing fluorescent probe should be stored in dark brown bottles, wrapped so as to prevent slow photobleaching from ambient light.

Water for all experiments was ultropure (10^{18} MΩ cm resistivity and <10ppb organic content).

5.3 Fluorescence imaging

The phase behavior of Langmuir monolayers was monitored using epifluorescence microscopy with an attached CCD camera mounted above the Langmuir trough (Nima model 601). The microscope stage can be translated to examine different regions of the surface film in the x and y directions. This apparatus allowed for the recording of

pressure-area compression isotherm and fluorescence imaging simultaneously. The key feature of fluorescence microscopy studies of Langmuir films is the addition to the monolayer of a small amount (typically 0.1-2.0 mol%) of a fluorescently labelled lipid that will partition itself between surface phases of different surface density so that optical contrast between these two phases is achieved.

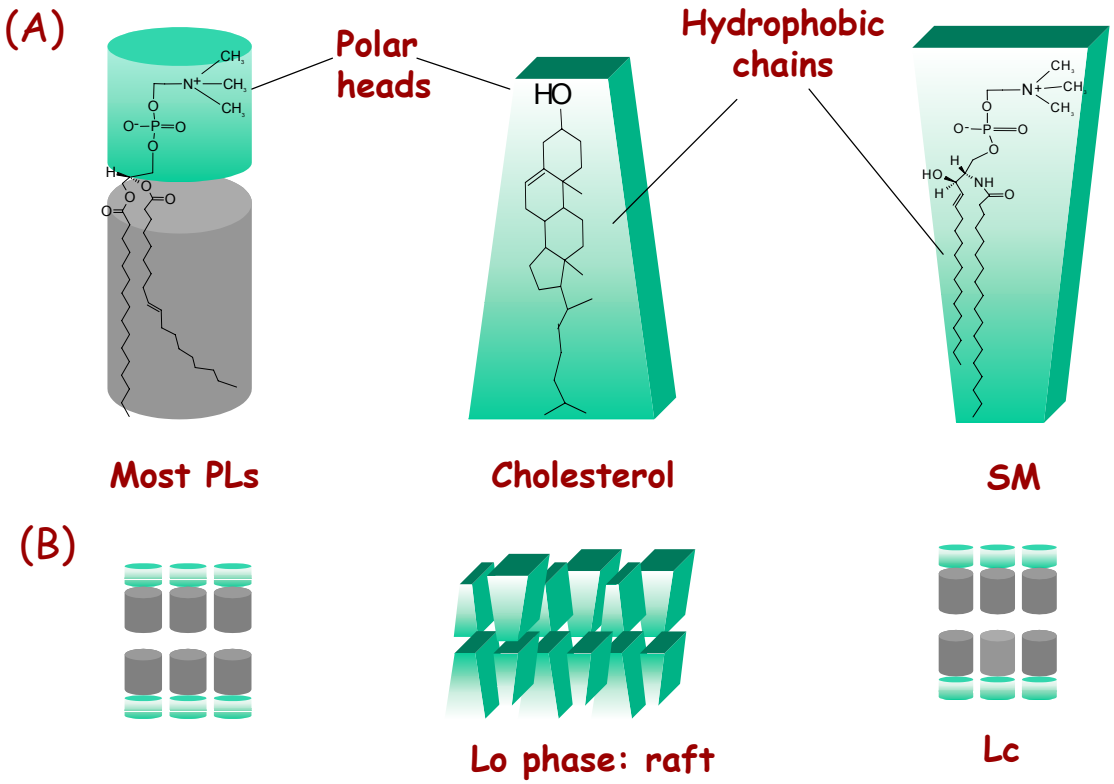

Figure 5.1: Lipid organisation in raft microdomains: a simplified model based on the theroretical shape of membrane lipids. (A) Glycerophospholipids (GPLs), which form the Lc phase of the plasma membrane, are indeed roughly cylindrical; however, cholesterol and sphingomyelin have a pyramidal or cone-like shape. In sphingomyelin the polar head group occupies a large area than does the hydrophobic region, whereas the converse is true fro cholesterol. (B) Any void between associated sphingomyelins is thought to be filled by cholesterol functioning as a molecular spacer. The enrichment of cholesterol in Lo phase domains is consist with this model.

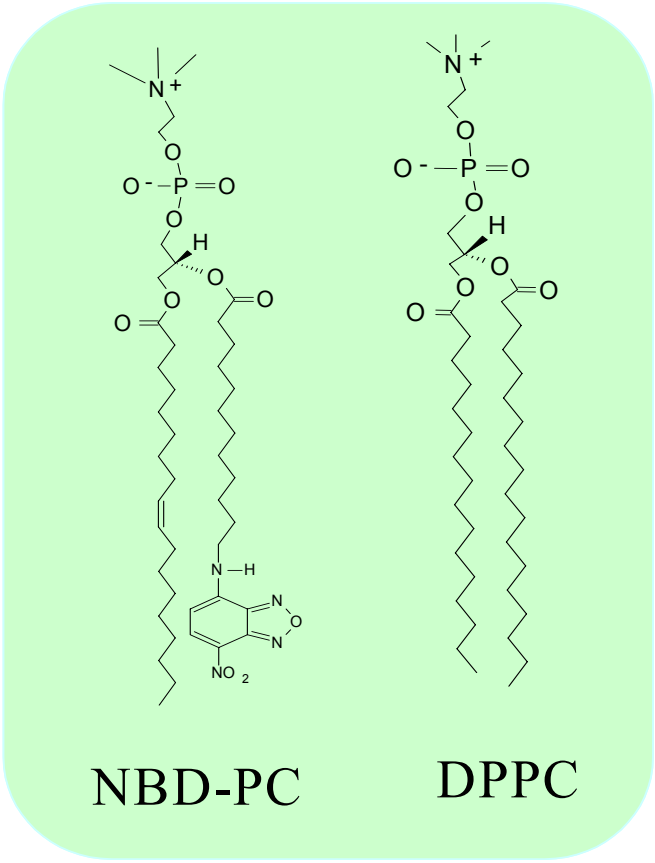

Figure 5.2: Chemical structures of DPPC and the probe (NBD-PC)

Proper behavior of the probe is crucial in these studies; if the probe is equally soluble in the two phases or segregates from the monolayer, no useful images or misleading images will be obtained. A number of suitable probes are commercially available. The most popular derivatives for monolayer studies have been the NBD-labelled (NBD = 7-nitro-2,1,3,-benzoxadiazol-4-l) phospholipids. In this study, a small amount (0.6%) of a fluorescent dye, NBD-PC, is used to provide contrast between coexisting phases. A standard filter set was used to monitor the fluorescence of NBD (excitation λ = 450-470 nm, dichroic mirrorλ = 480 nm, emission λ = 510-530 nm).

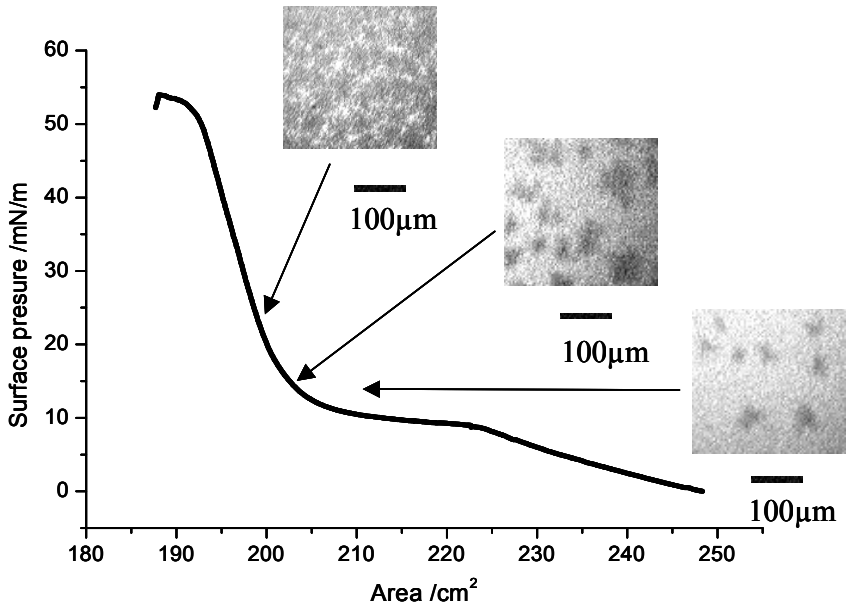

Figure 5.3: Fluorescence micrographs of phospholipids monolayers at the air-water interface at room temperature. Micrographs show fluorescence imaging and surface pressure-area isotherm of DPPC monolayer doped with 0.6mol% NBD-PC.

The existence of micro-domains or "lipid rafts" rich in cholesterol and sphingomyelin has been demonstrated in artificial membranes by using diverse biophysical techniques, although doubts about their presence in living cells still exist.[130] However, it is not clear whether 25-OH-Chol can form micro-domains with sphingomyelin. Therefore, epifluorescence images of Langmuir monolayers were recorded. By doping the monolayers with a fluorescent phospholipid analog (NBD-PC), any lipid phase separations can be visualized. In order to test the partitioning preference of the probe in different phases, Langmuir monolayers of DPPC with their well-studied phase behavior were imaged first. Fig. 5.3 shows that NBD-PC is largely excluded from micro-domains with a propeller shape, which is characteristic of DPPC monolayers at the air/water interface in the liquid expanded/liquid condensed phase coexistence region. This indicates that attaching bulky fluorophores to the acyl chains of PC (Fig. 5.2) can prevent

them from tightly interacting with the DPPC within micro-domains, because the fluorophore (NBD) disturbs the hydrophobic interaction between acyl chains of the lipids. Thus, NBD-PC could be used to identify the micro-domains. We employed also monolayers composed of POPC/SM/Chol (2:1:1) to further validate that approach. The coexistence of two phases was seen in the monolayers (Fig. 5.4) in agreement with other work.[131]

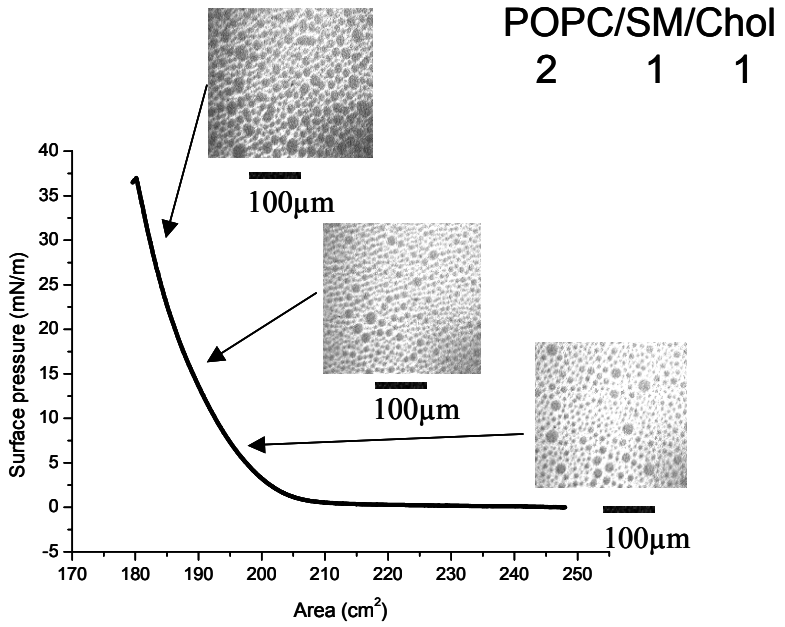

Figure 5.4: Fluorescence micrographs of phospholipids monolayers at the air-water interface at room temperature. Fluorescence micrographs and surface pressure-area isotherm of phospholipid monolayer composed of POPC/sphingomyelin/Cholesterol (2:1:1) doped with 0.6mol% NBD-PC.

25-hydroxycholesterol, a kind of oxidative derivate of cholesterol, which closely resembles cholesterol, only difference in the position C_{25} (Fig. 5.5), presumably also has the tendency to form ordered phases with SM. In order to address this question, the phase behavior of monolayers of POPC/SM/25-OH-Chol (2:1:1) was investigated under the same conditions as above. Fig. 5.6 clearly shows the micro-domain formation despite the replacement of cholesterol with 25-OH-Chol in this tertiary mixture.

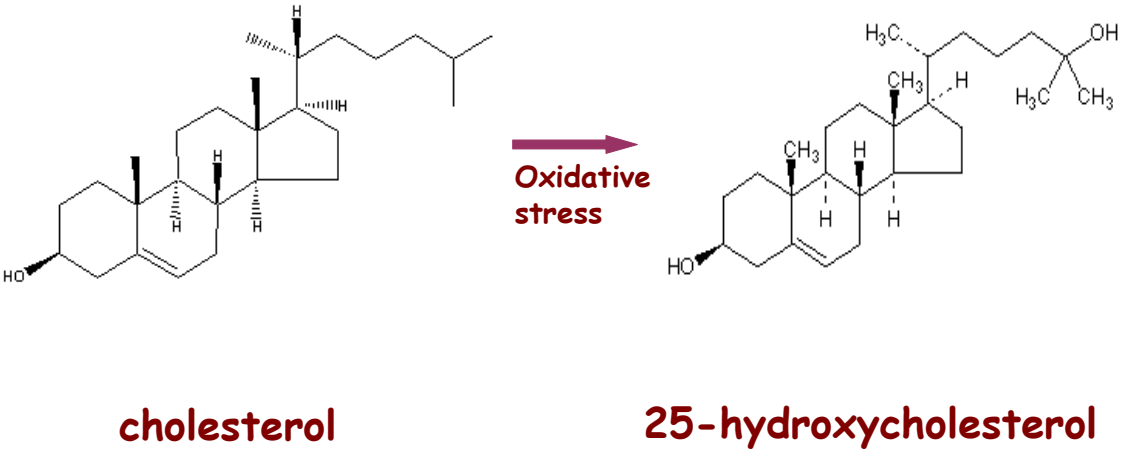

Figure 5.5: Schematic of the transformation of cholesterol to 25-hydroxycholesterol

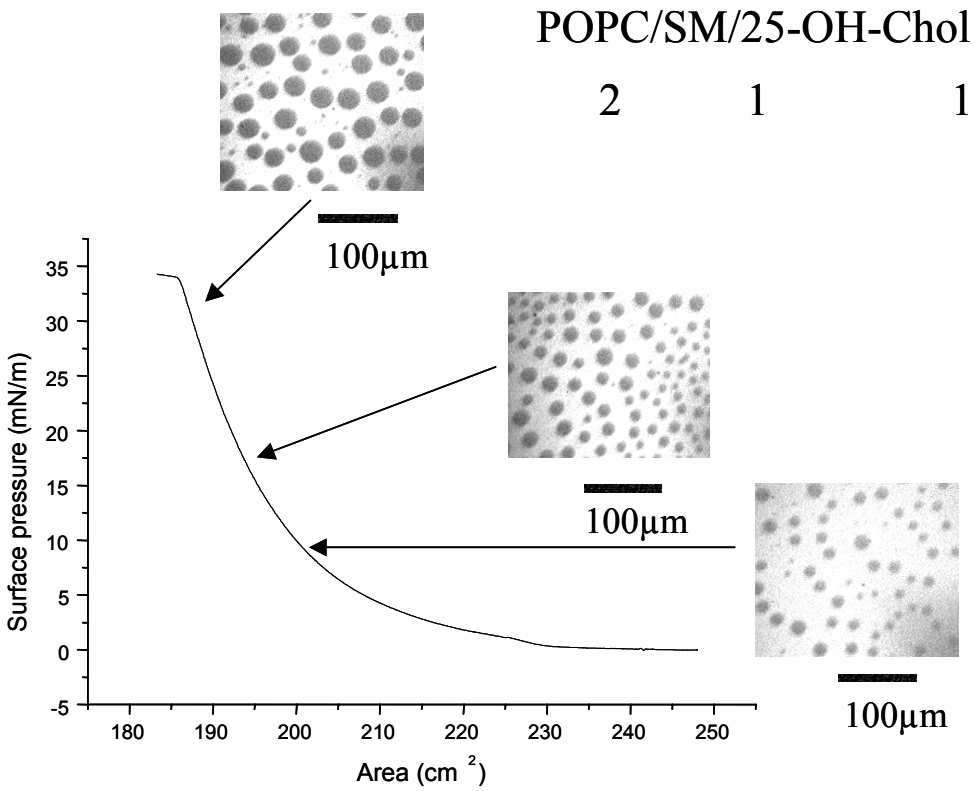

Figure 5.6: Effects of 25-hydroxycholesterol on the formation of micro-domains. The monolayers composed of POPC/sphingomyelio/25-hydroxycholesterol doped with 0.6mol% NBD-PC form micro-domains at above surface pressure of 5mN/m.

These observations suggest that 25-OH-Chol could also form ordered phases with SM as cholesterol does. This conclusion was further strengthened by the fact that the imaging of the micro-domains was critically dependent upon the 25-OH-Chol concentrations (Fig. 5.7), which indicated that 25-OH-Chol played a key role in the micro-domain formation.

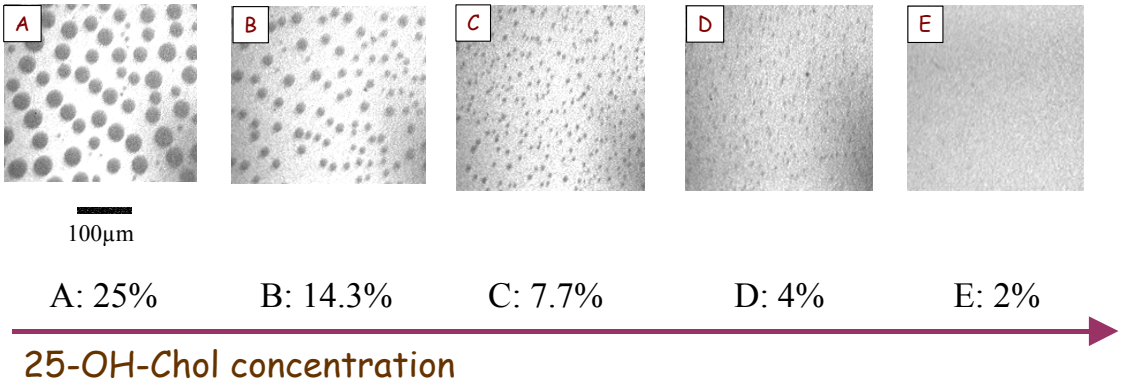

Figure 5.7: Effects of 25-hydroxycholesterol on the formation of micro-domains. The fluorescence images of the micro-domains markedly changed as the decrease in concentration of 25-hydroxycholesterol in the tertiary mixture, and micro-domains cannot be observed at the concentration of 2mol%

According the model for the formation of lipid rafts shown in Fig. 5.1, we postulate that 25-OH-Chol like cholesterol would effectively pack into the space between the sphingolipids in a manner analogous to the way it fills space between associated sphingolipids as a molecular spacer. Hydrogen bonding between the 3-OH /25-OH groups of 25-OH-Chol and the amide/the amide carbonyl of the sphingosine would stabilize this location of 25-OH-Chol.

The other model, historically the first to be proposed[132], considers the interaction between the chains as the primary determinant. This model places emphasis on the fact that saturated acyl chains are more extended than an unsaturated ones and pack well with each other into liquid-ordered phases. Cholesterol may interact more favourably with a

saturated than an unsaturated sphingolipid because cholesterol is a flat, rigid molecule. The interactions between acyl chains of sphingomyelin and cholesterol would be the critical factor in creating rafts. Therefore, an additional hydroxyl group in the side chain of 25-OH-Chol is assumed to prevent the formation of liquid-ordered phases because the polar group in the side chain would not able to associate with the nonpolar bilayer interior causing hydrophobic mismatch.

This assumption seems to be supported by the report that 25-OH-Chol did not appear to intercalate into the membrane bilayer and increase the acyl chain packing constraint in the background of POPC. Instead it appears that the molecule primarily associates with the hydrated surface of the bilayer. However, this observation obviously cannot be used to explain the interaction between 25-OH-Chol and saturated lipids such as sphingomyelin. That assumption is also challenged by the results of fluorescence microscopy that is 25-OH-Chol associates tightly with sphingomyelin.

A plausible explanation is that an additional OH group at C_{25} in the side chain of 25-OH-Chol actually can loop back to the interface possibly due to the squeezing by the hydrophobic chains between sphingomyelin molecules, and then also participate in the formation of hydrogen bonding with the interfacial region of sphingomyelin (Fig. 5.8). Our results are confirmed by the other work[133] that 25-OH-Chol appears to promote domain formation to a degree similar to cholesterol at 23 and 29°C by quenching measurements. Furthermore, the temperature dependence of quenching suggests that 25-OH-Chol stabilizes domain formation somewhat more than cholesterol, as exemplified by somewhat more domain formation in the 37-45 °C range. Thus, 25-OH-Chol seems to have stronger interaction with sphingomyelin than cholesterol.

These results indicate that the two polar groups of 25-OH-Chol do not affect the formation of micro-domains.

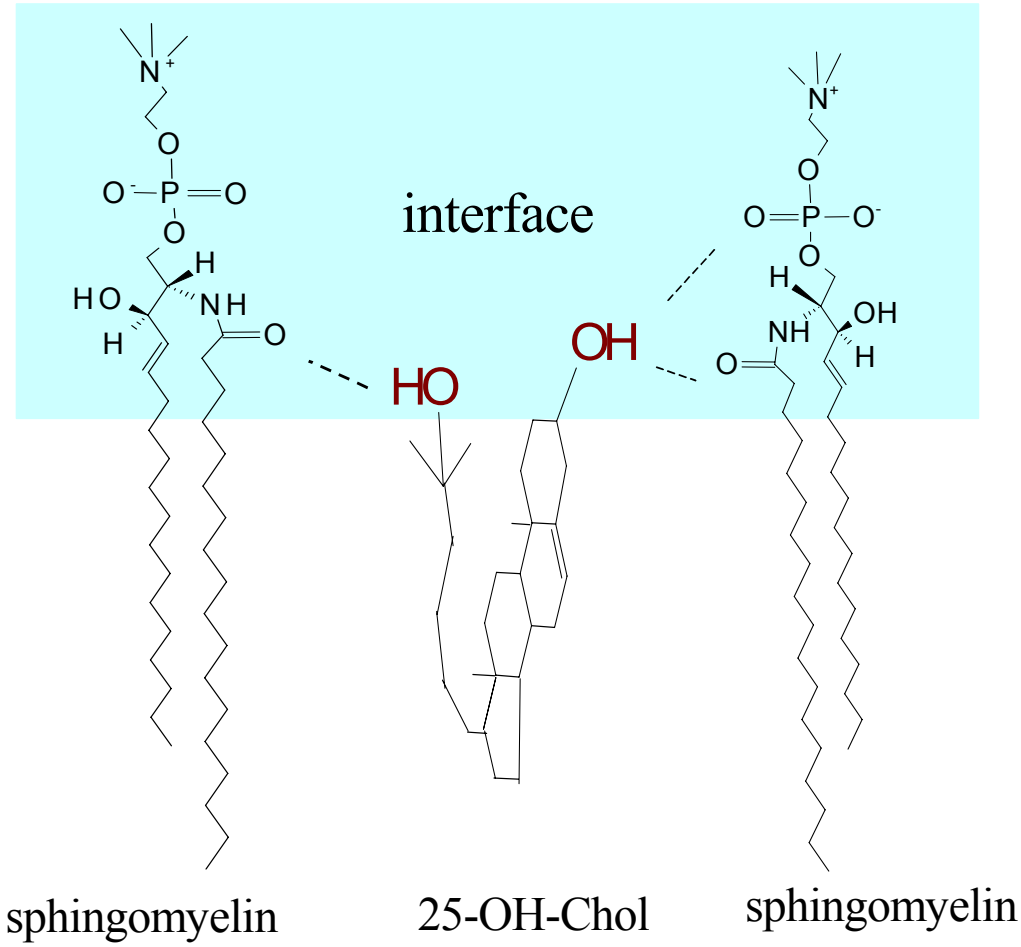

Figure 5.8: The assumption of the interaction of 25-OH-Chol and sphingomyelin at the air-water interface.

More important is the fact that the two-phase region of the monolayers was found above the surface pressure of 30mN/m, at which a well-defined second monolayer was deposited from the air-water interface by the Langmuir-Schaefer technique. Thus, it is believed that the micro-domains of the distal layers are preserved upon the formation of tethered lipid bilayers. The specificity of Aß binding to the model membrane should be closely related to the micro-domains mainly composed of SM and the sterols.

5.4 Detergent solubilization of experiments

In order to further confirm the association of sphingomyelein and 25-OH-Chol, we also examined the effects of 25-OH-Chol on the sensitivity of lipid mixtures to detergent solubilization because the formation of cholesterol-rich domains is closely associated with the appearance of lipid insolubility in the detergent Triton X-100.

Lipid vesicles containing 1mM of total lipid of were prepared in water as described in Chapter 2. The sample volume was 950µl. One set of the vesicles was composed of POPC, sphingomyelin and 25-OH-Chol at a mole ratio of 2:1:1, and the control set contained sphingomyelin (SM) and POPC (1:1). Then 50µl of 10% (w/v)

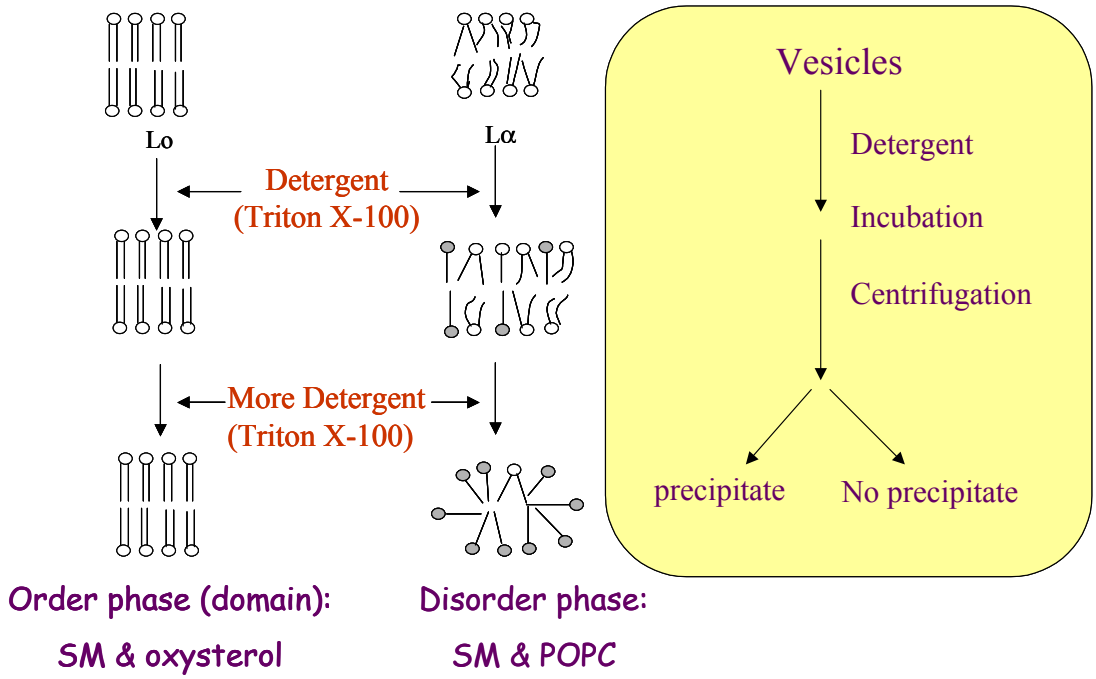

Figure 5.9: A schematic illustration of the effect of physical states of lipids on solubilization by the detergent. For the L_0 state, saturated acyl chains do not bind the detergent well, and are insoluble, and. For the Lα state, the detergent can bind well and form mixed bilayers with lipid at subsaturating concentrations. At higher detergent concentrations, micelles form.

Triton X-100 was added to the solution of the vesicles. After mixing and incubation at

22°C overnight (about 19h), the formation of pellets was detected by centrifugation for 10-15 min at medium speed (2600 rpm). For the sample containing 25-OH-Chol the pellets were observed after centrifugation. Solubilization was virtually complete with the control set. It is suggested that the tightly packed ordered phase can be resistant to both detergent binding and solubilization (Fig. 5.9). Therefore, these observations are indicative of the formation of domains in an ordered state that is stable to the extent that its lipid-lipid interactions are stronger than lipid-Triton X-100 interactions. Because SM/POPC mixtures are soluble in Triton X-100, it is most likely that the degree of insolubility reflects interaction between SM and 25-OH-Chol.

More significant is that the solubilization experiments were performed at room temperature, at which the formation of the micro-domains was observed by fluorescence microscopy. These results strongly support the notion that 25-OH-Chol has the ability to pack tightly with sphingomyelin into the ordered phases (micro-domains).

5.5 Conclusions

The results from SPFS and fluorescence imaging suggest that Aß preferentially binds to the micro-domains composed of SM and the sterols. The present results seem to be in line with the observation that Aß enriches in the detergent-insoluble membrane compartment of human neuroblastmoma cells.[134] It is assumed that secreted Aß is internalised into the plasma membrane by the specific interaction with the distinct membrane domains. It was further reported[135;136] that Aß with its sphingolipid-binding motif specifically interacted with SM at the air-water interface. In our case, Aß also prefers SM over POPC, and this preference can be markedly amplified by the addition of sterols. A plausible explanation is that the strong interaction of the sterols (cholesterol or 25-OH-Chol) with SM results in the exposure of more recognition sites to Aß due to the formation of the ordered phase. This hypothesis is supported by other report that the sphingomyelin undergoes the conformational change during the phase transition.[137] In other words, the conformation of SM in the ordered phase much more facilitates Aß to interact with the binding sites on SM than that in the disordered phase.

The results of our studies with SPFS and fluorescence microscopy suggest that 25-OH-Chol should have a stronger interaction with SM than with cholesterol possibly due to the formation of more hydrogen bonds with sphingomyelin. Studies in Chinese hamster ovary cells indicate that 25-OH-Chol stimulates the synthesis of SM. These observations implicate the possibly cooperative role of SM and the sterols in AD.

6 Conformation of Amyloid ß-protein adsorbed on the tethered artificial membrane probed by surface plasmon field-enhanced fluorescence spectroscopy

6.1 Introduction

The close association of amyloid plaques with AD suggest that it is important to understand the mechanism leading to aggregate formation. It is well known that the major component of the plaques is a 1-40 or 42-residue polypeptide (Aß) derived by the proteolytic cleavage of Aß precursor protein (APP), however, it is clear that Aß is a normal constituent of human biological fluids.[138;139] Key question arises as to what makes soluble Aß aggregates. Several reports indicate that the conformation adopted by Aß plays an important role in amyloid formation[140]. It has been demonstrated that Aß with high contents of ß-sheets is far more prone to aggregation.[141;142] Therefore, the conversion of soluble Aß conformation into ß-sheet-rich amyloidogenic intermediate appears to be a nucleation event in the formation of the aggregates. Several factors get involved in this conversion. One of the potential mechanisms for inducing the conformational change of Aß is direct interaction with the membranes. For example, membranes containing ganglioside favor the conversion of soluble Aß into aggregated Aß form. Additionally, the increase in cholesterol contents facilitated this conversion.[143] It is proposed, however, that cholesterol helps prevent the fibrillation by increasing incorporation into membrane if the contents of cholesterol higher than 30mol% (cf. Fig. 6.1).[144] It is obvious that cholesterol as a major component of mammalian cell membranes plays a key role in the formation of plaques.

Cholesterol is susceptible to oxidation to form oxidative derivatives of cholesterol by reactive oxygen species (ROS), which are continuously produced in the body.

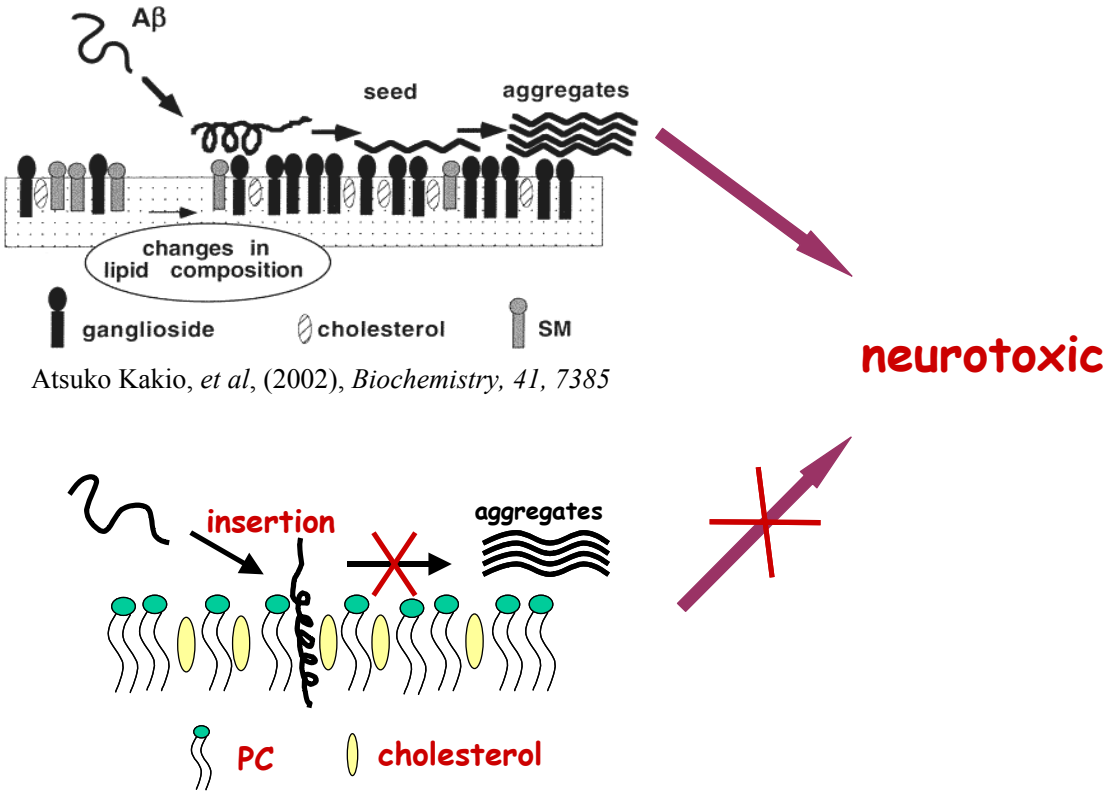

Atsuko Kakio, *et al*, (2002), *Biochemistry, 41, 7385*

Shang-Rong Ji, *et al,* (2002), JBC, 277, 6273

Figure 6.1: Effects of cholesterol contents on Aß-membrane interactions and the formation of aggregates.

It is known that aging is linked to the increased levels of ROS because of the reduction of antioxidants, resulting in excess production of oxysterols. Consequently, the oxidative changes of cholesterol due to ROS in general occur in age-related diseases, such as AD. Cytotoxicity of oxysterols on neurons has been demonstrated, and oxysterols may have been implicated in the etiology of AD. Although the neuronal death is closely related to the formation of oxysterols associated with Aß, it remains unclear whether amyloid plaques are byproduct of cholesterol oxidation. Recently, it is reported that ROS-induced oxidation of cholesterol much easily occurs in bilayers composed of POPC, sphingomyelin and sterol,[145] suggesting possibly prevalent presence of oxysterols in cell membranes during aging process. As mentioned above, the formation of plaques is critically dependent on the lipid composition of membranes, especially on cholesterol

present in membranes. Therefore, the knowledge of the effects of oxysterols on Aß-membrane interaction is very important. It is shown by cell-culture studies that most neuronal cells are very sensitive to 25-hydroxycholesterol (25-OH-Chol) neurotoxicity.[145] Earlier we showed that 25-OH-Chol markedly enhanced Aß adsorption on the membrane in the presence of sphingomyelin. In this Chapter, we further investigate whether this adsorption of Aß is propitious to fibrillogenesis. In order to address this question, we established the model membranes whose distal layers are composed of POPC/sphingomyelin/25-OH-Chol (2:1:1) as described above.

The evidence shows that the type of secondary structure adopted by Aß is closely correlated with the orientation of Aß on membranes. For example, it is reported that Aß with a ß-sheet-rich structure lies completely on the membranes.[146;147] On the other hand, a hydrophobic C-termius of Aß (residues 29-40) corresponding to a part of the transmembrane domain of APP (ß-amyloid procursor protein) is able to insert into membranes by hydrophobic interaction. Furthermore, it has been demonstrated that Aß adorpts mainly an α-helix upon insertion. This effect could be beneficial in reducing the formation of aggregation by depressing the ß-sheet conformation, suggesting that a possible pathway of Aß aggregation may be prevented by its membrane insertion.[148;149] Obviously, knowledge of the orientation of Aß adsorbed on membranes is important to clarify whether the Aß-membrane interaction is favorable to fibrillogenesis or not.

Epitope mapping using pairs of monoclonal antibodies (mAbs) is a tool in examining the surface topography of macromolecules. This method is always applied to characterization of the epitope specificities of mAbs. MAbs directed against separate epitopes will bind independently of each other, whereas mAbs against closely related epitopes will interfere with each other's binding. Aß is an amphilic peptide with a hydrophilic N-terminal domain (residues 1-28) and a hydrophobic C-terminus (residues 29-40), which should be exposed if Aß peptides lie on the membrane planes. Therefore, the orientation of Aß on the model membranes can be determined by testing the ability of a pair of mAbs to bind simultaneously to N- and C-terminal domains of Aß. In this case, a pair of mAbs directed against distinct epitopes (N- or C-terminus) was chosen to detect the orientation of Aß. Surface plasmon field-enhanced fluorescence spectroscopy (SPFS), is employed to measure the binding of the mAbs labelled with a fluorophore to Aß. The binding ability

of the mAbs to Aß was determined by a kinetic analysis of antibody-antigen interactions at the tethered bilayers. Simultaneous binding of paired mAbs to their epitopes (C- and N-terminus) respectively indicates that Aß is preferentially oriented parallel to the membrane surface.

It has been documented that melatonin secreted from the pineal gland can protect neurons against Aß toxicity by inhibiting the progressive formation of ß-sheets and fibrils.[150] In this work, therefore, we investigate whether the effect of melatonin on the conformation of Aß can be probed using pair-wise binding tests of mAbs to Aß on the membranes. Kinetic experiments indicate that the affinity of the first mAb recognizing conformational change in the C-terminus of Aß is significantly reduced due to the presence of melatonin. In contrast, remarkable increase in the affinity of the second mAb against the N-terminus of Aß was observed. These results show that surface plasmon field-enhanced fluorescence spectroscopy can be used to investigate a conformational transformation of adsorbed Aß by analysing the kinetics of binding of paired mAbs labelled with the fluorophores to Aß adsorbed on tethered membranes.

6.2 Materials

Monoclonal anti-ß-Amyloid (1-40) protein antibody directed against conformational epitope within C-terminus was obtained from Merck Biosciences Ltd. It dose not react with ß-amyloid (1-42) peptide. The information provided by the technical specialist of the company indicates that the changes in the conformation of the antibody would obscure the C-terminus of amyloid ß-peptide resulting in the decrease in the affinity of the antibody to the ß-peptide. (Dorothee Bechtloff, personal communication) Immunogen used was a synthetic peptide corresponding to the C-teriminus of the ß-amyloid (1-40) polypeptide, conjugated to KLH. Monoclonal anti-ß-Amyloid protein antibody directed against N-terminus was purchased from Sigma-Aldrich. Immunogen used was a synthetic peptide (1-40) conjugated to KLH. The epitope recognised by the antibody resides within amino acids 1-12 of the ß-amyloid protein.

6.3 Determination of the concentration of the fluorescent antibodies and the degree of labeling

After the labelling with Alexa Fluro 647, the concentration of the antibodies and the degree of labelling were determined by the measurement of the absorbance in a cuvette with a 1cm pathlength at both 280nm (A_{280}) and 650nm (A_{650}) as described in detail in Chapter 4. The concentrations of the antibody against N-terminus and the antibody against C-terminus calculated using the equation 4.1 were 9.0μM and 2.4μM, respectively. The moles dye per mole proteins against N-terminus and C-terminus calculated using the equation 4.2 were 3.5 and 3.1, respectively. The stock solutions of the labeled antibodies were diluted with PBS into the final concentration of 18nM before the pair-wise binding experiments. Moreover, both antibodies have almost the same degree of labeling.

6.4 Pair-wise binding of the fluorescent antibodies to Aß

The Aß solutions were prepared as described in the methods. The matrices were rinsed with PBS before Aß solutions were injected in the flow cell at a flow rate of 36μl/min. After incubation for 20min, the unbound peptide was rinsed out with PBS. The detection of Aß adsorbed on the membranes was conducted in PBS by in turn adding a pair of mAbs labeled with Alexa Fluro 647 directed against distinct epitopes of Aß. Once the background fluorescence was recorded, a 18nM solution of the first antibody was injected and the increase in fluorescence intensity measured as a function of time for 30min. After rinse with PBS for 20min to remove free and loosely associated dye molecules on the membranes, the injection of the same concentration of the second antibody was injected to increase the fluorescence signal.

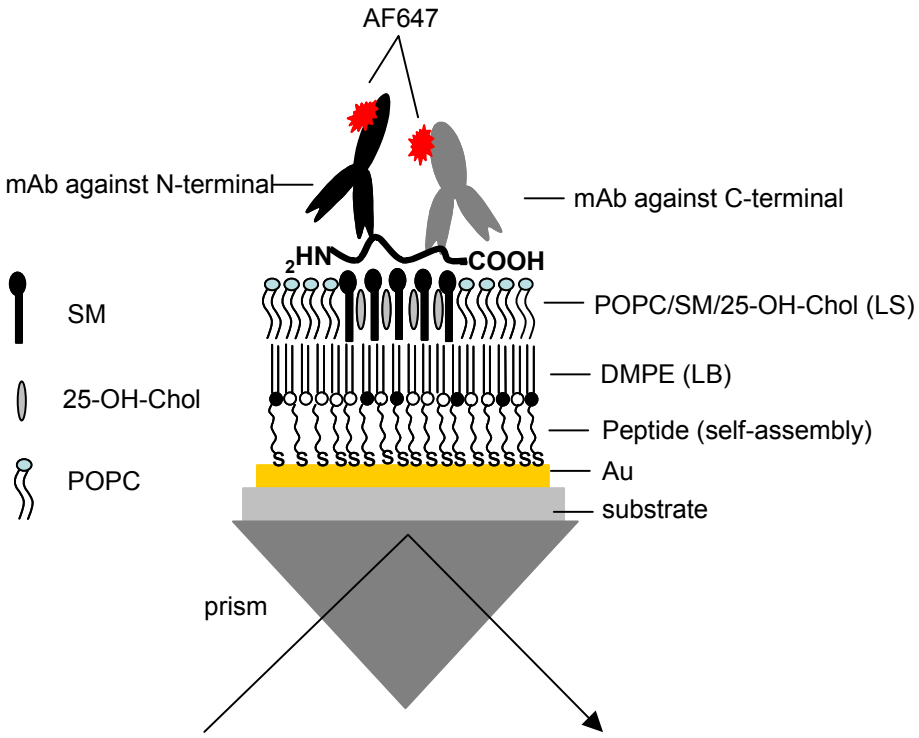

Figure 6.2: Schematic drawing of peptide-tethered membrane for Aß-membrane interaction and pair-wise binding test for the affinity of adsorbed Aß to the mAbs labelled with the AF 647 monitored by SPFS.

Kinetic/affinity parameters between the mAbs and Aß were obtained by fitting to a pseudo-single-exponential kinetic model. The corresponding association process is described by

$$I_{fl}(t) = (I_{max} - I_0)(1 - \exp(-(k_{on}c_0 + k_{off})\, t)) \qquad (1)$$

with I_{max} being the fluorescence intensity measured at the maximum coverage of the mAbs at the concentration of Aß c_0, I_0 is the initial background fluorescence. $I_{fl}(t)$ is the time dependent fluorescence during the association process, which is assumed to be proportional to the number of binding sites occupied by the mAbs at time t. According to the Langmuir model, the corresponding dissociation measured while rinsing pure PBS, i.e., $c_0 = 0$, should follow a single-exponential decay according to

$$I_{fl}(t) = (I_{max} - I_0) \exp(-k_{off} \cdot t) \qquad (2)$$

6.5 The preparation of melatonin sample

A concentrated melatonin solution, 4×10^{-3} M, was prepared as described by C.S.Shida. Similar to the preparation of lipid vesicles a certain amount of melatonin powder was dissolved in chloroform, and then the organic solvent was evaporated under a stream of N_2. Residual solvent was removed under vacuum for at least 3 hours. The solution of melatonin with the desired concentration was obtained in PBS by vortexing. It was clearly shown that melatonin is rather soluable in aqueous medium if it is prepared from a thin film on a glass surface. This is understandable considering that melatonin is an indoleamine for which the pyrrole ring can be polarized to the extent that the N-H group may participate in a hydrogen bond with a water molecule. Moreover, the heterocyclic indole could also form hydrogen bonds with water, similar to a benzene ring, as has been recently reported.[151] Therefore, the role of the film seems to make the melatonin molecule more accessible to water, compared to the packed structure of the powder microcrystals. Another important aspect of the melatonin preparation is that the biological activity of melatonin still holds. Furthermore, melatonin solubilized by this method is highly stable for up to 12 days.[152] The stock solution is kept below 4°C until use.

6.6 The orientation of Aß adsorbed on the model membranes

With the methods described above in detail in Chapter 3, we have successfully built up a model membrane whose distal layer is composed of POPC/SM/25-OH-Chol (2:1:1) to which the orientation of Aß was investigated.

IgG is a bivalent molecule (with two recognition sites per moleule). Antibodies behave very differently in solution than that at a surface. Studies of antibody binding using radiolabeled antibodies have shown the measured affinity constants at surfaces are sensitive to numerous experimental variables, such as the volume of incubation and the antigen surface density. Its binding constant to the surface-attached ligands is dependent on a ligand density due to the accecibility of antigenic epitope, which is usually termed as

"avidity" phenomena.[153] In the bivalent binding model the first event occurs when the bivalent antibody binds from the bulk solution phase to a surface-bound ligand. The second event occurs when a surface-bound monovalent complex binds a second ligand molecule at the surface.

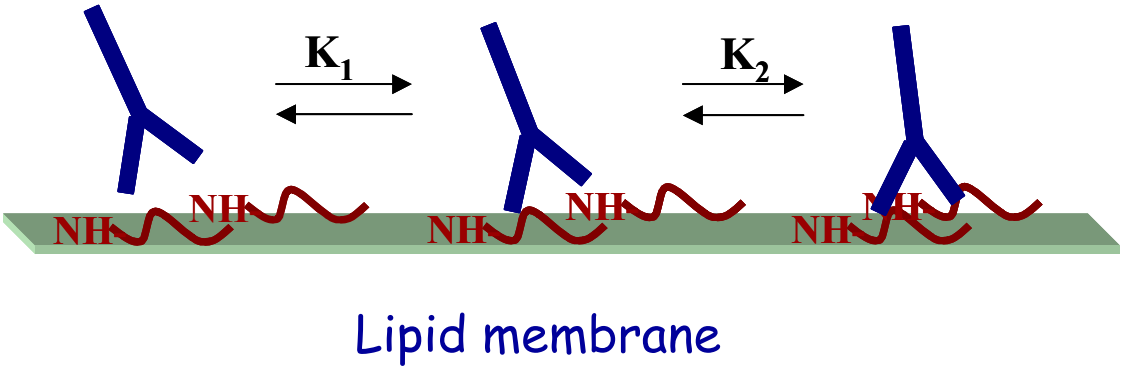

Figure 6.3: Cartoon depicting the two-step binding event of a bivalent antibody for two Aß peptides adsorbed onto the membrane surface.

For the first binding event between the antibody in solution phase and the peptides bound to the membrane surface, the antibody is free to sample all orientations in three-dimentsional space to adorpt the correct geometry for binding. For the second binding event, the two reactants are now both tethered to the surface and the resulting constraint on the number of accessible orientations of each reactant could possibly limit the association rate. It was reported that the observed rate for the second binding of a bivalent antibody to the antigens at a supported lipid monolayer was much slower than the first binding event,[154] and thus it is reasonable that monovalent binding of the antibody in the solution phase preferentially occurs to Aß bound to the model membrane. Furthermore, the purpose of this study is not to extract true intrinsic binding constants from the measurements, but to gain insight into the orientation of Aß at the surface by making a comparison between the affinities of paired mAbs to Aß. Therefore, we analyse the binding events between the antibodies and Aß using a simple bimolecular model. Fig.6.4 (A) and (B) show that a good fit could be obtained from a simple 1:1 binding algorithm,

which indicates a 1:1 interaction stoichiometry between the antibodies and the surface peptides.

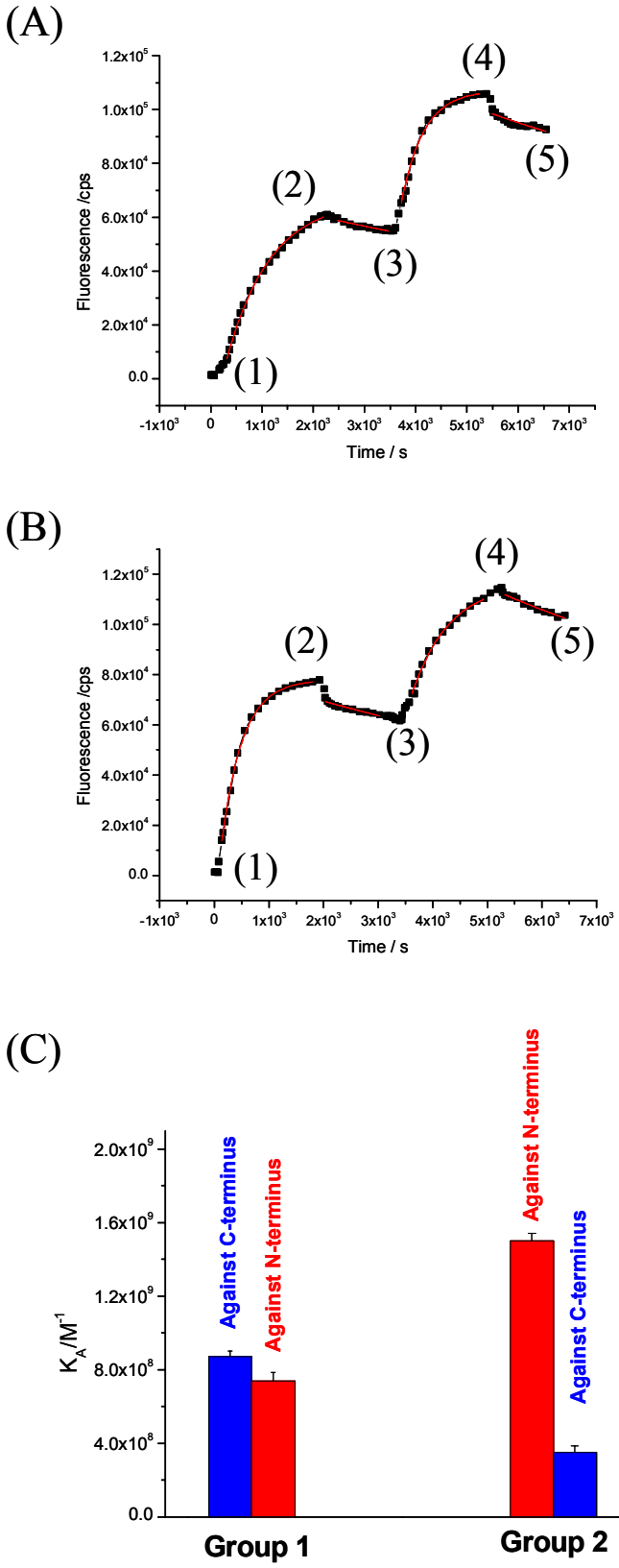

Figure 6.4: (A) The dashed curves depicting binding experiment between Aß adsorbed on the model membrane and the mAbs labelled with the fluorophores. (1)-(2) the mAb against C-terminal, (2)-(3) rinse with PBS, (3)-(4) the mAb against N-terminal, (4)-(5) rinse with PBS. Solid line curves were obtained by fitting to a pesudo-single-exponential kinetic model. (B) The dashed curves depicting binding experiment between Aß adsorbed on the model membrane and the mAbs labelled with the fluorophores. (1)-(2) the mAb against N-terminal, (2)-(3) rinse with PBS, (3)-(4) the mAb against C-terminal, (4)-(5) rinse with PBS. Solid line curves were obtained by fitting to a pesudo-single-exponential kinetic model. (C) Affinity of paired mAbs against separated epitopes to Aß adsorbed on the membrane. K_A, association constant; For group 1, the first mAb is against C-terminal (hatched bar) and the second mAb is against N-terminal (closed bar); For group 2, the first mAb is against N-terminal (closed bar) and the second mAb is against C-terminal hatched bar). For each group, left bar: the first antibody, right bar: the second antibody.

The kinetic data are considered to be reliable in a quantitative sense: the agreement between the measured time-dependent fluorescence intensities and the simulated kinetics is excellent over the whole experiment range. For group 1, both mAbs have similar affinity to Aß by fitting to a pesudo-single-exponential kinetic model if the antibody directed against C-terminus of Aß was firstly reacted with Aß petides on the membranes (Fig. 6.4C).

However, k_{on} values obtained from Eq. (1) show that the mAb against N-terminus has a stronger association with Aß at the surface than the mAb against C-terminus (cf. Table 6.1). The reason for the resulting lower overall affinity of the former antibody is the faster dissociation rate between the second mAb and Aß (cf. Table 6.1). In order to get more insight into mechanism of reduced affinity of the second mAb, reversed-order pair-wise binding of the mAbs to Aß was performed. Fig. 6.4C shows a significant increase in the affinity of the mAb against N-terminal (mAb-N) to Aß if it was fistly injected over the surface. Increased k_{on} and reduced k_{off} cooperatively contributed to the enhanced affinity of mAb-N to Aß. Compared to the mAb against C terminal (mAb-C) in group 1, remarkable decrease in the association constant was found in the interaction of the second antibody (mAb-C) and adsorbed Aß (shown in group 2). Association rate between mAb-C and Aß was slightly lower than that as the mAb being the first antibody, but very rapid dissociation rate resulted in a lower overall affinity. Obviously, the affinity of the mAbs to Aß was significantly affected by the injecting order of them over the membrane surfaces.

Table 6.1: Kinetic characterization of the interaction between paired mAbs and Aß adsorbed on the model membranes

A pair of monoclonal antibodies		k_{on} ($M^{-1}s^{-1}$)	k_{off} (s^{-1})	K_A (M^{-1})	K_D (M)
Group (1)	first /against C-terminal	6.1×10^{4}	7.0×10^{-5}	8.7×10^{8}	1.1×10^{-9}
	second /against N-terminal	1.2×10^{5}	1.6×10^{-4}	7.4×10^{8}	1.4×10^{-9}
Group (2)	first /against N-terminal	1.4×10^{5}	9.0×10^{-5}	1.5×10^{9}	6.5×10^{-10}
	second /against C-terminal	7.0×10^{4}	2.0×10^{-4}	3.5×10^{8}	2.9×10^{-9}

Rate constants, k_{on} and k_{off}, affinity constant, K_A, and the dissociation constant, K_D, as determined from the kinetic experiments for sequential binding of paired mAbs to Aß adsorbed on the membranes.

It was suggested that the N-terminal region of the ß-peptide is the immunodominant site in Aß,[155] which has higher binding affinity to the mAbs compared with the C-terminus of the ß-peptide. However, our results indicate that binding affinity of the mAb to N-terminus is lower than that of the mAb to C-terminus if the antibody against C-termimus was reacted with Aß followed by the mAb against N-terminus (cf. Fig.6.4C Group 1). The plausible reason for reduced binding affinity of the mAb against to N-terminus is that steric hindrance due to the occupation of the first mAb will interfere with the binding of the second one to Aß. Although we chose a pair of mAbs against distinct epitopes, it is possible for them to interfere with each other's binding to the Aß peptide on the membranes because the mAb (IgG) used in this work is a large protein (150 kDa) with a shape usually compared to a disk of diameter 12nm and thickness of 4-5nm.[156] Furthermore, the N-terminal domain (residues 1-12) and C-terminal domain (residues 29-40) respectively recognised by the antibodies, are not far away from each other. Therefore, the ability of the second antibody to bind to the surface peptides should decrease due to steric crowding if one of two binding sites of Aß is occupied by the first antibody. Without the interference of the mAb against C-terminus, the binding affinity of the antibody to the N-terminus is considerable higher than that of the antibody to the C-terminus. (cf. Fig. 6.4C)

Antibody-antigen interactions invole conformational changes in both antibody and antigen that can range from insignificant to considerable.[157-159] It was found that binding of high affinity of the mAb to N-terminal region of ß-peptide may alter the molecular dynamics of the whole protein chain or assembly. Increasing evidence indicates that only antibodies against N-terminus of ß-amyloid peptide are effective in leading to disaggregation of the fibrils and partial restoration of the peptide solubility, whereas those against C-terminal epitopes are inactive.[160;161] The transition of the α-helix to a ß-sheet conformation, with concomitant peptide aggregation, is a proposed mechanism of plaque formation. These findings suggest that the binding of the mAbs to the N-terminal region of Aß can induce significant conformational changes resulting in the decrease in the content of the ß-sheet. The binding of the mAb to the C-terminus has little influence on the conformation of Aß. Therefore, the reduced affinity of the antibody to N-terminus is only ascribed to the effect of steric hindrance. It is obvious that the decrease in the affinity of the antibody to the N-terminus is closely related to the binding of the mAb to the C-terminus of Aß. Because the mAb directed against C-terminus recognise conformational epitopes of Aß, the effects of not only the steric crowding but also the conformational change on the affinity of the antibody to the C-terminus should be taken into account. Compared to that in Group 1, the antibody did not efficiently recognize the C-terminus of Aß is presumably because the peptide underwent partial conformational changes upon the the binding of the mAb to the N-terminus of Aß.

These interpretations were supported by the fact that reversed-order binding tests have significant influence on the k_{off} values of both mAbs (cf. Table 6.1). K_{off} values show that the first binding has the effects of increasing dissociation rate between the second mAb and adsorbed Aß as fast as two times. In the case of the mAb against N-terminus, the great increase in dissociation rate is rational presumably because the antibody against C-terminus bound to Aß limits it to adopt correct orientation for binding which leads to rapid dissociation of the complex (antibody-Aß). The conformational changes also contribute to the high dissociation rate of the complex of the mAb-C and Aß. The decrease in k_{on} values of the mAbs was also observed if they reacted with Aß secondly, suggesting that availability and accessibility of the sites on the peptides were reduced due to the binding of the first antibody. Therefore, the interference tests of each other's

binding indicate that both mAbs directed against distinct sites (N- and C-terminus) are able to recognize Aß, suggesting that Aß preferably lies on the membrane surface. Taken together, we can depict the orientation of Aß on the model membrane by analysing kinetic/affinity parameters.

It is known that Aß may be oriented either parallel or perpendicular to the plane of bilayer, depending on the composition of lipid. Recently, sphingolipid-binding residues has been identified in Alzheimer, Prion and HIV proteins.[162] For the model membrane composed of POPC/SM/25-OH-Chol, therefore, SM is probably the binding sites of Aß-membrane interaction. The plausible explanation for the role of 25-OH-Chol in Aß binding is that it can induce the recognition sites of SM to expose to binding motif of Aß by changing the physical state of SM. This hypothesis is supported by other report that the sphingomyelin undergoes the conformational change during the phase transition.[163] This work presented above show that both N- and C-terminus of Aß were detected on the membrane surface, suggesting that the interaction of Aß with the membrane was mainly governed by the specific binding between Aß and SM instead of hydrophobic forces. Therefore, it may be concluded that lipid composition of this model membrane favors Aß adsorption taking an orientation parallel to the membrane surface possibly responsible for the nucleation of fibril formation, which is a neuropathologic feature of AD. It is proposed that insertion of Aß into membranes can prevent fibril formation. [148;149] In this regard, the coexistence of 25-OH-Chol and Sphingomyelin (SM) is obviously a potential risk factor for the onset of AD. On the other hand, it has been demonstrated that the formation of fibrils is critically dependent upon the secondary structure in Aß.[150] Several lines of observations are that ß-sheet conformation of Aß is prerequisite for the fibrillization of Aß.[122;164] In addition, membrane-mediated conformational transition from helix-rich to ß-sheet-rich structures has been extensively studied in many model systems,[147;149;165;166] which implicates a profound influence of membrane structure on the process of AD. Therefore, detecting conformational change of Aß adsorbed membranes will give an insight into the pathogenesis of AD.

6.7 Effects of melatonin on the binding of the mAbs to Aß

We assess whether the conformational change can be monitored by the immunoassay as described above. In this work, melatonin is employed to control conformation of Aß because it has been comprehensively reported as an inhibitor for the formation of ß-sheet of Aß.[150;167;168] It was reported by Miguel Pappolla that original ß-sheet content of Aß was markedly diminished after 24h incubation with melatonin, whereas random conformation significantly increased. Meanwhile, the increase of ß-sheet content of Aß incubated alone was observed. (cf. Table 6.2)

Table 6.2: Effects of melatonin on the secondary structure of Aß

	Aß alone incubation		Aß+ melatonin
	0h	24h	incubation 24h
α-helix	2	1	3
ß-sheet	52	66	24
ß-turn	29	26	18
random	16	7	55

Miguel Pappolla, *et al*, (1998), JBC, 7185-7188

In this case, the mAbs directed against C-terminal was always used as the first antibody. The ratio of melatonin and Aß used in this study was consistent with that under physiological conditions. We incubated Aß with melatonin for 48h in PBS to produce a significant change in the conformation of Aß. In order to exactly evaluate the effects of melatonin, Aß alone was also incubated under the same conditions as the mixture of Aß and melatonin. Binding behaviours of paired mAbs to Aß incubated alone and with melatonin were characterized by analysing kinetic parameters, respectively.

(A)

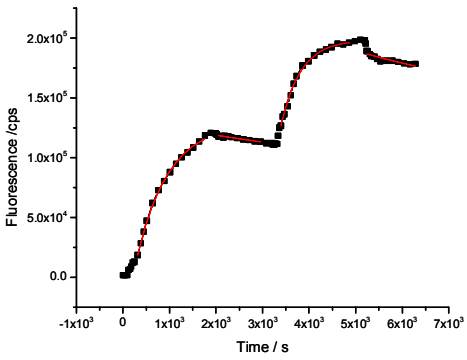
Fluorescence /cps
2.0x10^5
1.5x10^5
1.0x10^5
5.0x10^4
0.0
-1x10^3
0
1x10^3
2x10^3
3x10^3
4x10^3
5x10^3
6x10^3
7x10^3
Time / s

(B)

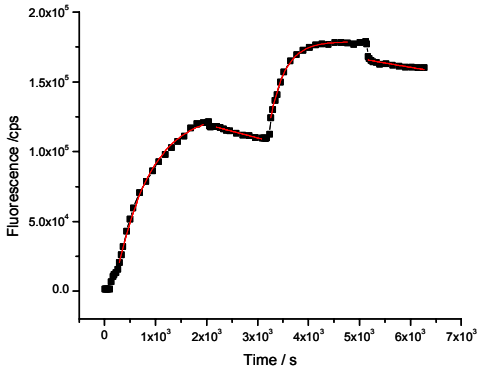
Fluorescence /cps
2.0x10^5
1.5x10^5
1.0x10^5
5.0x10^4
0.0
0
1x10^3
2x10^3
3x10^3
4x10^3
5x10^3
6x10^3
7x10^3
Time / s

(C)

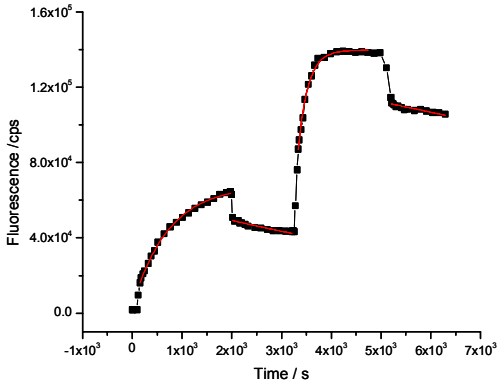
Fluorescence /cps
1.6x10^5
1.2x10^5
8.0x10^4
4.0x10^4
0.0
-1x10^3
0
1x10^3
2x10^3
3x10^3
4x10^3
5x10^3
6x10^3
7x10^3
Time / s

(D)

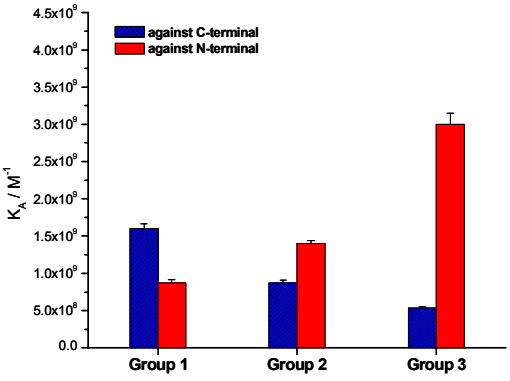
against C-terminal
against N-terminal
K_A / M^-1
4.5x10^9
4.0x10^9
3.5x10^9
3.0x10^9
2.5x10^9
2.0x10^9
1.5x10^9
1.0x10^9
5.0x10^8
0.0
Group 1
Group 2
Group 3

Figure 6.5: (A)-(C) The dashed curves depicting binding experiment between Aß adsorbed on the model membrane and the mAbs labelled with the fluorophores. Solid line curves were obtained by fitting to a pesudo-single-exponential kinetic model. (D) Effects of melatonin on the affinity between paired mAbs and Aß adsorbed on the model membranes. For three groups, it is always the case of the first mAb against C-terminal and the second mAb against N-terminal. For group1, Aß alone was stored at room temperature for 48h; For group 2, fresh Aß was mixed with melatonin for 10min; For group 3, fresh Aß incubated with melatonin for 48h. For each group, left bar: the first antibody, right bar: the second antibody.

A brief comment about the interaction of melatonin with the model membrane is needed before discussing the results obtained in pair-wise binding tests. It was reported that melatonin was able to interact with DMPC bilayer causing a significant fluidifying effect.[169] The increase in the membrane fluidity induced by melatonin should have little influence on the interaction of the antibodies and the model membrane, however, because our results shown above and other literature have evidenced that the adsorption of the proteins onto the membrane is mainly dependent on the lipid composition of the membrane. As to the interaction of Aß with the membrane, the fluidifying effect of melatonin on the membrane would presumably change the binding behaviour of Aß to the membrane. In order to exclude the effect of melatonin on Aß binding to the membrane, the same concentration of melatonin was employed to incubate with Aß. Therefore, the different affinity of the antibodies to Aß on the membrane just comes from the conformational changes of Aß caused by melatonin.

Fig. 6.5D shows that the bar graphs of group 1 and group 3 are markedly distinct. For Aß incubated alone (group 1), the affinity of the first antibody (mAb-C) to Aß is stronger than the second one (mAb-N). This result has a similar trend to that described above (Fig. 6.4C group 1), but much less affinity of the second mAb than that of the first one was observed. Table 6.2 shows that the contents of ß-sheet of Aß increase from 52 to 66 after 24-hour incubation. According to the product information provided by Merck Biosciences Ltd., the conformational changes of Aß will greatly affect the recognition of the antibody directed against C-terminus to Aß. Moreover, the affinity of the antibody to the C-terminus depends on the type of conformational change. The contribution of the C-terminal region of Aß in the initiation and progression of ß-sheet formation has been established.[170-172] Therefore, the antibody was generated using a synthetic peptide corresponding to the C-terminus of the ß-amyloid (1-40) as immunogen prefers to

recognise the conformation of ß-sheet. Thus, it is postulated that high contents of ß-sheet favor the binding of the antibody to C-terminus resulting in higher affinity of it to Aß on the membrane. More binding of the first antibody to the Aß peptides has a greater effect of reducing the binding of the second one due to steric crowding. After the incubation of Aß with melatonin for 48 hours, however, significant decrease in the affinity of the first antibody was observed compared to group 1 in Fig.6.5D. More interesting is that the ability of the second antibody (mAb-N) to bind to the Aß peptides considerably increased (Fig. 6.5D group3). The contribution of the C-terminal region of Aß in the initiation and progression of ß-sheet formation has been established.[173-175] Therefore, the antibody was generated using a synthetic peptide corresponding to the C-terminus of the ß-amyloid (1-40) as immunogen prefers to recognise the conformation of ß-sheet. When the conformation of Aß was changed greatly by melatonin, remarkable decrease in the contents of ß-sheet disfavoured the recognition of the antibody to C-terminus. The k_{on}/k_{off} values of mAb-C indicate that the presence of melatonin slightly decreased the association rate but significantly increased the dissociation rate (Table 6.3), suggesting that conformational change obscured the C-terminal recognised by the antibody. Consequently, incorrect binding of mAb-C to Aß destabilized the complex, which then dissociated at a faster rate. The rapid dissociation of mAb-C and Aß reduced the amount of the mAb-C bound to Aß on the surface, which gives the second antibody more freedom to seek out correct orientation for binging. Fig. 6.5D shows that the affinity between the second antibody and Aß is considerably stronger than the first one (group 3), most likely because the effects of steric hindrance have faded away. On the other hand, the present results show that the affinity of the mAb to the N-terminus is independent on the conformational changes of Aß, which is agreement with other's work and further supports the above results. The k_{on} values of mAb-N notablely enhanced after Aß incubated with melatonin (Table 6.2) comparable with the case of fresh Aß alone (Table 6.1). This increase is interpreted as being mainly caused by the increase in the number of accessible orientations of Aß. Therefore, the effects of melatonin on the conformation of Aß could be probed by calculating kinetic parameters of mAb-C.

Table 6.3: Effects of melatonin on the interaction between paired mAbs and Aß adsorbed on the model membranes

A pair of monoclonal antibodies		k_{on} ($M^{-1}s^{-1}$)	k_{off} (s^{-1})	K_A (M^{-1})	K_D (M)
Aß alone	first /against C-terminal	7.9×10^{4}	5.0×10^{-5}	1.6×10^{9}	6.4×10^{-10}
	second /against N-terminal	1.2×10^{5}	1.4×10^{-4}	8.7×10^{8}	1.1×10^{-9}
Aß+Mel 10min	first /against C-terminal	7.9×10^{4}	9.0×10^{-5}	8.7×10^{8}	1.1×10^{-9}
	second /against N-terminal	1.8×10^{5}	1.3×10^{-4}	1.4×10^{9}	7.2×10^{-10}
Aß+Mel 48h	first /against C-terminal	6.9×10^{4}	1.3×10^{-4}	5.3×10^{8}	1.9×10^{-9}
	second /against N-terminal	2.7×10^{5}	9.0×10^{-5}	3.0×10^{9}	3.3×10^{-10}

It was reported that the conformational changes of Aß occur immediately after addition of melatonin. In order to test whether the early changes can be detected, we performed the experiments for measuring the interactions of adsorbed Aß and the antibodies after mixing of Aß with melatonin for only10 minutes. Group 2 in Fig. 6.5D clearly shows that the affinity of mAb-C to Aß become lower than that of the second antibody (mAb-N). The effects of melatonin on Aß were only exhibited in increased k_{off} values of mAb-C, indicating that some antibodies bound to C-terminal are unstable at Aß possibly because of conformational transformation caused by melatonin. As discussed above, dissociated antibodies from Aß on the surface provides the second one more space for binding at a correct direction. As would be expected, the k_{on} and k_{off} values of the second antibody show the faster association and slower dissociation of the complex (antibody-Aß) after treatment with melatonin for 10 minutes (cf. Table 6.3). These results indicate that melatonin can change the conformation of peptides in a short time.

It has been proposed that proteolytic enzymes easily degrade Aß peptides with low contents of ß-sheets[150] induced by melatonin, which has implicated physiological role of melatonin in the physiopathology of AD. We assume that peptides adsorbed on membranes are readily removed by proteolytic degradation in normal brains because

melatonin prevents the formation of ß-sheet structure. We propose that there should be a dynamic competition between membrane structure and melatonin with respect to causing conformational transformation of Aß on membranes. When the level of melatonin is extremely low such as in AD[176], the lipid composition of membrane will play a dominant role in mediating conformational changes. Therefore, it is significant for the prevention of AD to identify the mechanism on age-related deficiency of this hormone and to slow or even reverse the reduction of melatonin.

6.8 Conclusions

Understanding of the details of interactions between Aß peptides and membranes is very important for the investigations on the pathogenesis and treatment of Alzheimer's disease. In this study, high sensitive SPFS allows for a very detailed and quantitative evaluation of the kinetics and the affinities of the association and dissociation reactions between paired mAbs against different epitopes and Aß peptides on the model membrane. The orientation and distribution of Aß adsorbed on peptide-tethered membranes were determined by carefully analysing kinetic parameters. The combination of SPFS and immunosensitive analysis based on paired monoclonal antibodies successfully detect the conformational changes caused by melatonin. The present work can certainly be extended to any study on protein-membrane interactions. Moreover, the peptide-tethered lipid membrane provides a novel experimental platform for these investigations.

7 SUMMARY

The amyloid peptide (Aß), a normal constituent of neuronal and non-neuronal cells, has been shown to be a major component of the extracellular plaque of Alzheimer's disease (AD). The interaction of Aß peptides with the lipid matrix of neuronal cell membranes plays an important role in the pathogenesis of AD. In this study, we have developed peptide-tethered artificial lipid membranes by the Langmuir-Blodgett and Langmuir-Schaefer methods. Anti-Aß40-mAb labeled with a fluorophore was used to probe the Aß40 binding to the model membrane system. Systematic studies on the antibody or Aß-membrane interactions were carried out in our model systems by Surface Plasmon Field-Enhanced Fluorescence Spectroscopy (SPFS). Aß adsorption is critically determined by the lipid composition of the membranes. Aß specifically binds with membranes of sphingomyelin, and this preferential adsorption was markedly amplified by the addition of sterols (cholesterol or 25-OH-Chol). Fluorescence microscopy indicated that 25-OH-Chol could also form micro-domains with sphingomyelin as cholesterol does at the conditions used for the built-up of the model membranes. Our findings suggest that micro-domains composed of sphingomyelin and the sterols could be the binding sites of Aß and the role of sphingomyelin in AD should receive much more attention. The artificial membranes provide a novel platform for the study on AD, and SPFS is a potential tool for detecting Aß-membrane interaction.

Numerous investigations indicate that the ability of Aß to form fibrils is considerably dependent upon the levels of ß-sheet structure adopted by Aß. Membrane-mediated conformational transition of Aß has been demonstrated. In this study, we focus on the interaction of Aß and the membranes composed of POPC/SM/25-OH-Chol (2:1:1). The artificial membrane system was established by the methods as described above. Immunoassy based on a pair of monoclonal antibodies (mAbs) against different epitopes was employed to detect the orientation of the Aß at the model membranes. Kinetics of

antibody-Aß binding was determined by surface plasmon field-enhanced fluorescence spectroscopy (SPFS). The attempt has also been made to probe the change in the conformation of Aß using SPFS combined with immunoassay. Melatonin was employed to induce the conformational change of Aß. The orientation and the conformational change of Aß are evaluated by analysing kinetic/affinity parameters. This work provides novel insight into the investigation on the structure of Aß at the membrane surface.

8 SUPPLEMENT

8.1 List of Figures

8.2 List of Tables

8.3 Bibliography

Reference List

1. Etemadi, A. *Biochimica et Biophysica Acta* **1980,** *604*, 347-422.
2. Selkoe, D. J. *Physiological Review* **2001,** *81*, 741-60.
3. Hardy, J.; Selkoe, D. J. *Science* **2002,** *297*, 353-56.
4. Glenner, G. G.; Wong, C. W. *Bicochemical and Biophysical Research Communication* **1984,** *120*, 885.
5. Mann, D. M. *Neurobiol.Aging* **1989,** *10*, 397-99.
6. Mann, D. M. *Neurobiol.Aging* **1989,** *10*, 397-99.
7. Hardy, J.; Allsop, D. *Trends Pharmacol.Sci.* **1991,** *12*, 383-88.
8. Selkoe, D. J. *Trends Cells Biol.* **1998,** *8*, 447-53.
9. Price, D. L.; Sisodia, S. S. *Annu.Rev.Neurosci.* **2005,** *21*, 479-505.
10. Younkin, S. G. *Ann.Neurol* **1995,** *37*, 287-88.
11. Wisniewski, T.; Frangione, B. *Neurobiol.Aging* **1994,** *15*, 143-52.
12. Yankner, B. A. *Neuron* **1996,** *16*, 921-32.
13. Haass, C.; et al *Nature* **1992,** *359*, 322-25.
14. Seubert, P.; et al *Nature* **1992,** *359*, 325-27.
15. Shoji, M.; et al *Science* **1992,** *258*, 126-29.
16. Soto, C.; Castano, E. M.; Kuma, R. A.; Beavis, R. C.; Frangione, B. *Neurosci.Lett.* **1995,** *200*, 105-08.
17. Jarret, J. T.; Berger, E. P.; Lansbury, P. T. *Biochemistry* **1993,** *32*, 4693-97.
18. Snyder, S. W.; Ladror, U. S.; Wade, W. S.; Wang, G. T.; Barrett, G. T. *Biophaysical Journal* **1994,** *67*, 1216-28.
19. Barrow, C. J.; Yasuda, A.; Kenny, P. T.; Zagorski, M. G. *J.Mol.Biol.* **1992,** *225*, 1075-93.
20. Soto, C.; Castano, E. M.; Frangione, B.; Inestrosa, N. C. *J.Biol.Chem* **1995,** *270*, 3063-67.
21. Soto, C.; Castano, E. M. *Biochem, J.* **1996,** *314*, 701-07.
22. Soto, C.; Castano, E. M. *Biochem, J.* **1996,** *314*, 701-07.
23. Soto, C. *Molecular Medicine Today* **1999,** *5*, 343-50.

24. Mclaurin, J.; Franklin, T.; Chakrabartty, A.; Fraser, P. E. *J.Mol.Biol.* **1998,** *278*, 183-94.

25. Choo-Smith, L.-P.; Garzon-Rodriguez, W.; Glabe, C. G.; Surewicz, W. K. *J.Biol.Chem* **1997,** *272*, 22987-90.

26. Matsuzaki, K.; Horikiri, C. *Biochemistry* **1999,** *38*, 4137-42.

27. Kakio, A.; Nishimoto, S.; Yanagisawa, K.; Kozutsumi, Y.; Matsuzaki, K. *The Journal of Biological Chemistry* **2001,** *276*, 24985-90.

28. Kakio, A.; et al *Biochemistry* **2002,** *41*, 7385-90.

29. Ji, S.; Wu, Y.; Sui, S. *The Journal of Biological Chemistry* **2002,** *277*, 6273-79.

30. Micelli, S.; Meleleo, D.; Picciarelli, V.; Gallucci, E. *Biophysical Journal* **2004,** *86*, 2231-37.

31. Koppaka, V.; Axelsen, P. H. *Biochemistry* **2000,** *39*, 10011-16.

32. Stenhagen, E. Determination of organic structures by physical methods*,* 1955.

33. Nutting, G. C.; Harkins, W. D. *J.Am.Chem.Soc.* **1939,** *61*, 1180-87.

34. Marsden, J.; Rideal, E. K. *J.Chem.Soc.* **1938,** 1163-71.

35. Puu, G.; Gustafson, I.; Artursson, E. *Biosens Bioelectron* **1995,** *10*, 463-76.

36. Duschl, C.; Boncheva, M.; Vogel, H. *Biochim.Biophys.Acta* **1998,** *1371*, 345-50.

37. Young, T. *Philos.Trans.R.Soc.London* **1805,** *95*, 65.

38. Zisman, W. A. Advances in Chemistry Series*,* 1964.

39. Fowkes *Ind.Eng.Chem.* **1964,** *12*, 52.

40. Driedger, O.; Neumann, A. W.; Sell, P. J. *Kolloid-Z.Z.Polym.* **1965,** *201*, 52.

41. Neumann, A. W.; Good, R. J.; Hope, M. S. *J.Colloid Interface Sci.* **1974,** *49*, 291.

42. Owens, D. K.; Wendt, R. C. *J.Appl.Polym.Sci.* **1969,** *13*, 1741.

43. van Oss, C. J.; Chaudhury, M. K.; Good, R. J. *Chem.Revs.* **1988,** *88*, 927.

44. Good, R. J.; van Oss, C. J. Moden Approaches to Wettability:Theory and Applications*,* 1992.

45. Stine, K. J. *Microsc Res Tech* **1994,** *27*, 439.

46. Rondelez, F. 1991.

47. Knobler, C. M. *Science* **1990,** *249*, 870.

48. Moewald, H. *Rep Prog Phys* **1993,** *56*, 653.

49. Ritchie, R. H. *Phys.Rev.* **1957,** *106*, 874.

50. E Kretschmann, Z. *Phys.* **1971,** *241*, 313.

51. Nelson, B. P.; Frutos, A. G.; Brockman, J. M.; Corn, R. M. *Analytical Chemistry* **1999,** *71*, 3928.

52. Frutos, A. G.; Weibel, S. C.; Corn, R. M. *Analytical Chemistry* **1999,** *71*, 3935.

53. Haeussling, L.; Ringsdolf, H.; Schmitt, F. J.; Knoll, W. *Langmuir* **1991,** *7*, 1837-40.

54. Schmidt, A.; Spinke, J.; Bayerl, T.; Sackmann, E.; Knoll, W. *Biophys.J.* **1992,** *63*, 1385-92.

55. Jung, L. S.; Nelson, K. E.; Campbell, C. T.; Stayton, P. S.; Yee, S. S.; Perez-Luna, V.; Lopez, G. P. *Sens.Actuators* **1999,** *B54*, 137-44.

56. Spinke, J.; Liley; M.; Guder, H. J. *Langmuir* **1993,** *9*, 1821-25.

57. Raether, H. Surface Plasmons on Smooth and Rough Surfaces and on Gratings, Springer-Verlag: 1988.

58. Nemetz, A.; Knoll, W. *Journal of Raman Spectroscopy* **1996,** *27*, 587-92.

59. Axelrod, D.; Burghardt, T. P.; Thompson, N. L. *Annual Review of Biophysics and Bioengineering* **1984,** *13*, 247-68.

60. Liebermann, T.; Knoll, W. *Colloid and Surfaces A-Physicochemical and Engineering Aspects* **2000,** *171*, 115-30.

61. Winzor, D. J.; Sawyer, W. H. Quantitative Characterisation of Ligand Binding, 1st Edition ed.; Wiley-Liss: 1995.

62. Atkins, P. W. Physical Chemistry, 6th Edition ed.; Oxford University Press: 1998.

63. Ji, S.; Wu, Y.; Sui, S. *The Journal of Biological Chemistry* **2002,** *277*, 6273-79.

64. Kakio, A.; et al *Biochemistry* **2002,** *41*, 7385-90.

65. Micelli, S.; Meleleo, D.; Picciarelli, V.; Gallucci, E. *Biophysical Journal* **2004,** *86*, 2231-37.

66. Ji, S.; Wu, Y.; Sui, S. *The Journal of Biological Chemistry* **2002,** *277*, 6273-79.

67. Mozsolits, H.; Wirth, H.-J.; Werkmeister, J.; Aguilar, M.-I. *Biochimica et Biophysica Acta* **2001,** *1512*, 64-76.

68. Kakio, A.; et al *Biochemistry* **2002,** *41*, 7385-90.

69. Buboltz, J. T.; Feigenson, G. W. *Biochimica et Biophysica Acta* **1999,** *1417*, 232-45.

70. Silvius, J. R. *Biochimica et Biophysica Acta* **2003,** *1610*, 174-83.

71. Jelinek, R.; Kolusheva, S. *Current Protein and Peptide Science* **2005,** *6*, 1-12.

72. Knoll, W.; Frank, C. W.; Heibel, C.; Naumann, R.; Offenhaeusser, A.; Ruehe, J.; Schmidt, E. K.; Shen, W. W.; Sinner, A. *Reviews in Molecular Biotechnology* **2000,** *74*, 137-58.

73. Rothman, J. E.; Lenard, J. *Science* **1977,** *195*, 743-53.

74. Etemadi, A. *Biochimica et Biophysica Acta* **1980,** *604*, 423-75.

75. Devaux, P. F. *Curr Opin Struct Biol* **1993,** *3*, 489-94.

76. Gordon, J. G.; Swalen, J. D. *Optics Communications* **1977,** *22*, 374-76.

77. Aust, E. F.; Sawodny, M.; Ito, S.; Knoll, W. *Scanning* **1994,** *16*, 353-61.

78. Marsh, D. *Biochemica et Biophisica Acta* **1996,** *1286*, 183-223.

79. Arispe, N.; Rojas, E.; Pollard, H. B. *Proc.Natl.Acad.Sci.USA.* **1993,** *90*, 567-71.

80. Pike, C. J.; Burdick, D.; Walencewicz, A. J.; Glabe, C. G.; Cotman, C. W. *J.Neurosci.* **1993,** *13*, 1676-87.

81. Iverson, L. L.; Mortishire-Smith, R. J.; Pollack, S. J.; Shearman, M. S. *Biochem.J.* **1995,** *311*, 1-16.

82. Mclaurin, J.; Chakrabartty, A. *Eur.J.Biochem.* **1997,** *245*, 355-63.

83. Fantini, J.; Garmy, N.; Mahfoud, R. Expert reviews in molecular medicine*,* 2002.

84. Kakio, A.; Nishimoto, S.; Yanagisawa, K.; Kozutsumi, Y.; Matsuzaki, K. *The Journal of Biological Chemistry* **2001,** *276*, 24985-90.

85. Mahfoud, R.; et al *The Journal of Biological Chemistry* **2002,** *277*, 11292-96.

86. Ji, S.; Wu, Y.; Sui, S. *The Journal of Biological Chemistry* **2002,** *277*, 6273-79.

87. Kakio, A.; Nishimoto, S.; Yanagisawa, K.; Kozutsumi, Y.; Matsuzaki, K. *The Journal of Biological Chemistry* **2001,** *276*, 24985-90.

88. Kakio, A.; et al *Biochemistry* **2002,** *41*, 7385-90.

89. Micelli, S.; Meleleo, D.; Picciarelli, V.; Gallucci, E. *Biophysical Journal* **2004,** *86*, 2231-37.

90. Ji, S.; Wu, Y.; Sui, S. *The Journal of Biological Chemistry* **2002,** *277*, 6273-79.

91. Vatassery, G. T.; Quach, H. T.; Smith, W. E.; Sjovall, J. *Lipids* **1997,** *3*, 879.

92. Chang, J. Y.; Phelan, K. D. Sterols and Oxysterols: Chemistry, Biology, and Pathobiology, Fliesler, S. J., Ed.; 2002.

93. Phillips, J. E.; Geng, Y.-J.; Mason, R. P. *Atherosclerosis* **2001,** *159*, 125-35.

94. Knoll, W.; Park, H.; Sinner, E.; Yao, D.; Yu, F. *Surface Science* **2004,** *570*, 30-42.

95. Snyder, S. W.; Ladror, U. S.; Wang, G. T.; Barrett, L. W.; Matayoshi, E. D.; Huffaker, H. J.; Krafft, G. A.; Holzman, T. F. *Biophys.J.* **1994,** *67*, 1216-28.

96. MacRichtie, F. *Adv.Protein Chem* **1978,** *32*, 283-326.

97. Montich, G. G.; Bustors, M.; Maggio, B.; Cumar, F. A. *Chem.Phys.Lipids* **1985,** *38*, 319-26.

98. Montich, G. G.; Scarlate, S.; MacLaughlin, S.; Lehrmann, R.; Seelig, J. *Biochim.Biophys.Acta* **1993,** *1146*, 17-24.

99. Israelachvili, J. N. Intermolecular and Surface Forces*,* 1985.

100. Lu, D. R. L. S. J.; Park, K. *J.Biomater.Sci., Polymer Edn.* **1991,** *3*, 17.

101. Wisniewski, N.; Reichert, M. *Colloids and Surfaces B: Biointerfaces* **2000,** *18*, 197-219.

102. Glasaemastar, K.; Larsson, C.; Hoeoek, F. *Journal of Colloid and Interface Science* **2002,** *246*, 40-47.

103. Ishihara, K. *J.Biomaterials Application* **1998,** *13*, 111-27.

104. Lewis, A. L. *Colloids Surf.B Biointerfaces* **2000,** *18*, 261-75.

105. Chapman, D.; Charles, S. A. *Chem.Br.* **1992,** *28*, 253-56.

106. Wisniewski, N.; Moussy, F.; Reichert, W. M. *Fresenius J Anal Chem* **2000,** *366*, 611-21.

107. Ishihara, K. *J.Biomaterials Application* **1998,** *13*, 111-27.

108. Jendrasiak, G. L.; Smith, R. L. *Chemisry and Physics of Lipids* **2001,** *113*, 55-66.

109. Malmsten, M. *Colloids and Surfaces* **1999,** *159*, 87.

110. Sankaram M.B.; Thompson, T. E. *Biochemistry* **1990,** *29*, 10610-75.

111. Rastedt, B.; Slotte, J. P. *FEBS Letters* **2002,** *26592*, 1-5.

112. Wisniewski, N.; Reichert, M. *Colloids and Surfaces B: Biointerfaces* **2000,** *18*, 197-219.

113. Matsuzaki, K.; Horikiri, C. *Biochemistry* **1999,** *38*, 4137-42.

114. Micelli, S.; Meleleo, D.; Picciarelli, V.; Gallucci, E. *Biophysical Journal* **2004,** *86*, 2231-37.

115. Mahfoud, R.; et al *The Journal of Biological Chemistry* **2002,** *277*, 11292-96.

116. Morishima-Kawashima, M.; Ihara, Y. *Biochemistry* **1998,** *37*, 15247-53.

117. Kakio, A.; et al *Biochemistry* **2002,** *41*, 7385-90.

118. Kakio, A.; Nishimoto, S.; Yanagisawa, K.; Kozutsumi, Y.; Matsuzaki, K. *The Journal of Biological Chemistry* **2001,** *276*, 24985-90.

119. Kakio, A.; et al *Biochemistry* **2002,** *41*, 7385-90.

120. Olsher, M.; Yoon, S.; Chong, P. L. *Biochemistry* **2005,** *44*, 2080-87.

121. Soto, C.; Castano, E. M.; Kumar, R. A.; Beavis, R. C.; Frangione, B. *Neurosci.Lett.* **1995,** *200*, 105-08.

122. Sunde, M.; Serpell, L. C.; Bartlmm, M.; Fraser, P. E.; Pepys, M. B.; Blake, C. C. *J.Mol.Biol.* **1997,** *273*, 729.

123. Singer, S. J.; Nicolson, G. L. *Science* **1972,** *175*, 720-31.

124. Simons, K.; Ikonen, E. *Nature* **1997,** *387*, 569-72.

125. Suzuki, T. *Neurosci Res* **2002,** *44*, 1-9.

126. van der Goot, F. G.; Harder, T. *Semin Immunol* **2001,** *13*, 89-97.

127. Kakio, A.; et al *Biochemistry* **2002,** *41*, 7385-90.

128. Golde, T. E.; Eckman, C. B. *Drug Discov Today* **2001,** *6*, 1049-55.

129. Kakio, A.; et al *J.Biol.Chem* **2001,** *276*, 24985-90.

130. Munro, S. *Cell* **2003,** *115*, 377-88.

131. Dietrich, C.; Bagatolli, L. A.; Volovyk, Z. N.; Thompson, N. L.; Levted, M.; Jacobson, K.; Gratton, E. *Biophy.J.* **2001,** *80*, 1417-28.

132. Israelachvili, J. N.; Marcelja, S.; Horn, R. G. *Q Rev Biophys* **1980,** *13*, 121-200.

133. Xu, X. L.; London, E. *Biochemistry* **2000,** *39*, 843-49.

134. Morishima-Kawashima, M.; Ihara, Y. *Biochemistry* **1998,** *37*, 15247-53.

135. Mahfoud, R.; et al *The Journal of Biological Chemistry* **2002,** *277*, 11292-96.

136. Soto, C.; Castano, E. M.; Frangione, B.; Inestrosa, N. C. *J.Biol.Chem* **1995,** *270*, 3063-67.

137. Steinbauer, B.; Mehnert, T.; Beyer, K. *Biophys.J.* **2003,** *85*, 1013-24.

138. Seubert, P.; et al *Nature* **1992,** *359*, 322-25.

139. Shoji, M.; et al *Sceince* **1992,** *258*, 126-29.

140. Barrow, C. J.; Yasuda, A.; Kenny, P. T.; Zagorski, M. G. *J.Mol.Biol.* **1992,** *255*, 1075-93.

141. Soto, C.; Castano, E. M. *J.Biol.Chem* **1995,** *270*, 3063-67.

142. Soto, C.; Castano, E. M. *Biochem, J.* **1996,** *314*, 701-07.

143. Kakio, A.; Nishimoto, S.; Yanagisawa, K.; Kozutsumi, Y.; Matsuzaki, K. *The Journal of Biological Chemistry* **2001,** *276*, 24985-90.

144. Micelli, S.; Meleleo, D.; Picciarelli, V.; Gallucci, E. *Biophysical Journal* **2004,** *86*, 2231-37.

145. Olsher, M.; Yoon, S.; Chong, P. L. *Biochemistry* **2005,** *44*, 2080-87.

146. Ishihara, K. *J.Biomaterials Application* **1998,** *13*, 111-27.

147. Kakio, A.; Nishimoto, S.; Yanagisawa, K.; Kazutsumi, Y.; Matsuzaki, K. *Biochemistry* **2002,** *41*, 7385-90.

148. Micelli, S.; Meleleo, D.; Picciarelli, V.; Gallucci, E. *Biophaysical Journal* **2004,** *86*, 2231-37.

149. Ji, S.; Wu, Y.; Sui, S. *The Journal of Biological Chemistry* **2002,** *277*, 6273-79.

150. Pappolla, M.; Bozner, P.; Soto, C.; Shao, H.; Robakis, N. K.; Zagorski, M.; Frangione, B.; Ghiso, J. *The Journal of Biological Chemistry* **1998,** *273*, 7185-88.

151. Suzuki, S.; Grenn, PG.; Bumgarner; R.E.; Dasgupta, S.; Goddard, W. A.; Blake, G. A. *Science* **1992,** *257*, 942-45.

152. Shoji, M.; et al *Sceince* **1992,** *258*, 126-29.

153. Yu, F.
Surface Plasmon Fluorescence Spectroscopy and Surface Plasmon Diffraction in Biomolecular Interaction Studies. 2004.
Ref Type: Thesis/Dissertation

154. Cooper, M. A.; Williams, D. H. *Analytical Biochemistry* **1999,** *276*, 36-47.

155. Solomon, B.; Koppel, R.; Frankel, D.; Hanan-Aharon, E. *Proc.Natl.Acad.Sci.USA.* **1997,** *94*, 4109-12.

156. Amzel, M. L.; Poljak, R. J. *Annu.Rev.Biochem* **1979,** *48*, 961-97.

157. Davies, D. R.; Cohen, G. H. *Proc.Natl.Acad.Sci.USA.* **1996,** *93*, 7-12.

158. Amit, A. G.; Mariuzza, R. A.; Philips, S. E. V.; Poljak, R. J. *Science* **1986,** *233*, 747-53.

159. Bhat, T. N.; Bentley, G. A.; Fishchmann, T. O.; Boulot, G.; Poljak, R. J. *Nature* **1990,** *347*, 483-85.

160. Solomon, B.; Koppel, R.; Frankel, D.; Hanan-Aharon, E. *Proc.Natl.Acad.Sci.USA.* **1997,** *94*, 4109-12.

161. Bard, F.; Cannon, C.; Barbour, R.; Burke, R. L.; Games, D.; Grajeda, H.; Guido, T.; Hu, K.; Huang, J.; Johnson-Wood, K. *Nat.Med.* **2000,** *6*, 916-19.

162. Mahfoud, R.; Garmy, N.; Maresca, M.; Yahi, N.; Puigserver, A.; Fantini, J. *The Journal of Biological Chemistry* **2002,** *277*, 11292-96.

163. Steinbauer, B.; Mehnert, T.; Beyer, K. *Biophys.J.* **2003,** *85*, 1013-24.

164. Soto, C.; Castano, E. M.; Kumar, R. A.; Beavis, R. C.; Frangione, B. *Neurosci.Lett.* **1995,** *200*, 105-08.

165. Matsuzaki, K.; Horikiri, C. *Biochemistry* **1999,** *38*, 4137-42.

166. Koppaka, V.; Axelsen, P. H. *Biochemistry* **2000,** *39*, 10011-16.

167. Skribnek, Z.; Balaspiri, L.; Mak, M. *J.Mass Spectrom.* **2001,** *36*, 1226-29.

168. Kim, J. E.; Lee, M. *Bicochemical and Biophysical Research Communication* **2003,** *303*, 576-79.

169. Saija, A.; Tomaino, A.; Trombetta, D.; Pellegrino, M. L.; Tita, B.; Caruso, F.; Castelli, F. *European Journal of Pharmaceutics and Biopharmaceutics* **2005,** *53*, 209-15.

170. Halverson, K.; Fraser, P.; Kirschner, D. A.; Lansbury, P. T. *Biochemistry* **1990,** *29*, 2639-44.

171. Hilbich, C.; Kisters-Woike, B.; Reed, J.; Masters, C. L.; Beyreuther, K. *J.Mol.Biol.* **1991,** *218*, 149-63.

172. Jarrett, J. T.; Lansbury, P. T. *Cell* **1993,** *73*, 1055-56.

173. Halverson, K.; Fraser, P.; Kirschner, D. A.; Lansbury, P. T. *Biochemistry* **1990,** *29*, 2639-44.

174. Hilbich, C.; Kisters-Woike, B.; Reed, J.; Masters, C. L.; Beyreuther, K. *J.Mol.Biol.* **1991,** *218*, 149-63.

175. Jarrett, J. T.; Lansbury, P. T. *Cell* **1993,** *73*, 1055-56.

176. Skene, D. J.; Vivien-Roels, B.; Sparks, D. J.; Hunsaker, J. C.; Pevet, P.; Ravid, D.; Swaab, D. F. *Brain Res.* **1990,** *528*, 170-74.